# MVDR Broadband Beamforming Using Polynomial Matrix Techniques

Ahmed Alzin

Centre for Signal & Image Processing
Department of Electronic & Electrical Engineering
University of Strathclyde, Glasgow

February 25, 2022

This thesis is the result of the author's original research. It has been composed by the author and has not been previously submitted for examination which has led to the award of a degree.

# Abstract

This thesis addresses the formulation of and solution to broadband minimum variance distortionless response (MVDR) beamforming. Two approaches to this problem are considered, namely, generalised sidelobe canceller (GSC) and Capon beamformers. These are examined based on a novel technique which relies on polynomial matrix formulations. The new scheme is based on the second order statistics of the array sensor measurements in order to estimate a space-time covariance matrix. The beamforming problem can be formulated based on this space-time covariance matrix. Akin to the narrowband problem, where an optimum solution can be derived from the eigenvalue decomposition (EVD) of a constant covariance matrix, this utility is here extended to the broadband case. The decoupling of the space-time covariance matrix in this case is provided by means of a polynomial matrix EVD.

The proposed approach is initially exploited to design a GSC beamformer for a uniform linear array, and then extended to the constrained MVDR, or Capon, beamformer and also the GSC with an arbitrary array structure. The uniqueness of the designed GSC comes from utilising the polynomial matrix technique, and its ability to steer the array beam towards an off-broadside direction without the pre-steering stage that is associated with conventional approaches to broadband beamformers.

To solve the broadband beamforming problem, this thesis addresses a number of additional tools. A first one is the accurate construction of both the steering vectors based on fractional delay filters, which are required for the broadband constraint formulation of a beamformer, as for the construction of the quiescent beamformer. In the GSC case, we also discuss how a block matrix can be obtained, and introduce a novel paraunitary matrix completion algorithm. For the Capon beamformer, the polynomial extension requires the inversion of a polynomial matrix, for which a residue-based method is proposed that offers better accuracy compared to previously utilised approaches.

These proposed polynomial matrix techniques are evaluated in a number of simulations. The results show that the polynomial broadband beamformer (PBBF) steers

the main beam towards the direction of the signal of interest (SoI) and protects the signal over the specified bandwidth, and at the same time suppresses unwanted signals by placing nulls in their directions. In addition to that, the PBBF is compared to the standard time domain broadband beamformer in terms of their mean square error performance, beam-pattern, and computation complexity. This comparison shows that the PBBF can offer a significant reduction in computation complexity compared to its standard counterpart.

Overall, the main benefits of this approach include beam steering towards an arbitrary look direction with no need for pre-steering step, and a potentially significant reduction in computational complexity due to the decoupling of dependencies of the quiescent beamformer, blocking matrix, and the adaptive filter compared to a standard broadband beamformer implementation.

# Acknowledgements

All praise is due to Allah who guides me to work with such wonderful people during my research over the past years. Starting with my supervisor, the research group colleagues, and ends with friends and family, who collectively have made my study and life in the UK delightful. Having said that:

I would like to express my extreme gratitude to my supervisor, Prof. Stephan Weiss for his invaluable advice, continuous support, and patience during my Ph.D. His immense knowledge and plentiful experience have encouraged me all the time during my academic research and my daily life. These words are not enough to express my thanks, gratitude, and appreciation for his great efforts at various times.

I would like to offer my special thanks to my examiners Prof. Robert Stewart and Prof. Jesus Selva for their constructive comments and suggestions.

I would like to thank all CeSIP centre members, more specifically I would like to thank colleagues with whom I shared the lab and those I worked with as a teaching assistant. It was such a productive environment full of a broad range of educational themes and discussions.

My Parents, from the bottom of my heart I would like to say a big thank you, I simply couldn't have done this without your prayers, motivation, and unconditional love. Special thanks are to my brothers and sisters for their spiritual support. To all of you - Thank You.

Finally, no words of gratitude are enough for my family, my children for bearing with my very busy days during their holidays, and my wife who made a significant impact during all these years via her patience and cooperation to make everything hold together.

# Author's Publications

- Ahmed Alzin, Fraser K Coutts, Jamie Corr, Stephan Weiss, Ian K Proudler and Jonathon A Chambers: Polynomial matrix formulation-based Capon beamformer, Institute of Mathematics and its Applications, 2016.
- Ahmed Alzin, Fraser K. Coutts, Jamie Corr, Stephan Weiss, Ian K. Proudler and Jonathon A. Chambers: Adaptive broadband beamforming with arbitrary array geometry, 2nd IET International Conference on Intelligent Signal Processing (ISP), 2015.
- Stephan Weiss, Samir Bendoukha, Ahmed Alzin, Fraser K Coutts, Ian K Proudler and Jonathan A Chambers: MVDR broadband beamforming using polynomial matrix techniques, 23rd European signal processing Conference (EUSIPCO), 2015.
- Mohamed A Alrmah, Jamie Corr, Ahmed Alzin, Keith Thompson and Stephan Weiss: Polynomial subspace decomposition for broadband angle of arrival estimation, Sensor Signal Processing for Defence (SSPD), 2014.

# Contents

# List of Figures

# List of Tables

# List of Abbreviations

| | |
|---|---|
| AoA | angle of arrival |
| CSD | cross-spectral density |
| DFT | discrete Fourier transform |
| ESPRT | estimation of signal parameters via rotational invariance techniques |
| EVD | eigenvalue decomposition algorithm |
| FDF | fractional delay filter |
| FIR | finite impulse response |
| GSC | generalised side-lobe canceller |
| LCMV | linearly constrained minimum variance |
| LMS | least mean square |
| MIMO | multiple input multiple output |
| MUSIC | multiple signal classification |
| MVDR | minimum variance distortion-less response |
| NLMS | normalised least mean square |
| PBBF | polynomial broadband beamformer |
| PEVD | polynomial eigenvalue decomposition |
| SBR | sequential best rotation |
| SG | spatial gain |
| SINR | signal to interference plus noise ratio |

| | |
|---|---|
| SMD | sequential satrix diagonalisation |
| SMI | sample matrix inversion |
| SNR | signal to noise ratio |
| SoI | signal of interest |
| TDL | tap delay line |
| ULA | uniformly linear array |

# List of Notations

| | |
|---|---|
| $d[n]$ | quiescent signal output |
| $s(t, \mathbf{r})$ | space time signal |
| $\mathbf{r}$ | vector of vocations of the antenna elements |
| $\omega$ | angular frequency |
| $\mathbf{k}$ | wavenumber vector |
| $\mathbf{u}$ | unit length vector |
| $\varphi$ | azimuth angle |
| $\vartheta$ | elevation angle |
| $M$ | number of array elements |
| $\tau$ | propagation delay or lag |
| $x_m[n]$ | input signal captured by m-th antenna element |
| $\mathbf{x}[n]$ | vector of antenna array element's signals |
| $\mathbf{v}[n]$ | noise vector |
| $\mathbf{a}(\varphi, \vartheta)$ | steering vector of the array towards direction $(\vartheta, \varphi)$ |
| $\mathbf{A}(\vartheta, \varphi)$ | array steering matrix |
| $d$ | inter-element spacing |
| $\mathbf{w}[n]$ | spatial weight vector |
| $\tau$ | time lag |
| $u[n]$ | vector of blocking matrix output |
| $e[n]$ | error signal |
| $\mu$ | LMS step size |
| $\mathbf{C}$ | constraint matrix |

| | |
|---|---|
| $\boldsymbol{A}(z)$ | polynomial matrix |
| $a_{ij}(z)$ | $(i,j)$-th element of a polynomial matrix $\boldsymbol{A}(z)$ |
| $\mathcal{E}\{\cdot\}$ | expectation operator |
| $(\cdot)^*$ | conjugate operator |
| $(\cdot)^{\mathrm{H}}$ | Hermitian operator |
| $(\cdot)^{\mathrm{P}}$ | para-Hermitian operator |
| $r[\tau]$ | auto or cross-correlation sequence |
| $f$ | frequency |
| $f_s$ | sampling frequency |
| $\sigma^2$ | variance or the power of a signal |
| $\mathbf{I}_n$ | $n \times n$ identity matrix |
| diag[$\cdot$] | diagonal matrix |
| $\Omega$ | angular frequency |

List of Tables

# Chapter 1

# Introduction

## 1.1 Background and Motivation

In many applications such as radar [1, 2], sonar [3, 4], microphone arrays [5], radio astronomy [4, 6], seismology, medical diagnosis [7], and wireless communications [8, 9], beamforming techniques play a vital role. A beamformer is a signal processing system consisting of an array of sensors; these sensors measure propagation fields with the aim to emphasize a signal from a certain direction, while attenuating signals from other directions. This emphasis is achieved by the beamformer operating as a spatial filter.

With respect to the bandwidth of the impinging signals, beamforming is categorized as either narrowband or wideband beamforming. Narrowband beamformers are designed to operate at a single frequency or narrow range of frequencies, whereby the inverse of the bandwidth is large compared to the time delay that the signal component experiences to travel between the reference and furthermost sensors in the array [10]. In contrast, broadband beamformers are utilized in a large range of applications which need to work over a wide frequency band that extends over several octaves, such as in audio or sonar signal processing [3, 11].

Many approaches exist for narrowband beamformering. These are categorised in terms of data dependency, where in a first category the beamforming weights do not depend on the arrays' data but only on geometry such as the angle of arrival of the signal of interest, as is the case of the delay and sum beamformer [12]. The second cate-

gory are statistically optimum beamformers where beamforming weights are optimized based on the arrays' data; these are also referred to as adaptive beamformers [4, 13]. Some approaches related to this category optimise the beamformer with respect to the signal to interference plus noise ratio (SINR) [14], minimum variance distortionless response (MVDR) [15, 16], or perform a sample matrix inversion (SMI) adaptive beamformer, which is preferable in applications where adaptive beamformers suffer from slow convergence due to a wide spread of the eigenvalues in the covariance matrix [17, 18].

Broadband beamformers are often implemented as digital systems. A first method is the implementation in time domain by using finite impulse response (FIR) filters or tapped delay lines following each array element [19, 20, 21, 22, 23, 24, 25]. The second is the frequency decomposition method [26], in which the time sequences measured at each sensor are projected into narrowband frequency bins using the discrete Fourier transform (DFT), and a broadband beam-pattern can then be created by applying synthesis techniques across all frequency bins. Many advantages and properties of the time domain broadband beamformer are reported in [27] and[28]. For instance, this method of broadband design does not suffer from latency, which makes it suitable to use in applications such as communications; the data can be updated for each new snapshot which is advantageous in processing transient signals and short pulses. In addition, it is proved in [27] that the time domain approach for broadband beamforming estimates the weights more accurately compared to its frequency domain counterpart, and functions better in scenarios where interference signals possess high power and occupy large bandwidths. This is because frequency domain methods that operate in independent DFT bin, while numerically very inexpensive, are known to have a very poor worst-case performance [29].

While most of the existing work has been reported on narrowband beamforming where a rich set of optimum tools are available, wideband beamforming technique solutions are specific to parameters such as the tap delay line length, and can be suboptimal. In addition, commonly, the design approaches of broadband beamforming incorporate a pre-steering delay for each sensor, which can be achieved physically at

the cost of extra hardware components in implementation. This in return can lead to higher power consumption. Accordingly, in [30] a broadband beamformer without pre-steering procedures was proposed, which simplifies the physical structure as well as reduces the processing time and cost. This can be very significant when an array consists of a large number of sensors.

From an implementation viewpoint, in the case of narrowband time domain beamforming the delay of signal samples between array elements is usually represented as a phase shift. However, in the case of broadband processing the time delay or lag value has to be taken into account when calculating the space-time covariance matrix that describes the interaction between the broadband sensor array signals. As a consequence, the elements of the space-time covariance matrix are formed by the complete auto- or cross-correlation sequences rather than just a single correlation coefficient as in the narrowband case. By applying the - $z$ transform to this matrix results in its corresponding cross-spectral density (CSD) matrix that takes a polynomial form. Within the polynomial matrix framework, a number of narrowband techniques have been extended to the broadband case [31].

Regarding the previous statement of advantages and disadvantages of broadband beamformers in time or frequency domain implementation, and also the benefit of discarding the pre-steering process, in this research we are particularly interested in time domain broadband beamforming with arbitrary look direction, since most beamformer designs assume pre-steering and look towards broadside. This method is achieved by manipulating the concept of polynomials in digital signal processing.

The proposed method shows a reduction of computational complexity and robustness particularly for off-broadside constraints for linear or planar arrays, or for arrays with an arbitrary configuration in three dimensions. This is achieved using the generalised sidelobe canceller (GSC) structure, which is an implementation of minimum variance distortionless response (MVDR) beamformer and relies on adaptive filtering algorithms, such as the normalised least mean square (NLMS) algorithm, to perform unconstrained adaptive optimisation in order to determine the beamforming weights. The MVDR beamformer in its generalised side-lobe canceller (GSC) structure addresses

the optimisation problem and can also respond to any change in the statistics of the array's data. However, if a part of the signal of interest leaks along with interference and noise through the system's blocking matrix to the adaptive filter, this can lead to cancellation of the signal that we would like to preserve. As a consequence the design of a blocking matrix that prevents such scenario is very important in order to optimally suppress interference and noise, and many approaches were proposed for this purpose [32, 33, 34]. In this work the design of a blocking matrix for broadband signals is accomplished by invoking polynomial tools [1], namely a polynomial eigenvalue decomposition algorithm (PEVD) which is an extension of the eigenvalue decomposition (EVD) of conventional Hermitian matrices [35].

This approach is tested under scenarios that assume a uniformly spaced linear array (ULA) as well as arbitrary array geometry and an environment without reverberation. The sole impairment that the desired signal encounters is due to interference and noise. The performance of the proposed design is compared with a standard beamformer by using MATLAB simulations. The metrics to assess the performance of the adaptive beamfomer are its directivity pattern, the mean square residual error, and its computational cost. The results show that the polynomial approach of designing a broadband beamformer provides low computational complexity and can outperform standard broadband beamforming.

To demonstrate the ease with which broadband array problems can be generalised from their well-known narrowband equivalents when using polynomial matrix formulations, this thesis further studies the Capon beamformer as an alternative form of addressing the MVDR problem. This form of formulation of the MVDR includes the inverse of the space-time covariance matrix, which is accomplished by a new polynomial matrix inversion technique based on the residue method. Within this context, a regularisation factor or diagonal loading is applied to the polynomial matrix in order to mitigate poor conditioning in space and frequency. This is examined for a specific regularisation parameter. This has also led to a reduction in sidelobe peak levels, and can enhance the overall performance of the polynomial broadband beamformer.

[1] http://pevd-toolbox.eee.strath.ac.uk/

This thesis also demonstrates the constraint design and broadband beamformer implementation for an array with arbitrary configuration in 3-dimensional space for the unconstrained adaptive MVDR beamformer. This is important since an equispaced, linear arrangement of the sensor array might be inadequate for some applications. Also, the spatial arrangement of the sensors overcomes the problem of the ambiguity cone of the ULA. The performance of the polynomial broadband beamformer (PBBF), with this type of sensor array configuration, is evaluated based on its beam-pattern, and the residual error. The results for a number of defined simulation scenarios show sufficient nulling of the interference and protection of the desired signal.

## 1.2 Contributions

This thesis aims to provide several novel aspects related to array processing and more precisely the design of broadband beamformers, which are detailed below.

- The polynomial formulation of the objective and constraints of MVDR optimisation problem for various MVDR beamforming techniques including GSC and Capon solutions, and for arbitrary array geometry [36, 37, 38].
- A solution to a broadband beamformer with no pre-steering process that respond to sources of interest that lie off-broadside[36].
- The construction of two of the main three parts of the GSC structure of the MVDR beamformer based on polynomial methods, namely, the polynomial quiescent beamformer and the blocking matrix [36].
- The development of novel approach, that relies on the residue theorem, for the numerical calculation of a polynomial matrix inverse [38].
- The application of the polynomial matrix inverse to compute the broadband Capon beamformer's weight vector [38].
- The implementation of the broadband Capon beamformer in three different ways, which depends on different combinations of the desired signal, interference, and

noise to obtain the space-time covariance matrix [38].

- The generalisation of the polynomial broadband beamformer to be adequate for processing sampled data captured by an array of sensors[37].

## 1.3 Thesis Organisation

The overall organisation of the thesis is as follows.

Chapter 2 starts with basic concepts about electromagnetic waves and array signal modelling and processing. Here, the beamforming techniques for narrowband signal are first discussed, and their categories are introduced such as data independent or statistically optimum [15, 39]. Also, their implementation steps are explained. The fractional delay filter is introduced in order to construct a broadband steering vector. General structures for time domain and frequency domain beamformers are also introduced. Since adaptive filters are usually incorporated in the design of adaptive beamformers, some algorithms related to these techniques are described. The chapter also reviews polynomial matrix techniques and algorithms in signal processing. The polynomial matrix structure, their properties and some related algorithms to process this type of matrices are treated in so far as they are required for implementation purposes in the context of this thesis.

Next, Chapter 3 discusses the formulation and implementation of a broadband MVDR beamformer using a GSC structure that relies on polynomial matrix techniques. It concentrates on the aspects and characteristics associated with broadband steering vectors and quiescent beamformer as well as the design of the blocking matrix and multichannel noise cancellation adaptive filter. The design is then examined by comparing its performance with a tap-delay-line-based time domain broadband beamformer in computer simulations.

Then, the Capon broadband beamformer is considered in Capter 4. Special consideration is given to the implementation process, which includes the inversion of the polynomial space-time covariance matrix. Implementation approaches are exemplified, and a numerical evaluation of each of the approaches is presented.

In Chapter 5, the extension of the broadband steering vector to a three dimensional array set up is derived. Based on this derivation, the GSC beamformer implementation is updated, and the performance of the beamformer is evaluated using metrics including beam patterns that can adequately reflect a dependency on three parameters — azimuth and elevation angles, as well as frequency.

The main points and observations of the work are summed up, together with some ideas for future work, in Chapter 6.

# Chapter 2

# Introduction to Beamforming

This chapter is concerned with fundamentals and concepts of array processing and beamforming. The chapter begins with a description of antenna arrays in Sec. 2.1 based on the organisation of array elements within a coordinate systems, along with the spatial signal representation and its mathematical model. General beamforming is reviewed in Sec. 2.2. In Sec. 2.3 the minimum variance distortionless response (MVDR) in its linearly constrained minimum variance (LCMV) beamformer and generalised sidelobe canceller (GSC) versions are presented. In order to extend this to the broadband case, in Sec. 2.4 the time domain approaches of broadband beamformer are discussed. In the last section of this chapter, some polynomial signal processing terminologies, definitions and algorithms are defined in order to complete some of the background that will be used in later chapters.

## 2.1 Antenna Array and Signal Model

### 2.1.1 Array Elements in Space and Wave Propagation

Antenna arrays comprise multiple antenna elements that can be organized into different geometric configurations which depend on the application. This set of antenna elements collects spatial samples of the signal impinging on the array. The output from the individual elements are processed and combined to obtain a single output that represent the antenna array output. In comparison with continuous aperture antennas,

the antenna array principle adds degrees of freedom to the array design, and also a capability to control its radiation pattern [40, 41, 42]. Flexibility to control the shape of the desired radiation pattern can improve the directivity and gain, and facilitate to electronically steer the beam towards the specific direction from which a source that emits a signal arrives at the array [43].

The mathematical representation of an impinging signal involves two parameters that play an important role for the signal discrimination, as it is described in later sections, with the aim of extracting information from the signal in the presence of interference and noise. The first parameter is the position vector of the antenna array elements, $\mathbf{r}$, and the second is the time, $t$, at which the signal is observed. Hence, such a signal is commonly known as a space-time signal, and it is symbolically indicated as $s(t, \mathbf{r})$. The location of the antenna elements, $\mathbf{r}$, can be described within a three dimensional right handed orthogonal coordinate system, such a rectangular or Cartesian coordinate system $x$, $y$, $z$, or its Spherical coordinate counterpart system $\rho$, $\vartheta$, $\varphi$. However, the description of a vector within either system can be easily converted to the other via

$$\boldsymbol{r}_m = \begin{bmatrix} x_m \\ y_m \\ z_m \end{bmatrix} \tag{2.1}$$

or

$$\boldsymbol{r}_m = \rho_m \begin{bmatrix} \cos\varphi_m \sin\vartheta_m \\ \sin\varphi_m \sin\vartheta_m \\ \cos\vartheta_m \end{bmatrix} , \tag{2.2}$$

where the transformation from the Cartesian to polar coordinate systems is achieved by substituting $x_m = \rho_m \cos\varphi_m \sin\vartheta_m$, $y_m = \rho_m \sin\varphi_m \sin\vartheta_m$, and $z_m = \rho_m \cos\vartheta_m$. The transformation (2.2) is illustrated in Fig. 2.1.

In the case when propagation occurs in free space, in which the medium is considered as homogeneous, dispersion free, and lossless, the space time signal $s(t, \mathbf{r})$ undergoes e.g. the Maxwell equations in case of propagation of an electromagnetic wave, and can

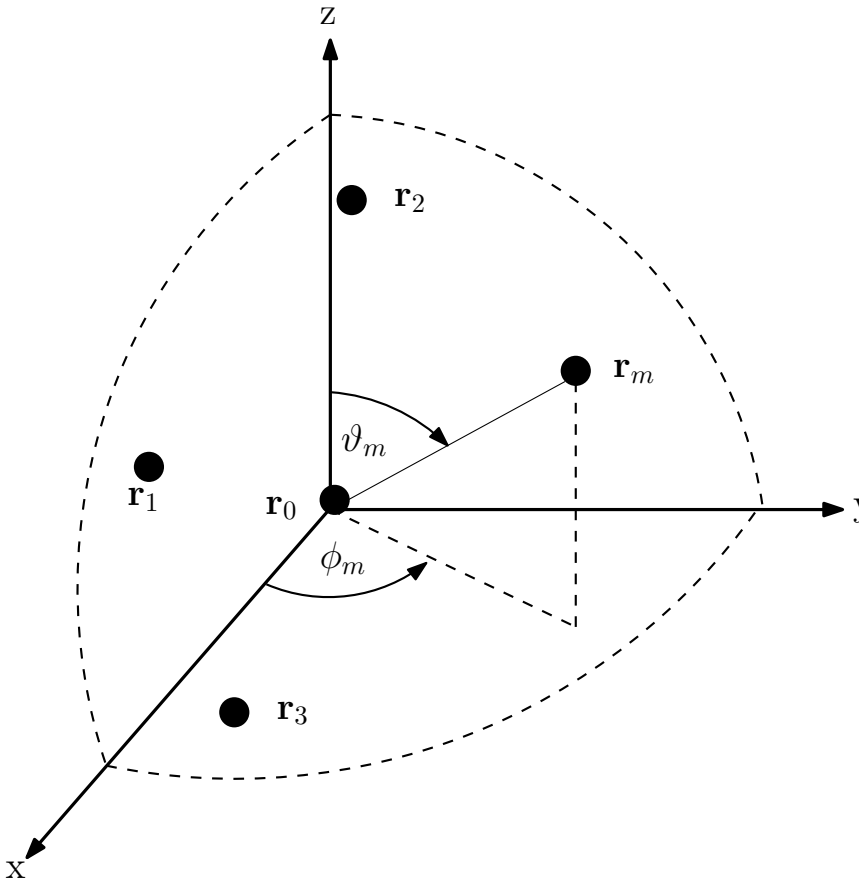


Figure 2.1: Antenna array with arbitrary configuration.

be solved accordingly by the scalar wave equation [40]

$$\nabla^2 s(t,\mathbf{r}) - \epsilon_0\mu_0 \frac{\partial^2 s(t,\mathbf{r})}{\partial t^2} = 0 \ , \tag{2.3}$$

where $\nabla^2$ denotes the Laplacian operator, and $\epsilon_0$ and $\mu_0$ the dielectric constant and magnetic permeability of free space, respectively. The solution for this differential equation provides that

$$\begin{aligned} s(t,\mathbf{r}) &= Se^{j(\omega t - \mathbf{k}^T\mathbf{r})} && (2.4)\\ &= Se^{j\omega t}e^{-j\mathbf{k}^T\mathbf{r}} \ , && (2.5) \end{aligned}$$

where $S$ refers to the signal amplitude, $\omega$ is the angular frequency, and $\mathbf{k}$ is a vector termed as the angular wavenumber vector and is defined by e.g. [44] as

$$\begin{aligned} \mathbf{k} &= \mathbf{k}(\vartheta,\varphi) && (2.6)\\ &= k.\mathbf{u} \ . && (2.7) \end{aligned}$$

The scalar $k$ represents the magnitude of $\mathbf{k}$ and is often termed wavenumber or the spatial frequency [25, 45],

$$k = \frac{2\pi}{\lambda} = \frac{\omega}{c}. \tag{2.8}$$

The vector $\mathbf{u}$ is a unit length vector that points to the direction specified by the azimuth angle $\varphi$ measured with respect to $x$ axis, and the elevation angle $\vartheta$ that is measured with respect to $z$ axis. Therefore, the unit vector is defined as

$$\mathbf{u} = \mathbf{u}(\vartheta,\varphi) = \begin{bmatrix} \cos\varphi_l \sin\vartheta_l \\ \sin\varphi_l \sin\vartheta_l \\ \cos\vartheta_l \end{bmatrix} \ , \tag{2.9}$$

with the azimuth angle $\varphi \in [0, 2\pi]$ , and the polar angle $\vartheta \in [-\pi/2, \pi/2]$.

### 2.1.2 Signal Model and Steering Vector

Assume that there are $L$ spatially discrete far field sources at locations $p_1, p_2, \ldots p_L$, and emitting signals whose baseband models are given by (2.5). Let $s_l[n]$ represents a signal from far field radiated by the $l$th source at time instance $n$. If this signal impinges on an antenna array with $M$ elements, then the array elements will spatially sample the plane wave, and the signal received by the $m$-th antenna element is

$$x_m[n] = s[n, \mathbf{r}_m] + v_m[n] \; . \tag{2.10}$$

The signals at the output of antenna elements, apart from being time-delayed, are all identical, whereby the delays depend on the angle of arrival (AOA) of the signal. With the reference element located at the origin of the coordinate system, the relative delay $\tau$ that a signal experience to travel to an $m$th element can be expressed as

$$\tau_m = \frac{\mathbf{r}_m^T . \mathbf{u}_l}{c} \; . \tag{2.11}$$

Thereby, the array signal components at each element due to the source signal in (2.10) can be organised to form a vector,

$$\mathbf{x}[n] = \begin{bmatrix} x_0[n] \\ x_1[n] \\ \vdots \\ x_{M-1}[n] \end{bmatrix} \tag{2.12}$$

By explicitly including the source signal and time delays, this becomes

$$\mathbf{x}[n] = \begin{bmatrix} s[n-\tau_0] \\ s[n-\tau_1] \\ \vdots \\ s[n-\tau_{(M-1)}] \end{bmatrix} + \begin{bmatrix} v_1[n] \\ v_2[n] \\ \vdots \\ v_{(M-1)}[n] \end{bmatrix} \; , \tag{2.13}$$

whereby $x_m[n] = s[n-\tau_m] + v_m[n]$ .

Alternatively, the signal vector can be expressed as a multiplication of the steering vector, that incorporates the phase shifts due to delays as a function of the angle of incidence, with a scalar signal, such that

$$\mathbf{x}[n] = \begin{bmatrix} e^{-j\mathbf{k}^T\mathbf{r}_0} \\ e^{-j\mathbf{k}^T\mathbf{r}_1} \\ \vdots \\ e^{-j\mathbf{k}^T\mathbf{r}_{M-1}} \end{bmatrix} s[n] + \mathbf{v}[n] \,, \tag{2.14}$$

with $\mathbf{v}[n]$ a noise vector characterised further below. The phase factor is also referred to as array steering vector and incorporates all the spatial characteristics of the array.

For a general case, when complex baseband signals related to $L$ spatially separated and uncorrelated sources are received by an array with $M$ elements at a single discrete time instance $n$, we assume the underdetermined case $L < M$. In addition to that, these signals are corrupted by zero-mean complex additive white Gaussian noise $v_m[n] \sim CN(0, \sigma^2)$. Then the array observation vectors can be represented by

$$\begin{bmatrix} e^{-j\mathbf{k}_1^T\mathbf{r}_0} & e^{-j\mathbf{k}_2^T\mathbf{r}_0} & \dots & e^{-j\mathbf{k}_L^T\mathbf{r}_0} \\ e^{-j\mathbf{k}_1^T\mathbf{r}_1} & e^{-j\mathbf{k}_2^T\mathbf{r}_1} & \dots & e^{-j\mathbf{k}_L^T\mathbf{r}_1} \\ \vdots & \vdots & \dots & \vdots \\ e^{-j\mathbf{k}_1^T\mathbf{r}_{M-1}} & e^{-j\mathbf{k}_2^T\mathbf{r}_{M-1}} & \dots & e^{-j\mathbf{k}_L^T\mathbf{r}_{M-1}} \end{bmatrix} . \tag{2.15}$$

Here, $\mathbf{a}(\varphi_l, \vartheta_l)$ denotes the steering vector of the array towards direction $(\vartheta_l, \varphi_l)$,

$$\mathbf{a}(\varphi_l, \vartheta_l) = \begin{bmatrix} e^{-j\mathbf{k}_l^T\mathbf{r}_0} \\ e^{-j\mathbf{k}_l^T\mathbf{r}_1} \\ \vdots \\ e^{-j\mathbf{k}_l^T\mathbf{r}_{M-1}} \end{bmatrix} , \tag{2.16}$$

and $\mathbf{v}[n]$ is the noise vector with elements representing the noise at each antenna

element. Using compact matrix notation, (2.14) becomes

$$\mathbf{x}[n] = \mathbf{A}(\varphi, \vartheta) \cdot \mathbf{s}[n] + \mathbf{v}[n] \,, \tag{2.17}$$

where $\mathbf{A}(\vartheta, \varphi)$ is the array steering matrix of dimension $M \times L$ which contains in its columns the steering vectors of the incoming signals, such that

$$\mathbf{A}(\varphi, \vartheta) = \left[ \begin{array}{cccc} \mathbf{a}(\varphi_1, \vartheta_1) & \mathbf{a}(\varphi_2, \vartheta_2) & \ldots & \mathbf{a}(\varphi_L, \vartheta_L) \end{array} \right] . \tag{2.18}$$

### 2.1.3 A Uniform Linear Array Signal Model Example

In light of this discussion, we exemplify how the above parameters are related to the arrangement of the array elements. If a particular geometric structure of the antenna array is considered, for instance, if we assume that this formulation is applied to the uniform linear array (ULA) in Fig. 2.2, then the antenna elements are illuminated by a planar wave coming from a source with direction of arrival $\vartheta$. If (2.11) is applied to evaluate the propagation time delay with respect to the first element, the time delay for the $m$-th element will be

$$\tau_m = \frac{d \cos \vartheta}{c}(m), \quad m = 0, 2, \ldots, M-1 \,. \tag{2.19}$$

The parameter $d$ is the space distance between two adjacent antenna elements in the array.

By drawing an analogy between the temporal sampling based on the Nyquist theorem [46] and spatial sampling [25], the distance $d$ is considered as being the spatial sampling period that has to be restricted to avoid spatial aliasing. For a bandlimited signal, and by exploiting the relationship of the wavenumber $k$ with the angular frequency $\omega$ in (2.8) for $\omega \leq \omega_{max}$ , the spatial sampling period has to be $d \leq \lambda_{min}/2$ .

Based on correct spatial sampling, the spatial signature of the source is represented

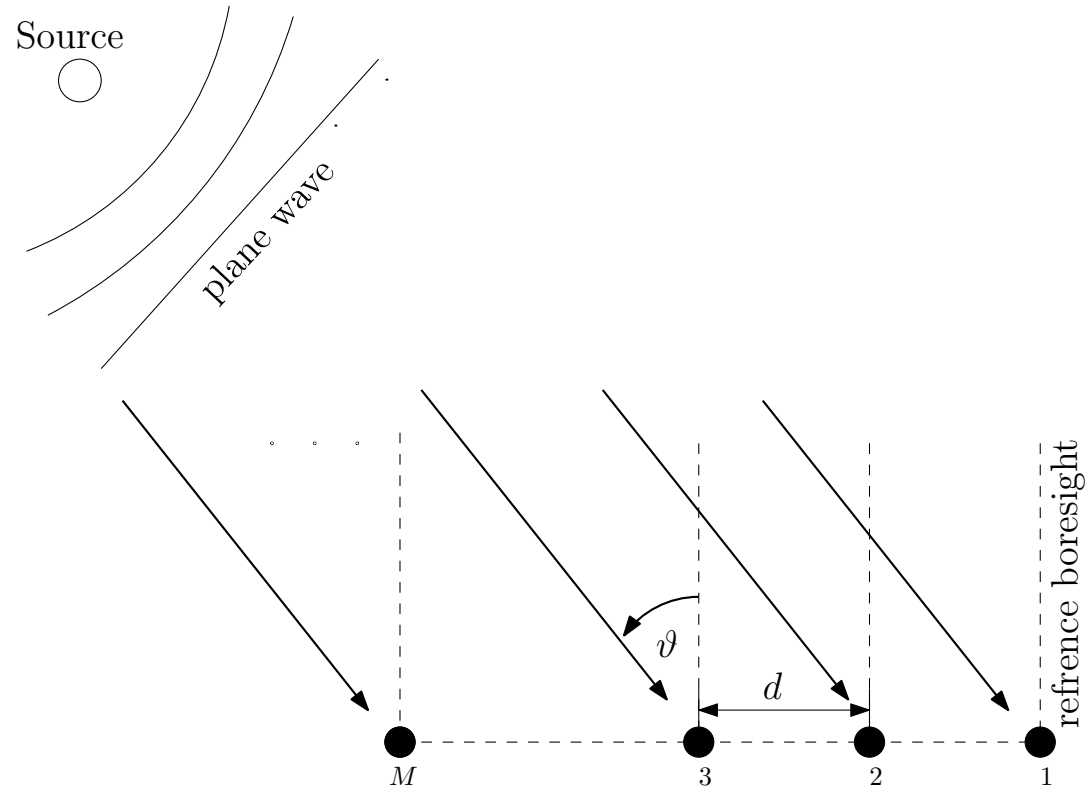


Figure 2.2: uniform linear array.

by the array steering vector

$$\mathbf{a}_{ULA}(\vartheta) = \begin{bmatrix} 1 \\ e^{-jkd\cos\vartheta} \\ \vdots \\ e^{-jkd\cos\vartheta(M-1)} \end{bmatrix} . \tag{2.20}$$

In the case of a monochromatic plane wave, this set of complex values represents phase shifts that substitute time delay processors $\delta[n-\tau_m]$, $m = 0, \ldots, (M-1)$ , and guarantee the components of the plane wave from the direction $\vartheta$ to be coherently added. If the noise $v_m[n]$ corrupting the sensors is assumed to be mutually independent, an enhancement of the signal to noise ratio (SNR) can be achieved which leads to the

socalled the array spatial gain (SG). The spatial gain is defined as

$$\mathrm{SG} = 10 \log \frac{\mathrm{SNR}_a}{\mathrm{SNR}_e} (\mathrm{dB}) \ , \tag{2.21}$$

where $\mathrm{SNR}_a$ and $\mathrm{SNR}_e$ are the signal to noise ratio of the array and of each element in the array respectively.

For generalization, if a number of plane waves are picked up by an array of sensors, and discrimination to a signal that comes from a specific direction is required, then it is important to process this signal in order to extract the spatio-temporal characteristics. To this end, direction finding algorithms need to be invoked, such as estimation of signal parameters via rotational invariance techniques (ESPRIT) [47] or multiple signal classification (MUSIC) algorithms [48], but these algorithms are beyond this research. The obtained information is processed by space time filters to spatially filter the SoI while simultaneously rejecting all other competing sources that are located spatially apart. This process is technically known as beamforming, which is going to be the core theme in the remainder of this thesis.

## 2.2 Beamforming Background

### 2.2.1 Beamforming Weights and Metrics

The capability of an antenna array to steer its beam pattern to a specific direction in space is termed as beamforming. Assume that a desired signal is coming from a direction $(\varphi_d, \vartheta_d)$ and propagates in a space shared with multiple interfering sources that propagate from different directions. Then the main objective, in this case, is to spatially filter the array signals such that the SoI is maintained while simultaneously nulling or suppressing undesired ones. To this end, a complex weight vector $\mathbf{w} = [w_0, w_1, \ldots, w_{M-1}]^H \in \mathbb{C}^{M \times 1}$ is applied to the array signal vector $\mathbf{x}[n]$ to perform a weighted sum over the different signals gathered by the array. Therefore the beamformer output is mathematically expressed as

$$y[n] = \mathbf{w}^{\mathrm{H}} \mathbf{x}[n] \ . \tag{2.22}$$

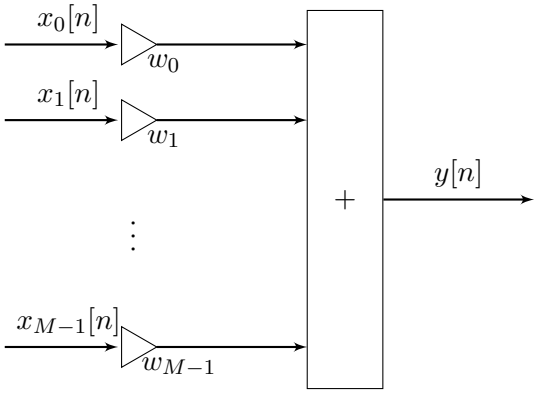


Figure 2.3: A narrowband conventional beamformer

In a simple type of beamformer called a delay-and-sum beamformer, the weighting in (2.22) is performed in order to compensate for the phase difference, and the array signals are, consequently, coherently combined. The process is depicted in Fig. 2.3, and this architecture, because of its structure and functionality, is generally called a delay-and-sum beamformer.

The way of calculating the weights classifies the beamformers into two categories, either as data independent or statistically optimum beamformers [18]. In the former the weights are fixed and do not depend on the received data, but on known angles of arrivals for both SoI and interferers. For the latter, the weights change or adapt based on the statistics of the array data, hence they optimize the array response to achieve a certain aim. This is used, for instance, to extract source signals when the array is used in the presence of multiple sources whose directions may be unknown.

For a single point source scenario, the weights are chosen to appropriately align the sensor signals such that they constructively interfer, as shown in Fig. 2.4. To this end, the phase shifts collected in the steering vector $\mathbf{a}(\vartheta_d)$ of the specific source are used to define the beamformer weights in order to steer the array's beam towards the desired

direction. Consequently, the choice of $\mathbf{w} = \mathbf{a}(\vartheta_d)$ satisfies this requirement, so that

$$\mathbf{w} = \frac{1}{\sqrt{M}} \begin{bmatrix} e^{-j\mathbf{k}_d^T \mathbf{r}_0} \\ e^{-j\mathbf{k}_d^T \mathbf{r}_1} \\ \vdots \\ e^{-j\mathbf{k}_d^T \mathbf{r}_{(M-1)}} \end{bmatrix} \tag{2.23}$$

where $\mathbf{k}_d$ represents the angular wavenumber vector of the desired signal. Once this factor is obtained, it is straightforward to define the characteristics of the array and to evaluate its performance by using metrics such as SNR or the directivity pattern of the array. The normalized directivity or gain pattern of a such beamformer as a function of the SoI's direction of arrival is depicted in Fig. 2.4, which is calculated via

$$y[n] = \mathbf{w}^{\mathrm{H}} \mathbf{a}(\vartheta) \, . \tag{2.24}$$

As it can be seen that the main beam, or the maximum power, is located at the angle of arrival of the SOI, and side-lobes are distributed over the other directions. The first side-lobe, adjacent to the main lobe, level is -6.2dB relative to the peak of the main lobe.

In contrast, SNR as a metric is related to the array average output power. This is expressed as

$$\mathcal{E}\{|y[n]|^2\} = \mathbf{w}^H \mathbf{R}_{xx} \mathbf{w} \, . \tag{2.25}$$

Hence, from (2.25) it can be noticed that, the output power depends on the array weights $\mathbf{w}$, as well as the data covariance matrix $\mathbf{R}_{xx}$ that is addressed in the following section.

### 2.2.2 Matrix Formulation of the Data Model

Most array processing approaches express the relationship between the array signals in $\mathbf{x}[n]$ by means of a spatio-temporal correlation matrix. In the narrowband case, the spatial correlation suffices to capture the phase differences that fully characterise signals impinging on the array from different angles of arrival.

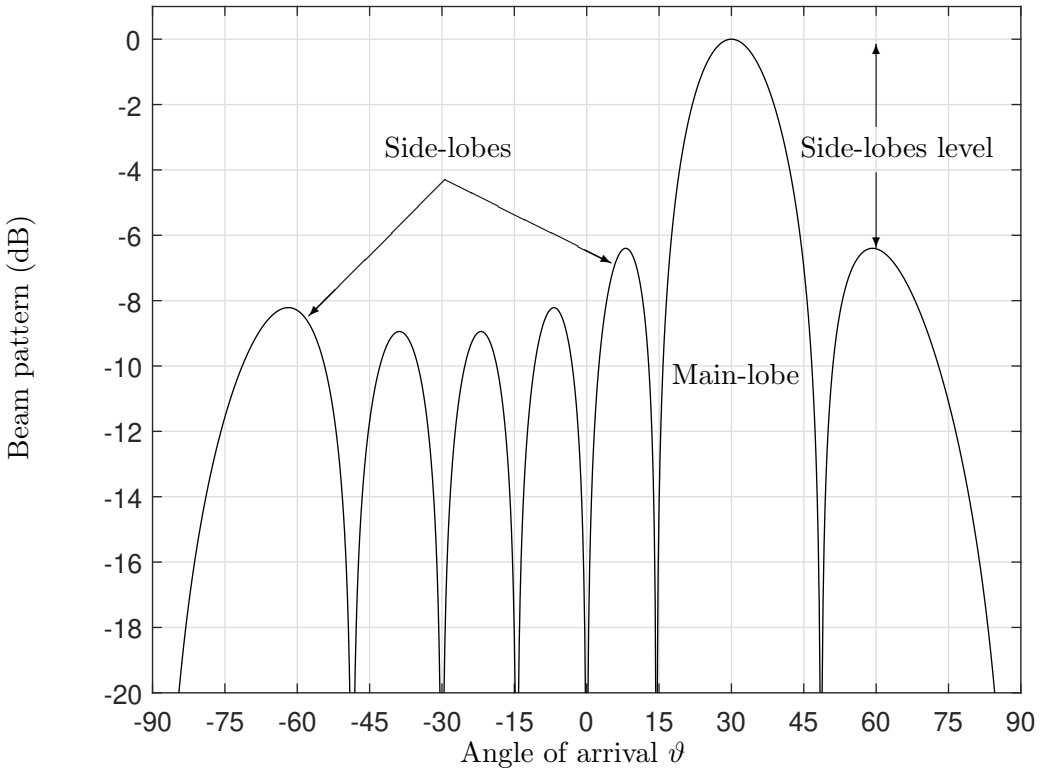


Figure 2.4: Beam pattern of a conventional beamformer with 8 array elements and an SoI from $\vartheta_s = 30°$.

The resulting spatial covariance matrix is

$$\mathbf{R}_{xx} = \mathcal{E}\{\mathbf{x}[n]\mathbf{x}^{\mathrm{H}}[n]\} \ . \tag{2.26}$$

In most cases, it can be assumed that the observation vectors $\mathbf{x}[n], n \in \mathbb{Z}$ are Gaussian random variables with zero mean, which makes the correlation and covariance matrices equivalent in such case. If this assumption is extended to the elements of the noise vector and we consider them as being spatially and temporally uncorrelated with variance $\sigma^2$, then

$$\mathcal{E}\{\mathbf{v}[n]\mathbf{v}^{\mathrm{H}}[n]\} = \sigma^2\mathbf{I} \, , \tag{2.27}$$

where $\mathbf{I}$ is an $M \times M$ identity matrix. By considering the data model in (2.17), the

matrix $\mathbf{R}_{xx}$ can be rewritten as

$$\mathbf{R}_{xx} = \mathbf{A}(\varphi, \vartheta)\mathbf{R}_{ss}\mathbf{A}^H(\varphi, \vartheta) + \sigma^2\mathbf{I} \,. \tag{2.28}$$

For $L$ independent sources, the $\mathbf{R}_{ss}$ is an $L \times L$ diagonal matrix containing the powers of the different contributing sources. By construction, the covariance matrix therefore is Hermitian and positive semi-definite. Hence $\mathbf{R}_{xx}$ possesses an eigenvalue decomposition with real non-negative eigenvalues,

$$\mathbf{R}_{xx} = \mathbf{U}\mathbf{\Lambda}\mathbf{U}^H \,. \tag{2.29}$$

The matrix $\mathbf{U}$ is unitary , and $\mathbf{\Lambda}$ is a diagonal matrix that contains the eigenvalues $\lambda_i, i = 1, \ldots, M$

$$\mathbf{\Lambda} = \mathrm{diag}\{\lambda_1, \lambda_2, \ldots, \lambda_M\} \,. \tag{2.30}$$

These eigenvalues are assumed to be spectrally majorised, which means that $\lambda_i \geq \lambda_{i+1} \geq 0$, $i = 1, \ldots, (M-1)$.

Recall that the average power in (2.25) does not only depend on the covariance matrix but also on the weight vector which needs to be adequately calculated to optimise the overall performance of the system. The computation of the weights is usually formulated as an optimisation problem. The basic formulation of such optimisation techniques is described in the following section.

## 2.3 Optimal Beamforming

Sec. 2.2 addressed fixed beamforming. One might notice that it yields significant improvement in terms of the gain of the received signal. In that way, the beamformer is fixed in the sense that the output signals from the elements are multiplied by a set of fixed weights, which do not rely on the received data characteristics. However, this method is not suitable in scenarios, for instance, when the AoA of an interferer may not be known precisely, sources might be (slowly) moving, or there might be calibration errors in the array. Which, in this case and in contrast to the conventional beamformer,

requires that the beamforming algorithms incorporate the statistics of the received data in the computation of the weights [49]. This permits these weights to change or adapt based on the received data in order to accomplish a certain goal, for example to adapt these weights to preserve the desired signal and improve rejection of interferers. To avoid the trivial solution $\mathbf{w} = \underline{0}$, we need to protect the look direction by a constraint. This leads to the concept of optimum beamforming which we will address in this section; more precisely, we consider the MVDR method and its GSC adaptive beamformer structure.

### 2.3.1 Minimum Variance Distortionless Response (MVDR)

The aim is to optimize the beamformer response, so that the output signal of the beamformer encompasses minimal contribution due to noise and signals impinging on the array from spatial angles other than the specific angle of the desired signal. This defines a constrained minimization problem, which permits a signal from the desired spatial angle to pass through the array with a specified gain [39, 50]. This can be written mathematically as

$$\min_{\mathbf{w}} \mathcal{E}\{|\mathbf{w}^{\mathrm{H}}\mathbf{x}|^2\} \tag{2.31}$$

$$\text{s.t.} \quad \mathbf{w}^{\mathrm{H}}\mathbf{a}(\vartheta, \Omega) = f, \tag{2.32}$$

where $\mathbf{a}(\vartheta, \Omega)$ is the steering vector.

This minimization of weights is usually solved by invoking the method of Lagrange multipliers, as detailed in Sec.4.3, setting the ultimate weight vector to be

$$\mathbf{w}_{opt} = \frac{\mathbf{R}^{-1}\mathbf{a}(\vartheta, \Omega)}{\mathbf{a}(\vartheta, \Omega)^{\mathrm{H}}\mathbf{R}^{-1}\mathbf{a}(\vartheta, \Omega)}, \tag{2.33}$$

which represents the LCMV optimal solution of the weight vector.

For a special case when the constraint response value $f$, is chosen to be unity, this leads to so called the minimum variance distortionless response (MVDR) solution. As the name suggests, the MVDR beamformer minimises the variance of the output signal while keeping the desired signal undistorted with a gain equal to unity in the

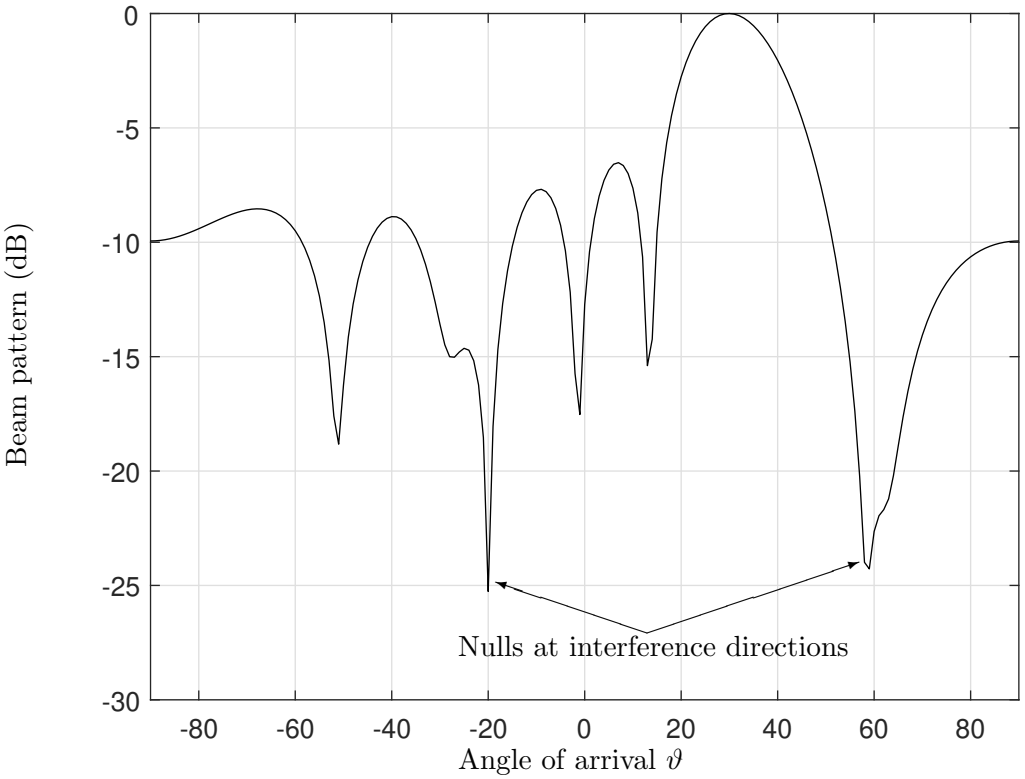


Figure 2.5: Beam pattern of optimal beamformer with 8 antenna array elements, $\vartheta_s = 30°$, and $\vartheta_{i=1,2} = [-20°, 60°]$

look direction. An example of a beam-pattern of an optimum narrowband beamformer with a ULA is depicted in Fig.2.5, where three sources in the far field imping on the array from angles 30° for the SoI, and $-20°$ and 60° for the interferers. Nevertheless, the computation of the weights based on this method is expensive due to the need of matrix inversion, that can be unacceptable for some applications. Consequently, another approach to solve this optimisation problem adaptively is suggested in [51] and summarised below.

### 2.3.2 Generalized Sidelobe Canceller

The GSC is another approach to implement the direct form of the constrained optimal filter in (2.33). The computation of the constraint weight vector involves the inverse of the covariance matrix , which renders the direct implementation of the LCMV to be computationally expensive.

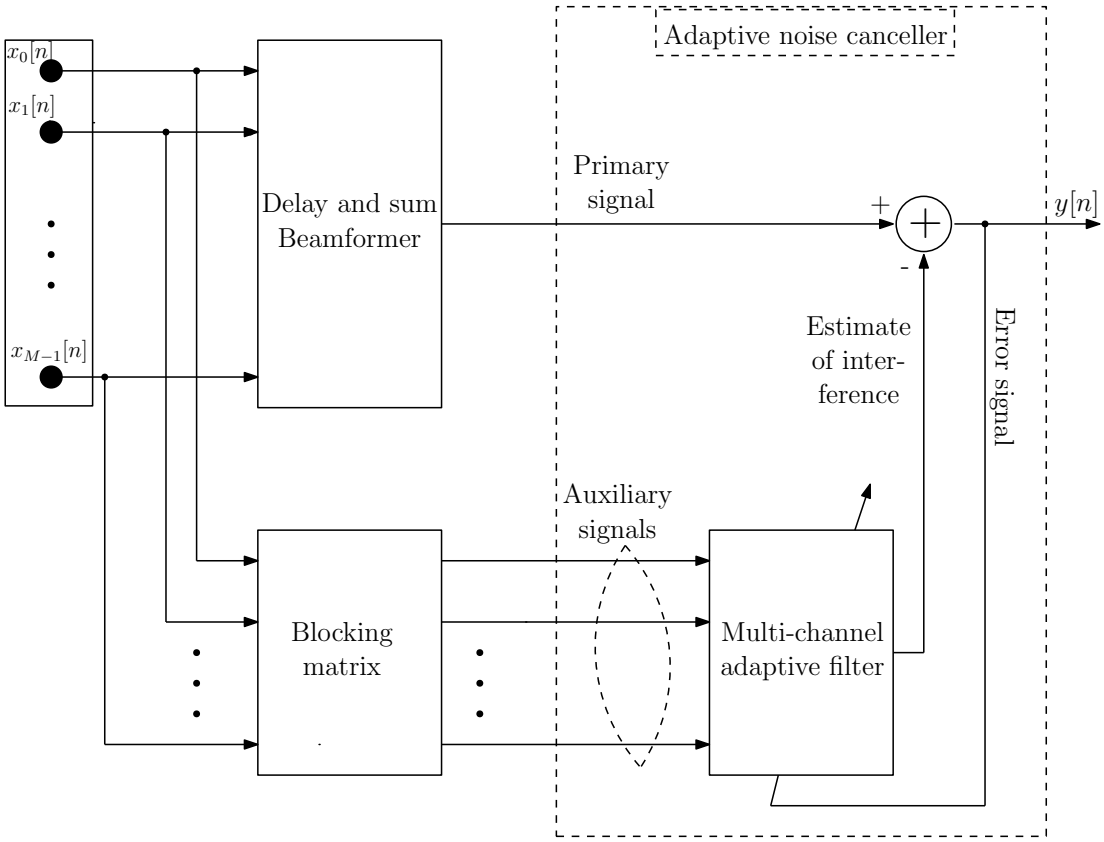


Figure 2.6: Descriptive blocks of MVDR beamformer in its generalised sidelobe canceller

An alternative approach, the GSC, can offer a less computationally costly implementation since it does not require the inverse of the covariance matrix $\mathbf{R}$. Moreover, it reduces the constrained optimisation problem to become an unconstrained minimization process. Fig. 2.6 shows the structure of the GSC as an adaptive beamformer. The derivation of the GSC begins by reformulation the problem in (2.32), which relies on the concept of projecting $\mathbf{w}$ onto the subspace spanned by $\mathbf{C}$, which generalises the constraint formulation in (2.32) to $\mathbf{C}^{\mathrm{H}}\mathbf{w} = \mathbf{f}$, to obtain a new vector $\mathbf{w}_q$, and in the null space of $\mathbf{C}$ to obtain a term $-\mathbf{B}\mathbf{w}_a$, which will be explained later. Consequently, the weight vector in (2.33) can be rewritten as [52]

$$\mathbf{w} = \mathbf{w}_q - \mathbf{B}\mathbf{w}_a \, . \tag{2.34}$$

The first part on the right hand side of (2.34), $\mathbf{w}_q$, is known as quiescent vector and works similarly to a conventional beamformer: it steers the mean beam towards the direction of the desired signal in order to enhance its gain relative to omnidirectional noise. The second part consists of a matrix $\mathbf{B}$, with dimension $M$ by $M - L$, that is called blocking matrix, and $\mathbf{w}_a$, an $M - L$ dimensional vector, is the adaptive filter vector weights. The blocking matrix and the adaptive weight vector are collectively responsible for minimising the total power at the output by reducing the contributions of noise and interference.

This can be mathematically expressed by substituting the decomposition of $\mathbf{w}$ back into the optimisation problem (2.32), which leads to

$$\min_{\mathbf{w}_a} \mathcal{E}\left\{|(\mathbf{w}_q - \mathbf{B}\mathbf{w}_a)^{\mathrm{H}}\mathbf{x}|^2\right\}. \tag{2.35}$$

this can be factorised to

$$\min_{\mathbf{w}_a} \mathcal{E}\left\{(\mathbf{w}_q - \mathbf{B}\mathbf{w}_a)^{\mathrm{H}}\mathbf{R}(\mathbf{w}_q - \mathbf{B}\mathbf{w}_a)\right\}. \tag{2.36}$$

The optimal solution of the adaptive filter weights thus becomes

$$\mathbf{w}_a = (\mathbf{B}^{\mathrm{H}}\mathbf{R}\mathbf{B})^{-1}\mathbf{B}^{\mathrm{H}}\mathbf{R}\mathbf{w}_q, \tag{2.37}$$

which minimises the mean square power in (2.25). For convenience, however, an approach to compute the values of the weights of the adaptive filter $\mathbf{w}_a$ is suggested in [51] in which they are obtained by invoking an adaptive algorithm such as the LMS algorithm, that is briefly described in the following section. The advantage of this solution, in fact, is to convert the constrained optimisation problem into an unconstrained one, for which many well-known solutions exist [52, 53].

### 2.3.3 LMS Algorithm

The least mean square (LMS) algorithm belongs to the family of stochastic gradient methods. Its simplicity, low cost, as well as robustness to stochastic of signals make it

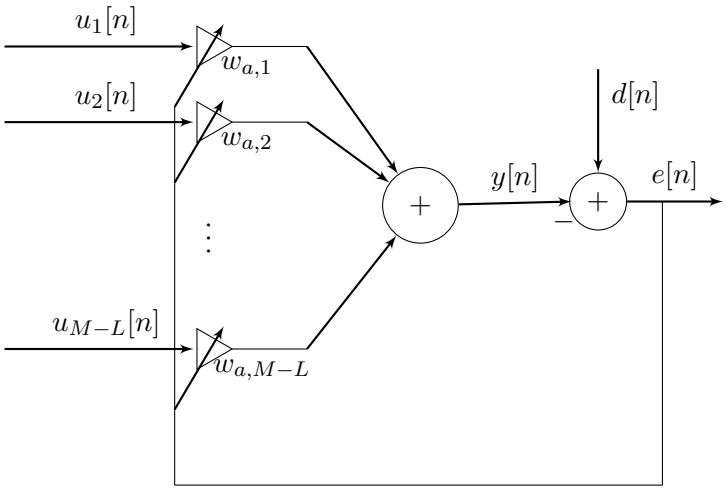


Figure 2.7: LMS adaptive filter

a popular adaptive algorithms for a wide range of applications.

For an $M-L$ tap adaptive filter the weight vector is defined as

$$\mathbf{w}_a[n] = \begin{bmatrix} w_{a,1}[n] & w_{a,2}[n] & \dots & w_{a,M-L}[n]] \end{bmatrix}^{\mathrm{H}} \tag{2.38}$$

as shown in Fig.2.7. If the signals from the blocking matrix, which referred to as auxiliary signals in Fig. 2.6, are arranged in a vector $\mathbf{u}[n]$, this results in

$$\mathbf{u}[n] = \mathbf{B}^{\mathrm{H}}\mathbf{x}[n], \tag{2.39}$$

where $\mathbf{u}[n] = \begin{bmatrix} u_1[n] & u_2[n] & \dots & u_{M-L}[n] \end{bmatrix}^T$. Then the output of the adaptive filter is given as

$$y[n] = \sum_{m=1}^{M-L} w_{a,m}[n]u_m[n] \, . \tag{2.40}$$

Assuming that $d[n]$ is the desired signal, or in the view of GSC beamformer is the quiescent beamformer output as explained in Sec.2.3.2, the aim to utilise the LMS is to minimise the error between $y[n]$ and $d[n]$ by using $\mathbf{w}_a$ as a mean for achieving

this aim. Then the error or the difference at time $n$ is

$$e[n] = d[n] - y[n] \ . \tag{2.41}$$

An adaptive process is used to adjust the filter tap weights so the error is minimised in some sense. The update equation of the weights is derived based on stochastic gradient approach, and its ultimate expression as follows

$$\mathbf{w}_a[n+1] = \mathbf{w}_a[n] + 2\mu e^*[n]\mathbf{u}[n] \tag{2.42}$$

and $\mu$ is a real scalar known as step size. It has a value which is bounded by

$$0 < \mu \leq \frac{2}{\lambda_{max}} \tag{2.43}$$

so that the convergence of $\mathbf{w}_a[n+1]$ is guaranteed as $n$ increases.

## 2.4 Broadband Beamformer

Broadband beamforming is a technique to extract or suppress the desired source or competing sources respectively. In contrast to the narrowband beamformer, these signals extend over a larger fractional bandwidth that can cover up to several octaves, and are known as broadband signals. In this section the generic time domain approach to broadband beamforming [19] and its amendment [30], which omits the pre-steering process in the former, will be discussed in sequence.

### 2.4.1 Generic Time Domain Broadband Beamformer Design

The time domain broadband beamformer is represented schematically in Fig. 2.8. From the figure it can be seen that each sensor in the array is followed by a tap delay line (TDL) or a finite impulse response filter (FIR) in order to perform space and time sampling on the impinging wave in (2.5).

With analogy to the narrowband beamformer, values of TDLs or FIR filter coefficients are considered as beamformer weights which respond to the range of frequencies

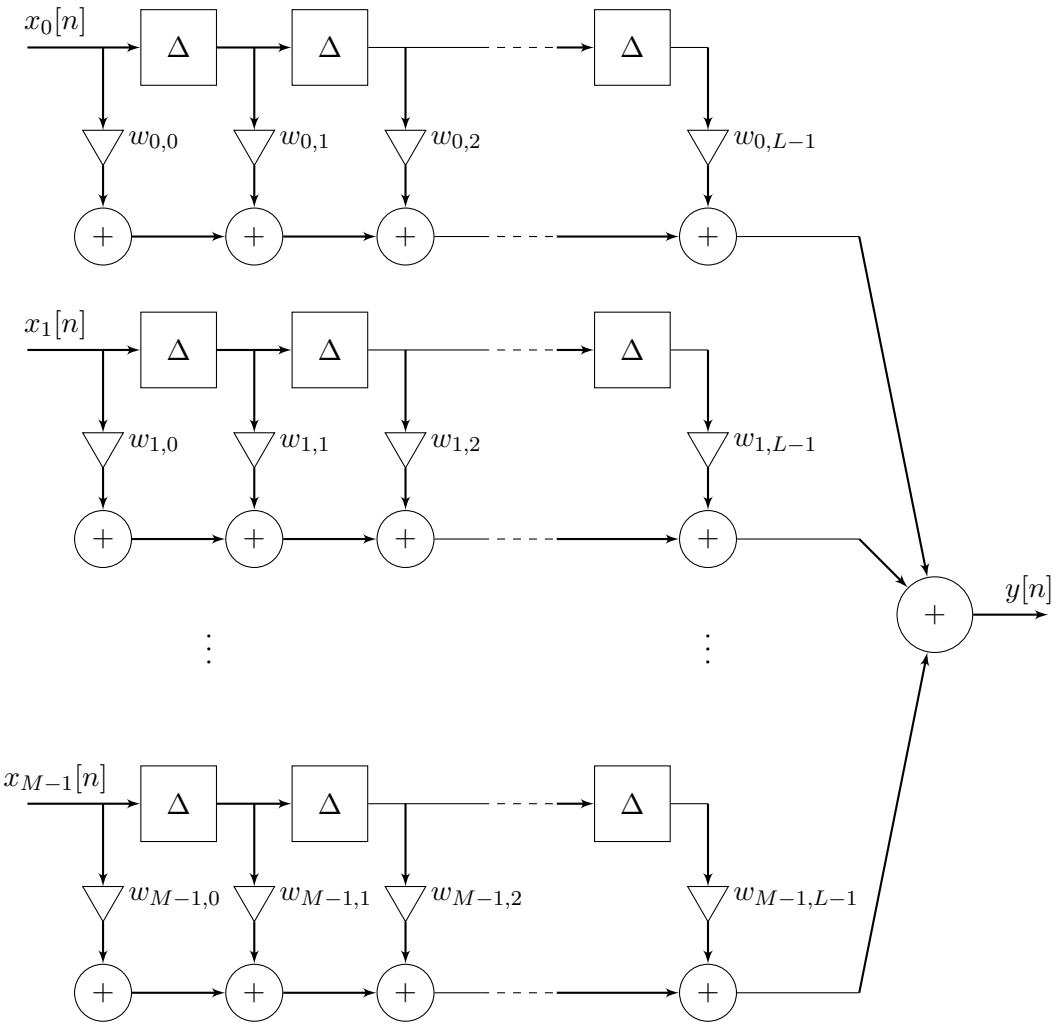


Figure 2.8: A wideband beamformer with $M$ sensors and $L-1$ delays after each sensor.

covered by the signal to compensate the phase difference for each frequency component. The pioneering work on this method [19] relies on the pre-steering concept, where the signal of each sensor is delayed such that the beamformer can treat its pre-steering inputs as if they had arrived from the broadside.

For a plane-wave signal arriving on a ULA from a direction $\vartheta$, for instance, the pre-steered signal of the $m$-th sensor in this direction becomes [25, 54]

$$x_m[n] = \hat{x}_m[n - T_m(\vartheta)], \tag{2.44}$$

where $\hat{x}_m[n]$ is a non pre-steered $m$th sensor signal, and $T_m(\vartheta)$ is the steering delay defined as

$$T_m(\vartheta) = T_0 + \tau_m(\vartheta), \tag{2.45}$$

and $T_0$ is the bulk delay [55], which by referring to (2.45) might take the values

$$T_0 \geq -\min_m(\tau_m(\vartheta)). \tag{2.46}$$

Consequently, from (2.44) the result of applying pre-steering to the receive signal can be noticed. It is obvious that after steering delays, the signal components related to the plane-wave arriving from direction $\vartheta$ are now aligned in time.

Hence , for $\mathbf{x}[n]$ and $\mathbf{w} \in \mathbb{C}^{MJ}$ that are the array signal and the beamformer weights, respectively, the beamformer output is

$$y[n] = \mathbf{w}^{\mathrm{H}}\mathbf{x}[n]. \tag{2.47}$$

Using (2.47) the mean square output of the beamformer is

$$\mathcal{E}\{|y[n]|^2\} = \mathbf{w}^{\mathrm{H}}\mathbf{R}\mathbf{w}\ , \tag{2.48}$$

where $\mathbf{R} \in \mathbb{C}^{MJ \times MJ}$ is the correlation matrix that is a non-negative definite. In order to protect the SoI, constraints are introduced to obtain $\mathbf{w}$ by minimisation of (2.47). The process of pre-steering the array's signals facilitates the design of the constraint

matrix of the broadband counterpart of the MVDR problem in (2.31) and (2.32). After pre-steering the signals, the constraint matrix can be given as

$$\mathbf{C} = [\mathbf{c}_1\ \mathbf{c}_2\ \ldots\ \mathbf{c}_L], \tag{2.49}$$

with $\mathbf{C} \in \mathbb{R}^{ML \times M}$, and

$$\mathbf{c}_l = [\underbrace{0, 0, \ldots, 0}_{M}, \quad \underbrace{0, 0, \ldots, 0}_{M}, \quad \ldots, \quad \underbrace{1, 1, \ldots, 1}_{l\text{th}, M}, \quad \underbrace{0, 0, \ldots, 0}_{M}]^T . \tag{2.50}$$

The existence of the steering delays, on one hand, makes the design of the constraints simple and straightforward, but on the other hand adds computational complexity. Since this approach incorporates a pre-steering delay for each sensor, this step might be achieved physically which requires extra hardware components in implementation. This in turn leads to more power consumption during processing. In [30, 56] a broadband beamformer without pre-steering procedures was proposed, which simplifies the physical structure as well as reduces the processing time cost. This can be very significant when an array consists of a large number of sensors. This method is discussed in the next section.

### 2.4.2 Time Domain Broadband Beamformer without Steering Delays

The proposed approach in[30, 56] relies on the knowledge of the steering vector in look direction. Hence, given the frequency response in look direction $\hat{A}(\varphi, \vartheta, \Omega)$. This steering vector is factorised into a set of frequency bins, such that its $k$-th frequency bin is expressed as

$$\hat{\mathbf{A}}(k) = \begin{cases} A(k), & k = 0, 1, \ldots, \frac{L-1}{2} \\ A^*(L-k), & k = \frac{L+1}{2}, \ldots, L-1\ , \end{cases} \tag{2.51}$$

then an $L \times L$ transformation matrix $\mathbf{C}_m$ is generated

$$\mathbf{C}_m = \begin{bmatrix} \tilde{A}_m(1) & \tilde{A}_m(2) & \dots & \tilde{A}_m(L) \\ \tilde{A}_m(L) & \tilde{A}_m(1) & \dots & \tilde{A}_m(L-1) \\ \vdots & \vdots & \ddots & \vdots \\ \tilde{A}_m(2) & \tilde{A}_m(3) & \dots & \tilde{A}_m(1) \end{bmatrix}, \tag{2.52}$$

where

$$\tilde{A}_m(u) = \sum_{k=0}^{L-1} A_m(k) e^{j2\pi mk} , \tag{2.53}$$

and $m = 0, 1, \dots, M-1$ and $u = 1, 2, \dots, L$.

The transformation matrix in (2.52) is applied to sensors' signals, such that the $m$-th sensor's signal becomes

$$\tilde{\mathbf{x}}_m[n] = \mathbf{C}_m^T \mathbf{x}_m[n], \tag{2.54}$$

where

$$\mathbf{x}_m = \begin{bmatrix} x_m[n] & x_m[n-T] & \dots & x_m[n-(M-1)T] \end{bmatrix}^T \tag{2.55}$$

Thus, the array signal vector is

$$\mathbf{x} = \begin{bmatrix} \tilde{\mathbf{x}}_0 \\ \tilde{\mathbf{x}}_1 \\ \vdots \\ \tilde{\mathbf{x}}_{M-1} \end{bmatrix} \tag{2.56}$$

and the covariance matrix is

$$\tilde{\mathbf{R}} = \mathcal{E}\{\mathbf{x}[n]\mathbf{x}^{\mathrm{H}}[n]\}, \tag{2.57}$$

the entries of this matrix contains information required to obtain the non pre-steering beamformer's weights by solving

$$\tilde{\mathbf{w}} = \tilde{\mathbf{R}}^{-1}\mathbf{C}(\mathbf{C}^T\tilde{\mathbf{R}}^{-1}\mathbf{C})^{-1}\mathbf{f} \tag{2.58}$$

with $\mathbf{C}$ as defined in (2.49), and

$$\mathbf{f} = [f_1, f_2, \ldots, f_L]^T \tag{2.59}$$

is a vector to constrain the frequency response of the beamformer in a specified direction.

This approach shows the possibility of obtaining beamformer without using any pre-steering stage. In this thesis, we will use a different approach to implement the time domain beamformer in its MVDR solution that does not require steering delays, and could be steered to an off-broadside. The proposed approach relies on using polynomial tools to construct the beamformer components. This leads us to Sec.2.5 where some of the terminologies, concepts and algorithms of polynomial in digital signal processing will be presented.

## 2.5 Polynomial Matrices and Algorithms in Digital Signal Processing

Polynomial matrices can be used to describe broadband systems with multiple inputs and outputs. Examples for successful deployment of polynomial matrix techniques in applications are optimum source coding [57], pre-coding and equalisation for MIMO communications [58, 59, 60, 61, 62, 63, 64, 65, 66, 67, 68, 69, 70], channel coding [71], blind source separation [72**?** ], identification of source-sensor transfer functions [73], speech enhancement [74], and angle of arrival estimation . In this context, this section is devoted to briefly review the polynomial matrix structure, properties and algorithms in so far as they are required later in this thesis.

### 2.5.1 Polynomial Matrices

Consider a matrix $\boldsymbol{A}(z)$ which is given as

$$\boldsymbol{A}(z) = \mathbf{A}_0 + z^{-1}\mathbf{A}_1 + z^{-2}\mathbf{A}_2 + \cdots + z^{-k}\mathbf{A}_k \tag{2.60}$$

with matrix-valued coefficients $\mathbf{A}_n \in \mathbb{C}^{M\times M}$, $n = 0, 1, 2$, and order or degree $k$ [**?** ]. An alternative approach to express (2.61) is via polynomial entries inside a matrix. The matrix $\boldsymbol{A}(z)$ then can be reformulated to become

$$\boldsymbol{A}(z) = \begin{bmatrix} a_{11}(z) & a_{12}(z) & \dots & a_{1M}(z) \\ a_{21}(z) & a_{22}(z) & \dots & a_{2M}(z) \\ \vdots & \vdots & \ddots & \vdots \\ a_{M1}(z) & a_{M2}(z) & \dots & a_{MM}(z) \end{bmatrix} . \tag{2.61}$$

If $\boldsymbol{A}(z)$ is assumed to be a polynomial matrix of degree $k$, then its $(i, j)$-th element can be given in the form

$$a_{ij}(z) = a_{ij}^{(0)} + a_{ij}^{(1)} z^{-1} + \cdots + a_{ij}^{(k)} z^{-k} . \tag{2.62}$$

In the following, we introduce a specific type of polynomial matrix which will aid in the formulation of broadband beamforming problems in subsequent chapters.

### 2.5.2 Space Time Covariance Matrix

Assume that an $M$-element sensor array measures the signal vector

$$\mathbf{x}[n] = \begin{bmatrix} x_1[n] & x_2[n] & \dots & x_M[n] \end{bmatrix}^T . \tag{2.63}$$

The covariance matrix of $\mathbf{x}[n]$ is calculated by taking the expectation, $\mathcal{E}\{\cdot\}$, of $\mathbf{x}[n]$ multiplied with its Hermitian

$$\boldsymbol{R} = \mathcal{E}\{\mathbf{x}[n]\mathbf{x}^{\mathrm{H}}[n]\} . \tag{2.64}$$

However, this matrix only accounts for instantaneous correlations but not for time lags between different array signals. In array signal processing, inclusion of the time lag is important since the relative delay between different array elements contains information about the angle of arrival (AoA) of the signal. The space time covariance matrix

therefore is formulated as [80, 81]

$$\mathbf{R}[\tau] = \mathcal{E}\{\mathbf{x}[n]\mathbf{x}^{\mathrm{H}}[n-\tau]\} \ . \tag{2.65}$$

This matrix captures both spatial and temporal correlation within and between signals. The diagonal of this matrix contains the autocorrelation sequences of the $M$ signals, while the off-diagonal terms are occupied by cross correlation sequences. If $\mathbf{R}[\tau]$ is expanded, then it can be expressed as

$$\mathbf{R}[\tau] = \begin{bmatrix} \mathcal{E}\{x_1[n]x_1^*[n-\tau]\} & \mathcal{E}\{x_1[n]x_2^*[n-\tau]\} & \dots & \mathcal{E}\{x_1[n]x_M^*[n-\tau]\} \\ \mathcal{E}\{x_2[n]x_1^*[n-\tau]\} & \mathcal{E}\{x_2[n]x_2^*[n-\tau]\} & \dots & \mathcal{E}\{x_2[n]x_M^*[n-\tau]\} \\ \vdots & \vdots & \ddots & \vdots \\ \mathcal{E}\{x_M[n]x_1^*[n-\tau]\} & \mathcal{E}\{x_M[n]x_2^*[n-\tau]\} & \dots & \mathcal{E}\{x_M[n]x_M^*[n-\tau]\} \end{bmatrix} , \tag{2.66}$$

or equivalently

$$\mathbf{R}[\tau] = \begin{bmatrix} r_{11}[\tau] & r_{12}[\tau] & \dots & r_{1M}[\tau] \\ r_{21}[\tau] & r_{22}[\tau] & \dots & r_{2M}[\tau] \\ \vdots & \vdots & \ddots & \vdots \\ r_{M1}[\tau] & r_{M2}[\tau] & \dots & r_{MM}[\tau] \end{bmatrix} \tag{2.67}$$

where $r_{ij}[\tau] = \mathcal{E}\Big\{x_i[n]x_j^*[n-\tau]\Big\}$ is the cross-correlation sequence between the signals of the $i$-th and the $j$-th sensors, and the auto-correlation sequence when $i = j$, and $i, j \in \mathbb{Z}$. Its $z$-transform, $\boldsymbol{R}(z) \bullet\!\!-\!\!\circ \mathbf{R}[\tau]$ is the cross spectral density (CSD) matrix. This Laurent polynomial matrix inherits the symmetry of the space-time covariance matrix, where $\mathbf{R}[\tau] = \mathbf{R}^{\mathrm{H}}[-\tau]$, such that $\boldsymbol{R}(z) = \boldsymbol{R}^{\mathrm{P}}(z) = \boldsymbol{R}^{\mathrm{H}}(1/z^*)$. A polynomial matrix fulfilling the later equality is termed a para-Hermitian matrix.

### 2.5.3 Para-Hermitian and Para-Unitary Operators

The para-Hermitian operator transposes, complex conjugates (transjugates) and time reverses the polynomial matrices, such that

$$\boldsymbol{A}^{\mathrm{P}}(z) = \boldsymbol{A}^{\mathrm{H}}(1/z^*) \ . \tag{2.68}$$

A polynomial matrix is para-Hermitian, if its transpose complex conjugate and time reverse version is identical to the matrix itself, i.e.

$$\boldsymbol{A}(z) = \boldsymbol{A}^{\mathrm{P}}(z) \; . \tag{2.69}$$

If a matrix satisfies

$$\boldsymbol{A}(z)\boldsymbol{A}^{\mathrm{P}}(z) = \boldsymbol{A}^{\mathrm{P}}(z)\boldsymbol{A}(z) = \mathbf{I} \tag{2.70}$$

then $\boldsymbol{A}(z)$ is called a para-Unitary matrix, in analogy to the unitary property for constant matrices. As a result $\boldsymbol{A}(z)$ is straightforwardly inverted, and is also termed a lossless filter bank [80] in analogy to the norm-preserving property of a unitary matrix.

### 2.5.4 Polynomial Eigenvalue Decomposition

A para-Hermitian polynomial matrix can be diagonalised by a polynomial eigenvalue decomposition [81, 82, 83], which can be considered as a generalisation or an extension of the conventional EVD, since it relies on similar procedures. When the conventional EVD is used to transform a Hermitian matrix, $\mathbf{A}$, it computes a unitary matrix, $\mathbf{U}$, that can be used to find a diagonal matrix related to $\mathbf{A}$, such that $\mathbf{\Lambda} = \mathbf{U}^H\mathbf{A}\mathbf{U}$ where the eigenvalues of $\mathbf{A}$ appear on the main diagonal of the matrix $\mathbf{\Lambda}$.

By analogy with the EVD, the PEVD takes a polynomial para-Hermitian matrix and factorises it into a diagonal matrix and a para-Unitary matrix, such that

$$\boldsymbol{A}(z) \approx \boldsymbol{Q}^{\mathrm{P}}(z)\boldsymbol{\Lambda}(z)\boldsymbol{Q}(z) \; . \tag{2.71}$$

The matrix $\mathbf{\Lambda}(z)$ is a diagonal para-Hermitian matrix and its diagonal entries contain auto-correlation sequences. In the frequency domain the diagonal entries of this matrix will represent power spectral density that are ordered, or spectrally majorised [80], over the entire frequency band covered by the signal. Thus for

$$\mathbf{\Lambda}(z) \cong \mathrm{diag}\{\lambda_{11}(z),\ \lambda_{22}(z),\ \ldots\ , \lambda_{MM}(z)\}\ , \tag{2.72}$$

the majorisation property means that on the unit circle, $\lambda_{11}(e^{j\Omega}) \geq \lambda_{22}(e^{j\Omega}) \geq \cdots \geq$

$\lambda_{MM}(e^{j\Omega})$ [84].

The matrix $\boldsymbol{Q}(z)$ is a para-Unitary matrix satisfying (2.70) . In the context of the PEVD, $\boldsymbol{Q}(z)$ transforms a para-Hermitian matrix into diagonal form, such that for the CSD matrix $\boldsymbol{R}(z)$

$$\boldsymbol{\Lambda}(z) \approx \boldsymbol{Q}^{\mathrm{P}}(z)\boldsymbol{R}(z)\boldsymbol{Q}(z) \; . \tag{2.73}$$

It is possible to achieve equality for the PEVD in (2.73), which however requires Laurent series of potentially infinite order [82, 83, 85]. For the purpose of the work in this thesis, we will typically content ourselves with a polynomial approximation of sufficient accuracy.

### PEVD Mechanism and Algorithms

We approach the PEVD via an iterative algorithm. We start with $\boldsymbol{R}(z)$, and in every rotation, aim to reduce off-diagonal energy by (i) a delay and (ii) a rotation step. The general procedure is described below, while the details differ for two families of algorithms – the second order sequential best rotation (SBR2) [57, 81, 86, 87, 88] and sequential matrix diagonalisation (SMD) families [89, 90, 91, 92, 93, 94, 95]. For an $i$th iteration, the algorithm starts by a search step. The output of this step are a column $k^{(i)}$ and a lag index $\tau^{(i)}$. These two parameters are used to generate a diagonal matrix which is termed as a shift matrix $\mathbf{D}^{(i)}(z)$. For $\mathbf{D}^{(i)}(z) \in \mathbb{R}^{M\times M}$ this is expressed as

$$\boldsymbol{D}^{(i)}(z) = \mathrm{diag}\left\{ \underbrace{1 \; \ldots \; 1}_{k^{(i)}-1}, \; z^{-(i)} \; \underbrace{1, 1, \ldots, 1}_{M-k^{(i)}} \right\} \; . \tag{2.74}$$

Applying $\boldsymbol{D}^{(i)}(z)$ to a partially diagonalised para-Hermitian matrix, lets say $\boldsymbol{S}^{(i-1)}(z)$ obtained from the $(i-1)$th iteration, leads to a shift of its $k$th row produces $\boldsymbol{S}^{(i)\prime}$. Where

$$\boldsymbol{S}^{(i)\prime}(z) = \boldsymbol{D}^{(i)}(z)\boldsymbol{S}^{(i-1)}(z)\boldsymbol{D}^{(i)\mathrm{P}}(z), \;\; i = 1 \; \ldots \; I \; , \tag{2.75}$$

and $I$ is a pre-determined upper limit of the number of iterations.

The $i$th iteration of PEVD ends by transferring the zero lag's off-diagonal energy

onto the diagonal by using

$$\boldsymbol{S}^{(i)}(z) = \mathbf{Q}^{(i)}\boldsymbol{S}^{(i)\prime}(z)\mathbf{Q}^{(i)\mathrm{H}}, \tag{2.76}$$

where $\mathbf{Q}^{(i)}$ is a unitary matrix that rotates the off-diagonal energy onto the diagonal and applied on the entire lags of $\boldsymbol{S}^{(i)\prime}(z)$, although it is generated from its zero lag.

The PEVD algorithms stop once the forgoing pre-determined upper limit of iterations $I$ is reached, or the low threshold of the off-diagonal energy is exceeded. The way of calculating the latter stopping criterion differs based on the algorithm as will be discussed specifically for the SBR2 and SMD families below.

#### 2.5.4.1 Sequential Best Rotation Algorithm-2 (SBR2)

The diagonal matrix of the decomposition, in this algorithm, is built by keeping the $k^{(i)}$th column elements of $\mathbf{S}^{(i)}[\tau]$ in $\hat{\mathbf{s}}^{(i)}[\tau] \in \mathbb{C}^{M-1}$ but excluding the diagonal element in this column [96, 97, 98]. At the same time the row index, $m^{(i)}$, of the maximum element in the column is extracted. Consequently, the search of the off-diagonal element can be expressed as

$$\{m^{(i)}, k^{(i)}, \tau^{(i)}\} = \arg\max_{m,k,\tau} \parallel \hat{\mathbf{s}}_k^{(i)}[\tau] \parallel_\infty \tag{2.77}$$

In order for the diagonalisation in (2.77) to be completed, the unitary rotation matrix in (2.76)is obtained from a scalar Jacobi rotation matrix

$$\mathbf{Q}^{(i)} = \begin{bmatrix} \mathbf{I}_1 & & & \\ & cos\varphi^{(i)} & \dots & e^{j\vartheta^{(i)}}sin\varphi^{(i)} \\ & \vdots & \mathbf{I}_2 & \vdots \\ & -e^{-j\vartheta^{(i)}}sin\varphi^{(i)} & \dots & cos\varphi^{(i)} \\ & & & & \mathbf{I}_3 \end{bmatrix} \tag{2.78}$$

where $\{\vartheta, \varphi\}$ represent the rotation angles, and $\mathbf{I}_1, \mathbf{I}_2$ and $\mathbf{I}_3$ are identity matrices with dimensions that are related to the maximum element in the $k^{(i)}$th column as $(\min\{m^{(i)}, k^{(i)} - 1\})$, $(|m^{(i)} - k^{(i)}| - 1)$ and $(M - \max\{m^{(i)}, k^{(i)}\} + 1)$ respectively.

The stopping criteria of the SBR2 algorithm are either a set maximum number of iterations, or the energy of the maximum off-diagonal element that can be set to a specific threshold value, for example $\eta$

$$\max_{k,\tau} \parallel \hat{\mathbf{s}}_k^{(I)}[\tau] \parallel_\infty < \eta \ . \tag{2.79}$$

#### 2.5.4.2 Sequential Matrix Diagonalisation (SMD)

The diagonalisation procedures in the SMD algorithm begins with initial diagonal matrix given by

$$\mathbf{S}^{(0)}[0] = \mathbf{Q}^{(0)}\mathbf{R}[0]\mathbf{Q}^{(0)\mathrm{H}} \ , \tag{2.80}$$

where $\mathbf{R}[0]$ is the zero lag matrix of $\mathbf{R}[\tau]$, and $\mathbf{Q}^{(0)}$ is the modal matrix obtained from the scalar EVD of $\mathbf{R}[0]$. For every iteration new rows and columns are shifted to $\mathbf{S}^{(i)}[0]$, followed by transferring their energy onto the diagonal by the means of the scalar EVD [89, 98]. Hence, the diagonalisation is applied on more than an element for each iteration. The search step is modified to be adequate for this purpose and the parameter selection in the $i$th iteration becomes

$$k(i), \tau(i) = \arg\max_{k,\tau} \parallel \hat{\mathbf{s}}_k^{(i-1)}[\tau] \parallel_2 \tag{2.81}$$

The stopping criterion of the SMD is similar to that for the SBR2; it depends on the iteration limit or the off-diagonal energy threshold.

#### 2.5.4.3 Computational Complexity

For both SBR2 and SMD, efficient implementation schemes have been explored for PEVD algorithms. This includes numerical tricks such as search space reduction, symmetry considerations, divide-and-conquer schemes, as well as fast Givens rotations and approximate EVDs [99, 100, 101, 102, 103, 104, 105, 106], but also approximations such as truncation [107, 108, 109], which aid with the grow of polynomial terms as SBR2 and SMD iterations progress. The impact of numerically efficient schemes is typically well controlled, and can dependent on both the environment [110] and the selected

algorithm, see e.g. [111] in the context of angle of arrival estimation.

Nonetheless, a precise computational cost of SBR2 or SMD is difficult to state. Since SBR2 and SMD operate iteratively, and the polynomial order growth at each step is not known a priori, the overall cost will depend on the parahermitian matrix that is to be factorised, despite the above tools to improve the computational efficiency of SBR2 and SMD.

For many applications, such as the beamformers discussed in this thesis, a PEVD via SBR2 or SMD only needs to be calculated once — this can therefore often be performed off-line, such that the actual complexity of algorithms such as SBR2 or SMD is less critical. Of importance, however, is the polynomial order of the PEVD factors that these methods yield, in particular the matrix of polynomial eigenvectors, which may continuous process the data to e.g. perform a subspace projection [77, 78] or dimensionality reduction [112]. Thus, for example for a matrix $\boldsymbol{Q}(z) : \mathbb{C} \rightarrow \mathbb{C}^{M\times M}$ of order $L$, we require $M^2(L+1)$ multiplications and additions per sampling period — hence the extracted order is crucial for the computational complexity of an implementation. Therefore, truncation methods [107, 108, 109, 113] or decompositions that pursue low order polynomial factors [114, 115, 116] can be important to keep the computational complexity of an implementation such as beamforming low.

## 2.6 Summary

This chapter has reviewed some principles of broadband beamforming, starting from extensions of narrowband beamformers to tap delay line structures capable of implementing physical delays. These delays are required to resolve the propagation delay with which the AoA of broadband signals must be characterised, as simple phase shifts as in the narrowband case are no longer sufficient.

This has also led to the introduction of polynomial matrices as descriptions for broadband multichannel signals and for capturing the second order statistical information of sensor signals via the space-time covariance matrix. In the following Chapters 3–5, we will particularly use the tools provided by polynomial matrix algebra to for-

mulate and solve broadband beamforming problems.

# Chapter 3

# Polynomial MVDR Beamforming for Uniform Linear Arrays

## 3.1 Introduction

The aim of this chapter is to demonstrate an alternative and simplified design for adaptive broadband beamformers. The approach adopts the concept of conventional time domain broadband beamforming and adaptive filters algorithms described in Sec. 2.4. However, this has been addressed in a different perspective based on polynomial matrix techniques, which simplifies the problem formulation and broadband solution, and surprisingly can also reduce the computational complexity compared to a standard time domain broadband beamformer.

More precisely, the developed algorithm is presented in the context of formulating a solution to the MVDR problem using a GSC structure. The main reason for choosing this structure is its widespread use in practical applications such as wireless communications [117], and audio acquisition systems [118] to name a few.

As it has been described in Chap. 2, if broadband signals need to be resolved by an array of sensors, the sensors usually have to be followed by tap delay lines in order to capture the relative lag rather than just a phase shift between signals. This has led to the extension of many narrowband beamforming techniques to the broadband case, such as MVDR beamforming and one of its realisations, the GSC [39].

In general, the covariance and transfer functions of broadband array signals as well as MIMO systems can be denoted as polynomial matrices [80]. For processing such quantities, narrowband techniques such as the EVD and SVD have been extended to the polynomial domains, with applications in denoising-type [119] or decorrelating preprocessors [35], in transmit and receive beamforming across broadband MIMO channels [120, 121], broadband angle of arrival estimation [122], or in optimum sub-band partitioning of beamformers [123].

In this chapter, polynomial matrix techniques are extended to the MVDR problem. We show that this can provide an elegant framework for designing a beamformer that steers its beam towards an angle of arrival other than the look direction of the array, without the need to pre-steer the array signals. In constrast, most existing beamformer designs assume presteering and look towards broadside [124, 125, 126], where the constraint can be inexpensively implemented [25]. Consequently, this work complements the sparse literature on designs with an arbitary look direction [56], for which a significant reduction in computational complexity can be achieved.

The chapter begins in Sec. 3.2 with the formulation of polynomial MVDR beamforming, where the components of its GSC structure are designed. Most of the GSC components are easily transferable to the polynomial domain; however, the blocking matrix of the GSC requires the completion of a paraunitary matrix, which is separately addressed in Sec. 3.3. In Sec. 3.5, the performance of the beamformer is evaluated by examining its beam pattern, residual error and the computational complexity. Sec. 3.6 provides a numerical example to compare the proposed beamformer with its standard tap delay line-based time domain counterpart and discussion of the result. Finally, conclusions are presented in Sec. 3.7.

## 3.2 Proposed Approach

### 3.2.1 Polynomial MVDR and GSC

An appropriate choice of weights in the event when beamformers are designed to deal with broadband signals is considered as a cumbersome process. A single weight pro-

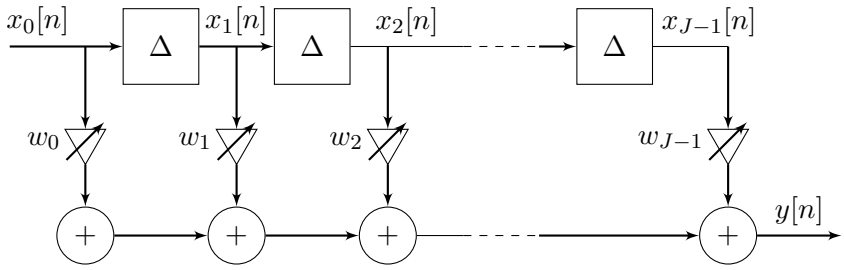


Figure 3.1: Tapped delay line processor for a single channel.

cessor behind each array element, as in narrowband case, works for a single frequency $\Omega_i$ but will not be appropriate when opterating at another frequency $\Omega_j \neq \Omega_i$. This is because of the dependency of the steering vector on the frequency and implicitly on the wavelength $\lambda$, which makes the array pattern susceptible to deviation as the value of $\lambda$ changes. Therefore for every possible operating frequency, a different set of weights is required to maintain the desired characteristic of the beamformer's beampattern, and prevent the deterioration of its performance.

To generalise a narrowband beamformer requires the substitution of single weights by tapped delay lines or a transversal filters as shown in Fig. 3.1. The overall system therefore implements a multichannel processor, where the total output of the channel is the sum of scaled and delayed versions of the input signal, as shown in Fig. 3.2.

Using vector notation with

$$\mathbf{x}[n] = \begin{bmatrix} x_1[n] \\ \vdots \\ x_M[n] \end{bmatrix} \quad , \qquad \mathbf{w}[n] = \begin{bmatrix} w_1^*[-n] \\ \vdots \\ w_M^*[-n] \end{bmatrix} \quad , \tag{3.1}$$

the output is compactly written as

$$e[n] = \mathbf{w}^{\mathrm{H}}[-n] * \mathbf{x}[n] = \sum_{\nu} \mathbf{w}^{\mathrm{H}}[-\nu]\mathbf{x}[n-\nu] = \sum_{\nu} \sum_{m=1}^{M} w_m[\nu] x_m[n-\nu] \; . \tag{3.2}$$

The complex conjugation in the definition of the weights in (3.1) is undone by the Hermitian transpose in (3.2), which is used for convenience [4]; the time reversal in the

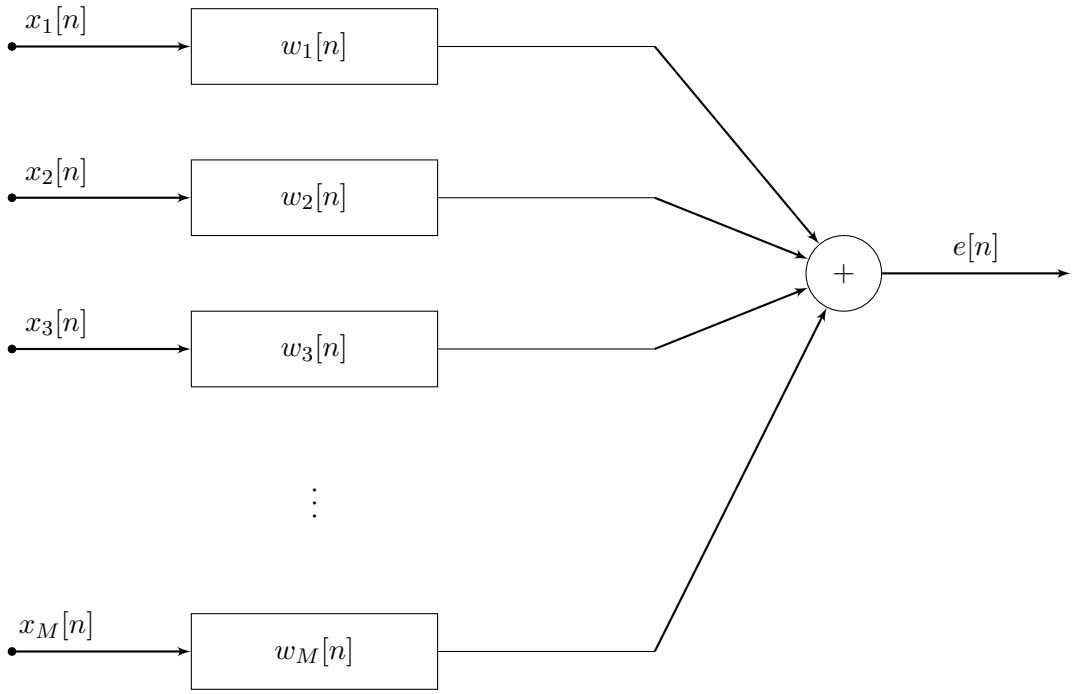


Figure 3.2: Beamformer for Broadband signal processing

definition of $\mathbf{w}[n]$ is to accommodate the extension to the polynomial domain. In the $z$-domain, if it was permissible to define $\boldsymbol{x}(z) \bullet\!\!-\!\!\circ\, \mathbf{x}[n]$ and $E(z) \bullet\!\!-\!\!\circ\, e[n]$, then with $\boldsymbol{w}(z) \bullet\!\!-\!\!\circ\, \mathbf{w}[n]$, we can write for the output $E(z) = \boldsymbol{w}^{\mathrm{P}}(z)\boldsymbol{x}(z)$, whereby the para-hermitian operation performs the complex conjugation and restores the chronological order of the coefficients.

With these definitions, we have for the output auto-correlation sequence

$$\begin{aligned}
\mathcal{E}\{e[n]e^*[n-\tau]\} &= \mathcal{E}\left\{\left(\sum_{\nu} \mathbf{w}^{\mathrm{H}}[-\nu]\mathbf{x}[n-\nu]\right)\left(\sum_{\mu} \mathbf{x}^{\mathrm{H}}[n-\tau-\mu]\mathbf{w}[-\mu]\right)\right\} \\
&= \sum_{\nu} \mathbf{w}^{\mathrm{H}}[-\nu] \sum_{\mu} \mathcal{E}\left\{\mathbf{x}[n-\nu]\mathbf{x}^{\mathrm{H}}[n-\tau-\mu]\right\} \mathbf{w}[-\mu] \\
&= \sum_{\nu} \mathbf{w}^{\mathrm{H}}[-\nu] \sum_{\mu} \mathbf{R}[\tau+\mu-\nu]\mathbf{w}[-\mu] \\
&= \sum_{\nu} \mathbf{w}^{\mathrm{H}}[-\nu] \left(\mathbf{R}[\tau-\nu] * \mathbf{w}[\tau-\nu]\right) \\
&= \mathbf{w}^{\mathrm{H}}[-\tau] * \mathbf{R}[\tau] * \mathbf{w}[\tau] \,. \qquad (3.3)
\end{aligned}$$

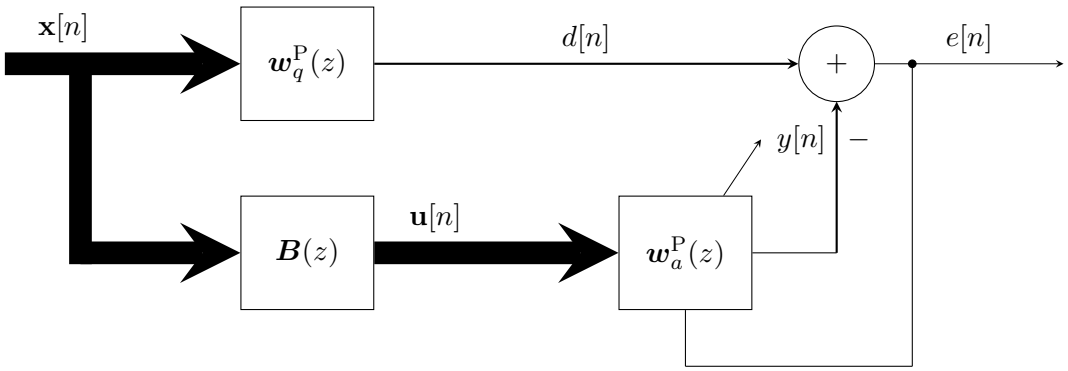


Figure 3.3: Generalised sidelobe canceller with polynomial quiescent vector and polynomial blocking matrix; the system $\boldsymbol{w}_{\mathrm{a}}(z)$ represents a multichannel adaptive filter.

In the $z$-domain, the power spectral density $R_e(z) \bullet\!\!-\!\!\circ\, \mathcal{E}\{e[n]e^*[n-\tau]\}$ is therefore given by

$$R_e(z) = \boldsymbol{w}^{\mathrm{P}}(z)\boldsymbol{R}(z)\boldsymbol{w}(z)\ , \tag{3.4}$$

based on $\boldsymbol{R}(z)$ being the CSD matrix of the array signals.

Based on the output PSD in (3.4), the output power is obtained by integrating over the unit circle. This leads to the MVDR problem formulation

$$\min_{\boldsymbol{w}(z)} \oint_{|z|=1} R_e(z)\frac{dz}{z} \tag{3.5}$$

$$\text{s.t.} \quad \boldsymbol{a}^{\mathrm{P}}(\vartheta_{\mathrm{s}}, z)\boldsymbol{w}(z) = F^{\mathrm{P}}(z)\ . \tag{3.6}$$

The broadband steering vector $\boldsymbol{a}(\vartheta_{\mathrm{s}}, z)$ defines the look direction of the array with a desired transfer function $F(z)$. For simplicity $F(z) = 1$ is assumed. The constraint in (3.6) depends on spatial and temporal properties of the desired broadband signal and is an extension of (2.32) for the narrowband LCMV.

To solve (3.5) and (3.6), we propose the polynomial GSC shown in Fig. 3.3. Analogously to Sec. 2.3.2, the design of the illustrated components relies on decomposing the weight vector $\boldsymbol{w}(z)$ into segments in two mutually orthogonal subspaces: the constraint (or range) subspace and the null (or noise) subspace. Thus the quiescent beamformer

$\boldsymbol{w}_{\mathrm{q}}(z)$ is derived from the constraint (3.6) as a vector lying in the constraint space, which in turn defines a blocking matrix $\boldsymbol{B}(z)$ with columns spanning the null space, thus making them orthogonal to the quiescent beamformer. A multichannel filter with coefficients in $\boldsymbol{w}_{\mathrm{a}}(z)$ is adaptively calculated by using an adaptive algorithm which in this work is chosen to be the normalized LMS.

The quiescent beamformer $\mathbf{w}_{\mathrm{q}}(z)$ is derived from the constraint (3.6), which in turn defines a blocking matrix $\boldsymbol{B}(z)$ and a multichannel adaptive filter with coefficients in $\boldsymbol{w}_{\mathrm{a}}(z)$. The designs of these components based on polynomial techniques will be elaborated in turn below. These are, in general, an extension of their narrowband counterparts, but with elements of vectors and matrices represented as polynomials.

### 3.2.2 Broadband Steering Vector and Quiescent Beamformer

The performance of a polynomial MVDR beamformer depends on the accuracy of the steering vector implementation. Hence this section is devoted to fractional delay filters as the core tool to obtain broadband steering vectors. Thereafter, the relationship between the steering vector and the quiescent weight vector will be discussed.

#### 3.2.2.1 Broadband Steering Vector

A broadband steering vector $\boldsymbol{a}(\vartheta, z)$ contains explicit delays rather than phase shifts as in the narrowband case, such that $\mathbf{a}_{\vartheta}[n] \circ\!\!-\!\!\bullet\, \boldsymbol{a}(\vartheta, z)$

$$\mathbf{a}_{\vartheta}[n] = \frac{1}{\sqrt{M}} \begin{bmatrix} d[n] \\ d[n - \tau_2(\vartheta)] \\ \vdots \\ d[n - \tau_M(\vartheta)] \end{bmatrix}, \tag{3.7}$$

where $d[n - \tau]$ is an ideal fractional delay by $\tau \in \mathbb{R}$ samples. The first array element is assumed to be the reference element at the origin of the coordinate system, such that $\tau_1 = 0$.

A waveform from direction $\vartheta$ experiences a lag $\tau_m(\vartheta)$ relative to element $m = 1$ when it arrives at the $m$-th sensor. Evaluating (3.7) at frequency $\Omega$ turns the delays

$d[n-\tau_m(\vartheta)]$ into phase shifts and $\mathbf{a}_\vartheta[n]$ into a narrowband steering vector as discussed in Sec. 2.2. With (3.7), $\boldsymbol{a}^{\mathrm{P}}(\vartheta,z)\boldsymbol{a}(\vartheta,z)=1$ is easily verified.

To implement a broadband steering vector according to (3.7) requires fractional delay filters. The impulse response of the $m$-th fractional delay is obtained by sampling shifted versions of the sinc function. This might not be by integer multiples of the sampling period [127]. With the definition for the sinc function[46]

$$\mathrm{sinc}(t)=\frac{\sin(\pi t)}{\pi t}\ , \tag{3.8}$$

sampling with period $T_\mathrm{s}=1$ and starting at the origin, this yields an impulse, $d[n]=\frac{\sin\pi n}{\pi n}=\delta[n]$ due to the sinc function's regular zero crossings. Sampling with a time offset $\tau\in\mathbb{R}$ however leads to

$$d[n-\tau]=\frac{\sin\pi(n-\tau)}{\pi(n-\tau)} \tag{3.9}$$

which decays with $1/n$ , and therefore is (i) not absolutely summable and (ii) of infinite support and hence not implementable.

Since the sinc function extends over an infinite time period, this leads to impracticality of this approach unless this function limited in its support. This is done by truncation which in turn can lead to ripples in the fractional delay filters' passband due to Gibbs phenomena, and causes imperfections of the fractional delay response behavior in terms of its magnitude and phase [31, 128]. The truncated response therefore approximates but no longer precisely matches the ideal fractional delay defined in (3.7).

A tapered windowing technique can be used to reduce the effects of truncation. The accuracy to which the steering vector matches the ideal delay can be assessed in the frequency domain. There an error function can be formulated between the frequency response of the ideal fractional delay filter and the approximated ones in the steering vector. A relatively moderate order for a fractional delay filter (FDF) can yield high accuracy close up to half of the sampling rate can be achieved by using, for example, windowed sinc functions [127, 129], as will be exemplified later. This technique is

therefore employed in this thesis to implement broadband steering vectors. We here use the proposition in [127] and apply a raised cosine or Hann window of length $2L$ to the sinc, such that

$$d[n-\tau] = \begin{cases} g[n] & -L+\tau < n < L+\tau, \\ 0 & \text{otherwise} \end{cases} \tag{3.10}$$

for (3.7) with

$$g[n] = \frac{\sin \pi(n-\tau)}{\pi(n-\tau)} \left(1 + \cos \frac{\pi}{L}(n-\tau)\right) . \tag{3.11}$$

Examples of broadband steering vectors are depicted in Fig. 3.4 and 3.5, showing the impulse responses of $\boldsymbol{a}(\vartheta, z)$ with $\vartheta = 0°$ and $\vartheta = 30°$ for a linear, critically sampled array with $M = 8$ equispaced elements. Each filter $q_m[n]$ represents a polynomial of order $T = 50$. For instance, in Fig. 3.4 where the vector demonstrates a steering vector for a signal arriving from broadside, it can be seen that the filters have identical impulse responses, where at the output of every individual filter the signal is delayed equally with a value of the number of samples related to a half of the filter order. This, alternatively, can be examined by the group delay of the filters. The group delay of $Q_m(e^{j\Omega}) \bullet\!\!-\!\!\circ\, q_m[n]$ is defined as

$$g_m(e^{j\Omega}) = -\frac{d}{d\Omega} Q_m(e^{j\Omega}) . \tag{3.12}$$

The group delays for the broadband steering vector examples above are shown in Fig. 3.6 and 3.7.

A comparison of the accuracy of an FDF, $\mathbf{a}(\vartheta, z)$, with moderate order, $T = [50, 100]$, for $\vartheta = 30°$ and a linear, critically sampled array with M = 8 equispaced elements is shown in Fig. 3.8. It can be seen from Fig. 3.8 that for both orders the error function between the frequency response of the ideal and the approximated FDFs is in an acceptable level, however as the order increases a closer approximation to the ideal FDF can be achieved.

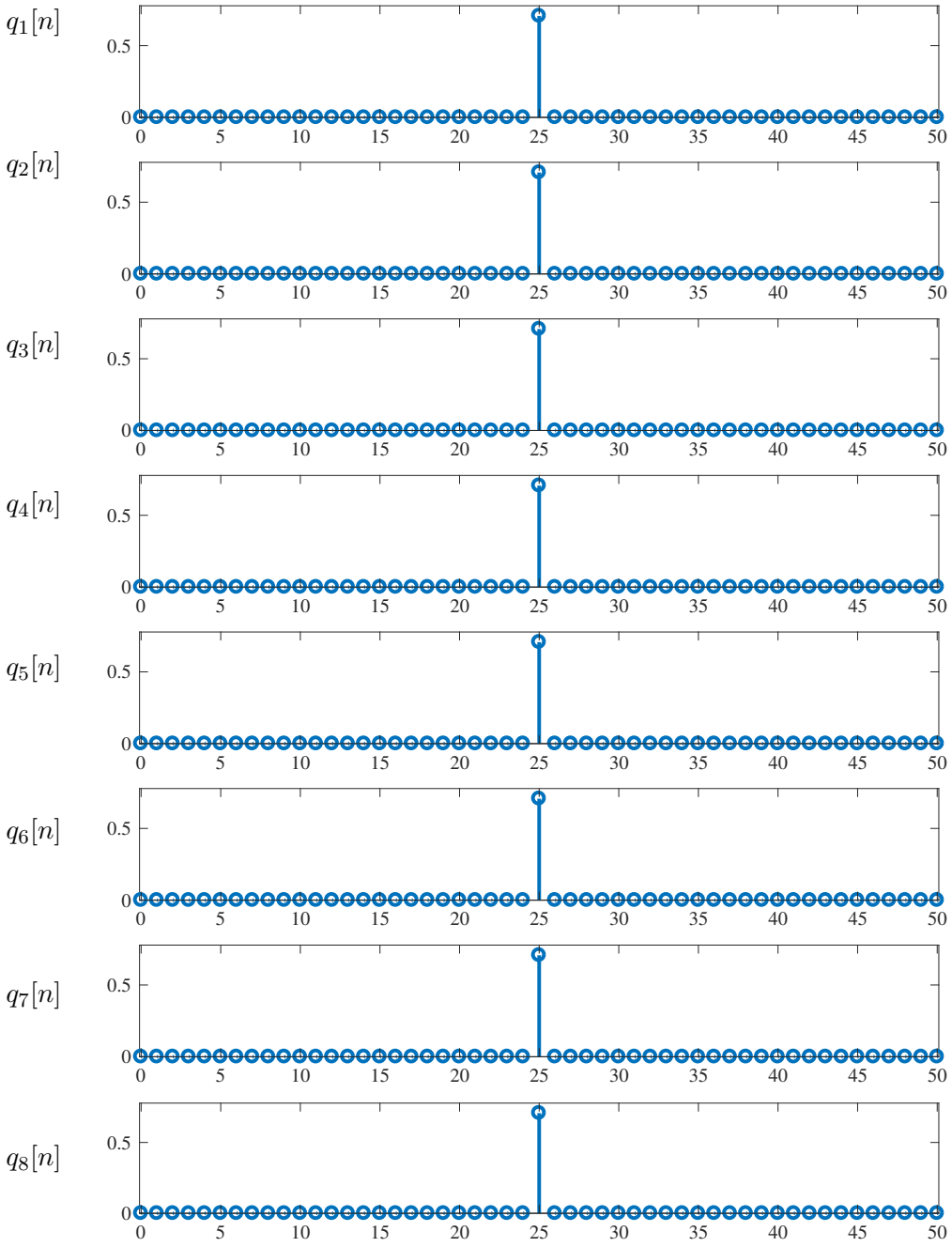


Figure 3.4: Fractional delay filters of $\boldsymbol{a}(\vartheta, z)$ with $\vartheta = 0°$.

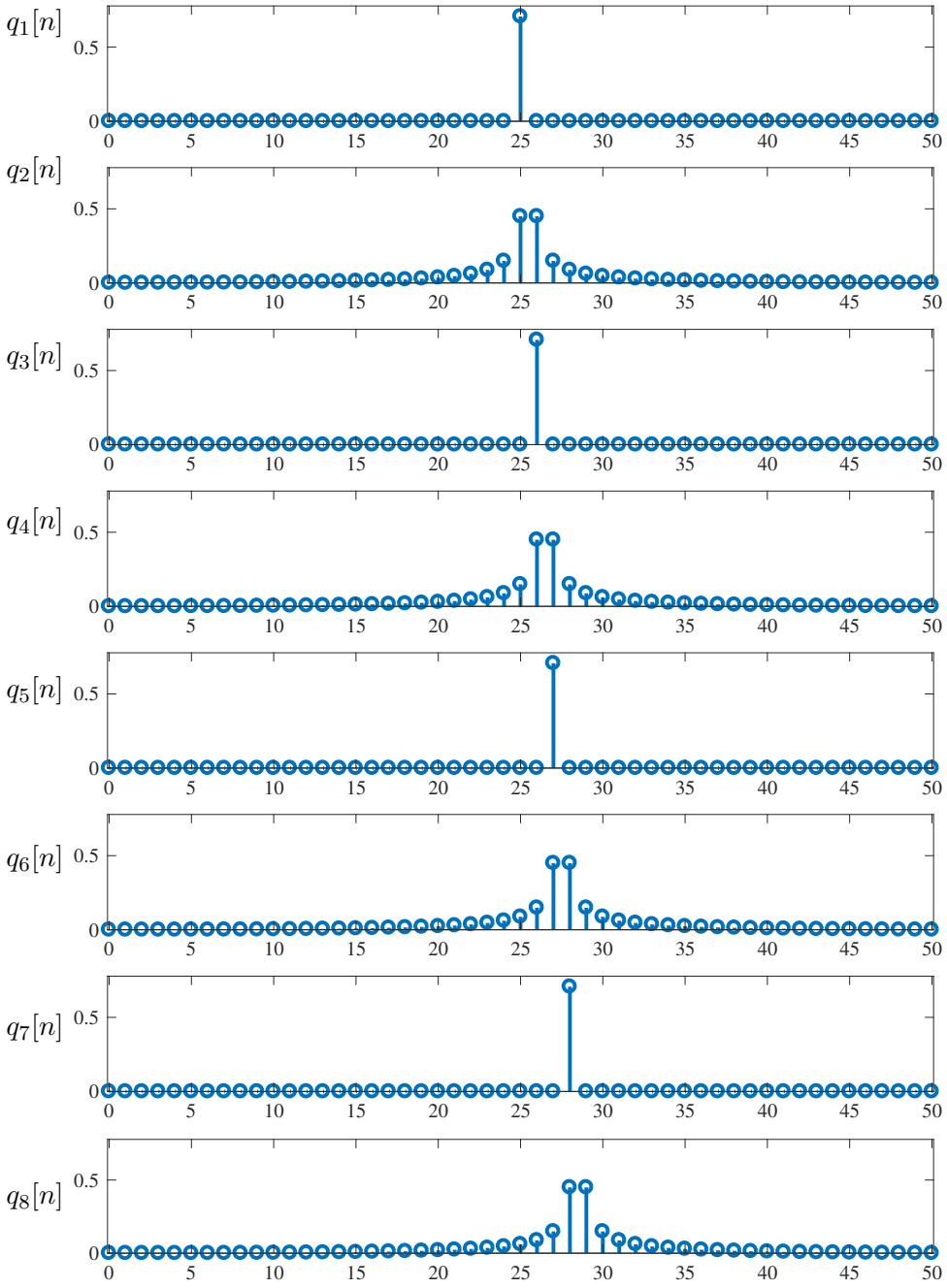


Figure 3.5: Fractional delay filters of $\boldsymbol{a}(\vartheta, z)$ with $\vartheta = 30°$.

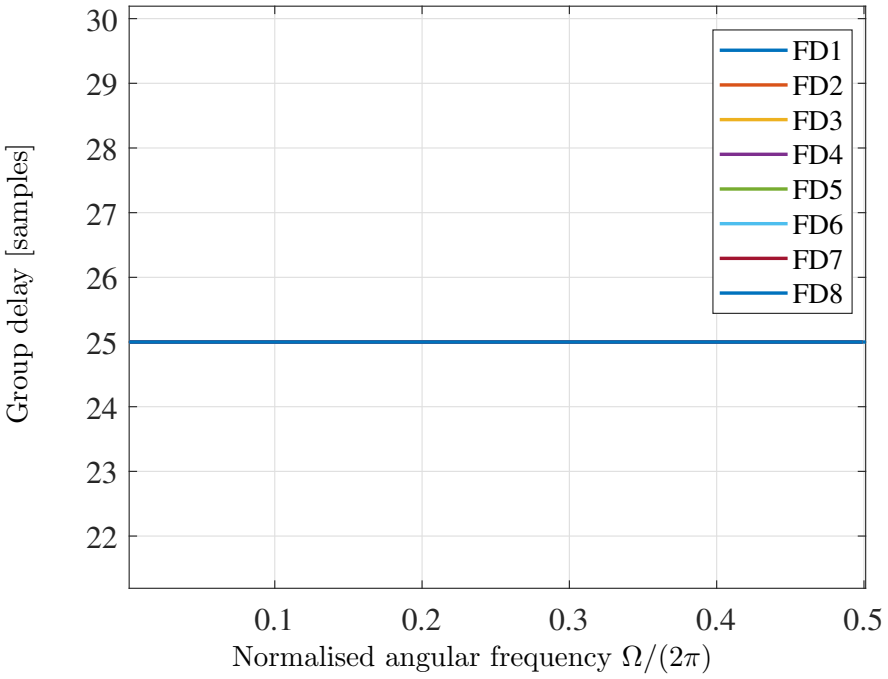


Figure 3.6: Delays associated with Fractional delays filters with $\boldsymbol{a}(\vartheta, z)$ and $\vartheta = 0°$.

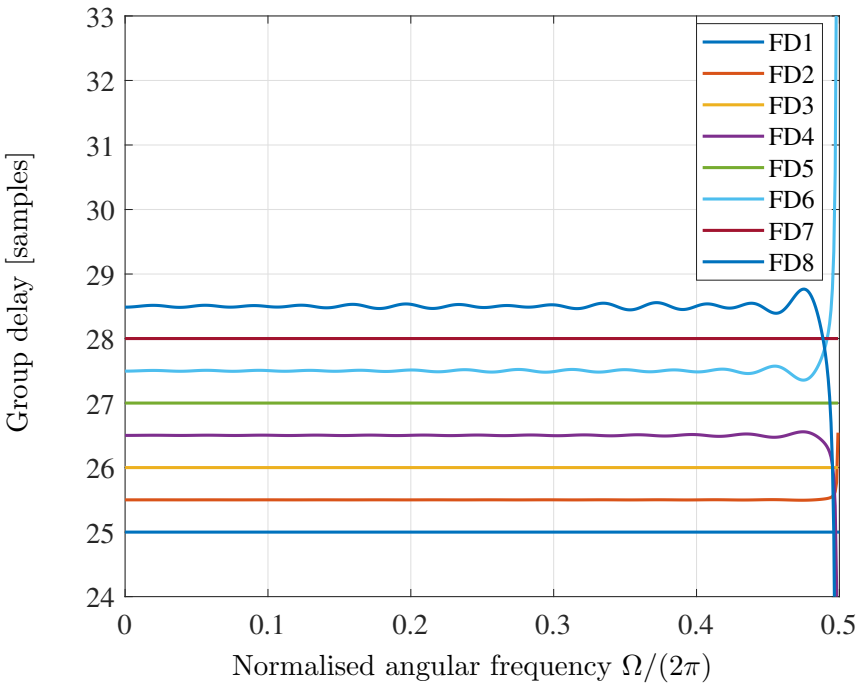


Figure 3.7: Delays associated with Fractional delays filters with $\boldsymbol{a}(\vartheta, z)$ and $\vartheta = 30°$.

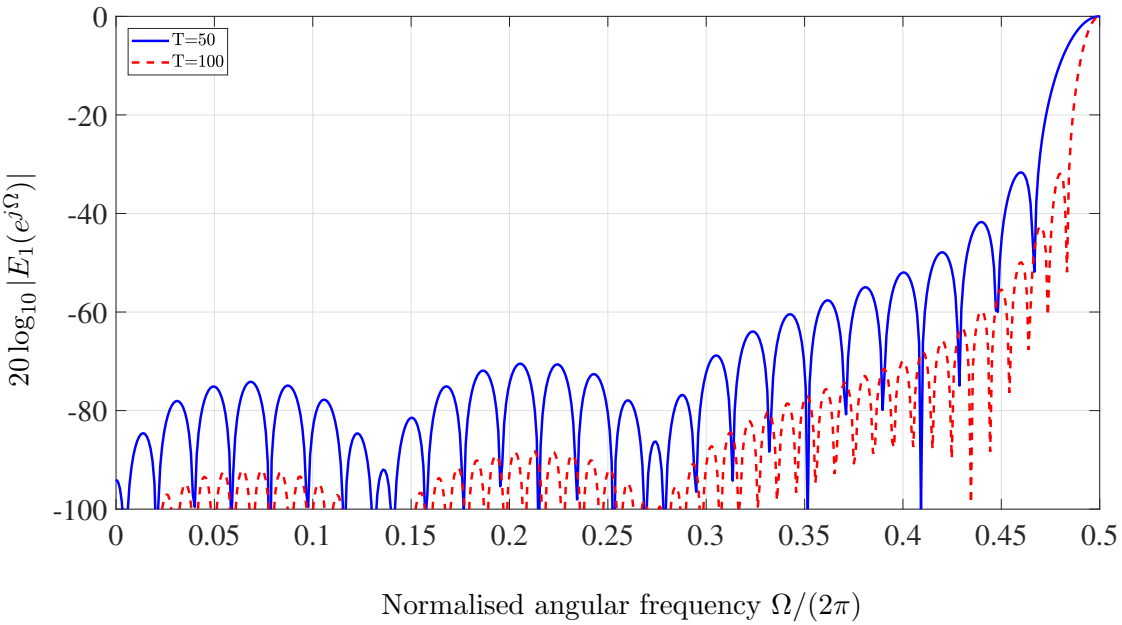


Figure 3.8: Error $E_1(z) = \boldsymbol{a}^{\mathrm{P}}(30°, z)\boldsymbol{a}(30°, z) - 1$ evaluated on the unit circle, with windowed sinc functions of order $T$ as fractional delay filters.

#### 3.2.2.2 Quiescent Beamformer

The quiescent beamformer $\boldsymbol{w}_{\mathrm{q}}(z)$ is derived from the constraint (3.6). Assuming that $\boldsymbol{a}^{\mathrm{P}}(\vartheta, z)\boldsymbol{a}(\vartheta, z) \approx 1$ for the steering vectors constructed above, and for the given assumption $F(z) = 1$ to be fulfilled, this requires $\boldsymbol{w}_{\mathrm{q}}(z) = \boldsymbol{a}(\vartheta_{\mathrm{s}}, z)$, ie, the quiescent weight vector is the matched filter of the SoI's steering vector. Therefore, the output from the quiescent beamformer, $d[n]$ in Fig. 3.3 is given by

$$d[n] = \sum_{\nu=0}^{T} \mathbf{w}_{\mathrm{q}}^{\mathrm{H}}[-\nu]\mathbf{x}[n-\nu], \tag{3.13}$$

hence the quiescent weight vector might be realised as a conventional beamformer. Note that $\boldsymbol{w}_{\mathrm{q}}(z) \bullet\!\!-\!\!\circ\, \mathbf{w}_{\mathrm{q}}[n]$ is of order $T$ and holds the parahermitian transpose of the actual coefficients.

### 3.2.3 Blocking Matrix

The quiescent weight vector was derived in Sec. 3.2.2.2 from the optimisation problem in (3.6), where it has to satisfy the constraint. Thus, the beamformer constructively interfers the SoI, but does not suppress any specific interferers[1]. To perform adaptive noise cancellation on $d[n]$ to cancel any remaining interference requires a reference signal that consists of the interference only. The blocking matrix $\boldsymbol{B}(z) : \mathbb{C} \to \mathbb{C}^{(M-1)\times M}$ in Fig. 3.3 has the purpose of generating this reference signal by passing any signal components other than the look direction defined by the constraint in (3.6).

Consequently, the relationship between the quiescent vector and the blocking matrix must satisfy

$$\boldsymbol{B}(z)\boldsymbol{w}_{\mathrm{q}}(z) = \underline{0} \quad . \tag{3.14}$$

This requires orthonormality between the row vectors of $\boldsymbol{B}(z)$ and $\boldsymbol{w}_{\mathrm{q}}(z)$. To achieve that, a paraunitary matrix

$$\boldsymbol{Q}(z) = [\boldsymbol{w}_{\mathrm{q}}(z) \;\; \boldsymbol{B}^{\mathrm{P}}(z)] \tag{3.15}$$

[1]The case where the constrain equation also includes interfers will be addressed as part of the polynomial Capon beamformer in Chap. 4.

needs to be constructed, with $\boldsymbol{Q}(z)\boldsymbol{Q}^{\mathrm{P}}(z) = \mathbf{I}$.

In the narrowband case involving constant matrices and vectors, a design for the block matrix can be derived from (3.15) by a variety of methods such as singular value decomposition of the constraint matrix, or orthogonalisation of the columns in (3.15) using Gram-Schmidt or QR decompositions [130]. However, the polynomial case is more involved and will be separately addressed in Sec. 3.3.

The output of the blocking matrix as shown in Fig. 3.3 is $\mathbf{u}[n] \in \mathbb{C}^{M-1}$. It ideally does not contain any trace of the desired signal components, but serves as a reference for interference plus noise, such that

$$\mathbf{u}[n] = \sum_{\nu=0}^{N} \mathbf{B}[\nu]\mathbf{x}[n-\nu], \tag{3.16}$$

where $\mathbf{B}[n] \circ\!\!-\!\!\bullet\, \boldsymbol{B}(z)$ is of order $N$. This order $N$ impacts on the computational complexity of $\boldsymbol{B}(z)$ and will arise from its construction in Sec. 3.3.

### 3.2.4 Multichannel Noise Cancellation

The output from the quiescent beamformer in the upper part of Fig. 3.3 includes not only the SOI signal, but also noise and interference. With $\boldsymbol{w}_{\mathrm{q}}(z)$ and $\boldsymbol{B}(z)$ as defined previously, a multichannel filter $\boldsymbol{w}_{\mathrm{a}}(z) : \mathbb{C} \to \mathbb{C}^{M-1}$ can be employed to minimise the GSC beamformer output power by removing the remaining interference from the quiescent beamformer output $d[n]$. This is done by using $\mathbf{u}[n]$ in Fig. 3.3 as a reference signal. With $\boldsymbol{w}_{\mathrm{a}}(z)$ containing the parahermitian transpose of the actual filter coefficients akin to (3.2), the beamformer output is

$$e[n] = d[n] - \sum_{\nu=0}^{J} \mathbf{w}_{\mathrm{a}}^{\mathrm{H}}[-\nu]\mathbf{u}[n-\nu], \tag{3.17}$$

whereby $\mathbf{w}_{\mathrm{a}}[n] \circ\!\!-\!\!\bullet\, \boldsymbol{w}_{\mathrm{a}}(z)$ is of order $J$.

The multichannel filter $\boldsymbol{w}_{\mathrm{a}}(z)$ can be determined through unconstrained minimisation of $\mathcal{E}\{|e[n]|^2\}$. Various tools exist for this need, such as the MMSE or Wiener approach for a direct solution, or adaptively by employing iterative algorithms such

as LMS or RLS [49]. For simulations in Sec. 3.6, the multichannel normalised LMS (NLMS) algorithm will be used. Compared to the LMS, the NLMS has a step size which is independent of the input signal power [131]. NLMS shares the LMS' low computational complexity of $\mathcal{O}\{L\}$, where the RLS typically possesses a complexity of order $\mathcal{O}\{L^2\}$.

## 3.3 Paraunitary Matrix Completion

This section explains one possible approach to find the blocking matrix $\boldsymbol{B}(z)$ via the matrix $\boldsymbol{Q}(z)$ in (3.15), i.e. by completing a paraunitary matrix from $\boldsymbol{w}_{\mathrm{q}}(z)$. For this, we employ a polynomial eigenvalue decomposition (PEVD, [81]) of the rank one matrix

$$\boldsymbol{w}_{\mathrm{q}}(z)\boldsymbol{w}_{\mathrm{q}}^{\mathrm{P}}(z) = \bar{\boldsymbol{Q}}(z)\boldsymbol{D}(z)\bar{\boldsymbol{Q}}^{\mathrm{P}}(z). \tag{3.18}$$

The PEVD approximately diagonalises and spectrally majorises $\boldsymbol{D}(z)$ by means of a paraunitary matrix $\bar{\boldsymbol{Q}}(z)$. Spectral majorisation is equivalent to the ordering of the singular values in the SVD [130], and ensures that the energy is compacted into as few polynomial eigenvalues in $\boldsymbol{D}(z)$ as possible. Since $\boldsymbol{w}_{\mathrm{q}}(z)$ has unit norm and (3.18) is rank one by construction, we obtain

$$\boldsymbol{D}(z) = \mathrm{diag}\{1 \;\; 0 \;\; \ldots \;\; 0\}\,. \tag{3.19}$$

The paraunitary matrix $\bar{\boldsymbol{Q}}(z)$ is ambiguous even if (3.18) had full rank. If

$$\bar{\boldsymbol{Q}}(z) = [\bar{\boldsymbol{q}}_1(z) \;\; \bar{\boldsymbol{q}}_2(z) \;\; \ldots \;\; \bar{\boldsymbol{q}}_M(z)]\,, \tag{3.20}$$

then $\bar{\boldsymbol{q}}_1(z)$ could, for example, be a shifted version of the polynomial vectors $\boldsymbol{w}_{\mathrm{q}}(z)$,

$$\bar{\boldsymbol{q}}_1(z) = z^{-\Delta}\boldsymbol{w}_{\mathrm{q}}(z)\,, \tag{3.21}$$

and still satisfy both (3.18) and (3.19). A more general ambiguity allows each eigenvector to be modified by an arbitrary allpass filter without violating paraunitarity of

$\bar{\boldsymbol{Q}}(z)$ [82, 83].

Similarly, the remaining columns $\bar{\boldsymbol{q}}_m(z)$ could be arbitrarily allpass filtered or shifted. Therefore, when defining

$$\boldsymbol{B}^{\mathrm{P}}(z) = [\bar{\boldsymbol{q}}_2(z) \ \ \ldots \ \ \bar{\boldsymbol{q}}_M(z)]\,, \tag{3.22}$$

$\boldsymbol{B}^{\mathrm{P}}(z)\boldsymbol{w}_{\mathrm{q}}(z) = \underline{0}$ is guaranteed, but $\boldsymbol{B}(z)$ may have a larger order than necessary. Through appropriate shift of rows and truncation of small outer coefficients of $\boldsymbol{B}(z)$ [**?** ], this order can be reduced.

Using the previous example of $\boldsymbol{w}_{\mathrm{q}}(z) = \boldsymbol{a}(30°, z)$ with $T = 50$ and the above procedure, $\boldsymbol{B}(z)$ is calculated by sequential matrix diagonalisation [89], which implements an iterative PEVD algorithm. Measuring how much of the signal of interest leaks through the blocking matrix is important, as this can result in signal cancellation in the GSC. The following error metric defined over a set of frequencies $\{\Omega_i\}$,

$$E_2(e^{j\Omega_i}) = \max_{m\in\{2\ldots M\}} |\bar{\boldsymbol{q}}_m^{\mathrm{H}}(e^{-j\Omega_i})\boldsymbol{w}_{\mathrm{q}}(e^{j\Omega_i})| \tag{3.23}$$

will be zero if $\boldsymbol{B}(z)\boldsymbol{w}_{\mathrm{q}}(z) = \underline{0}$; in case of a deviation, (3.23) extracts the maximum error across all $M-1$ inner products at every frequency. The result for truncation of $\boldsymbol{B}(z)$ by 1% and 0.1% of its energy is shown in Fig. 3.9. The error is acceptable particularly at low frequencies. It is dominated by inaccuracies in the construction of the broadband steering vector, as evident from the increasing error towards half of the sampling rate $\Omega = \pi$, where fractional delay filters are known to break down [132] and by the iterative PEVD or the truncation of $\boldsymbol{B}(z)$.

## 3.4 Relationship between Aperture, the FDF, and Adaptive Multichannel Filter Orders

The order of the FDF relies on several parameters, namely the AoAs' of the impinging sources, the bandwidth, the SNR, and the number of antenna elements, $M$. Later on, in Sec. 3.6 the impact of the latter parameter on the performance of the PBBF is

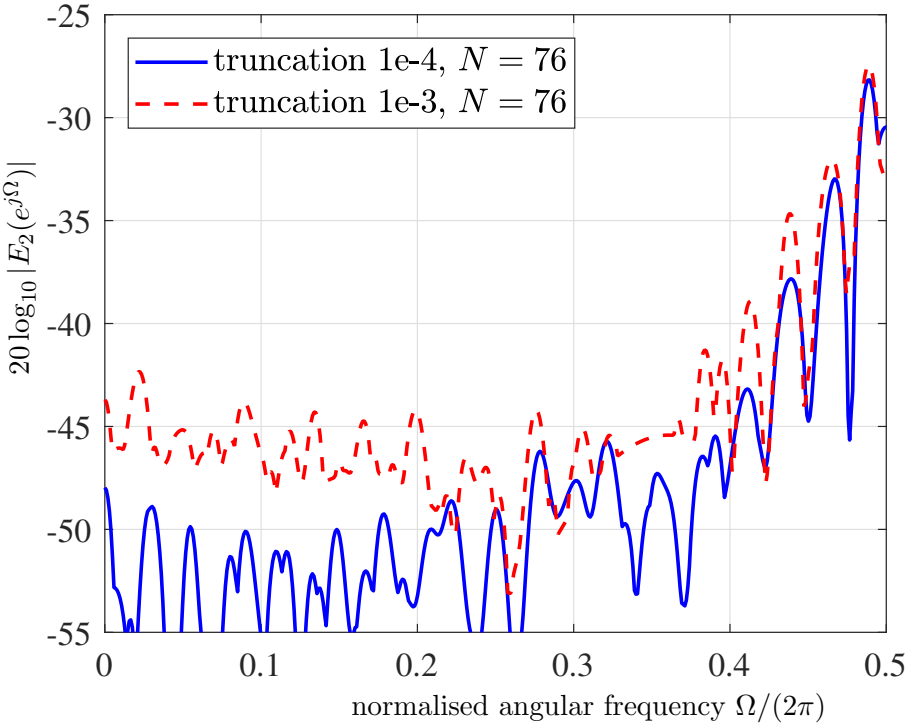


Figure 3.9: Leakage of blocking matrix according to (3.23).

studied with assumption that the other parameters are fixed. The experiment indicates that the FDF order needs to be increased as $M$ increases. The length of the FDF has a significant impact on the beamformer response, particularly, to the interference signals. Fig. 3.10 is produced based on the simulation scenario in Sec.3.6, where SOI's AoA is $\vartheta_s = 30°$ and interference sources' AoAs are $\{-40°, -70°, 80°\}$. The figure reveals that the performance of the PBBF, in terms of nullifying interfering signals, depends on the FDF order and the interference's AoA. As it can be noticed that for a specific number of array elements and low order FDFs ( with respect to a factor that is discussed beneath) the PBBF is still suitable to suppress interference in the vicinity of the broadside. However, as the interference moves towards the ULA antenna's endfires, the capability of the beamformer to sufficiently deal with interference degrades when FDF's order is less than twice of the spatial filter length. Thereby, a mathematical expression of the relationship between $T$ and $M$, for this particular scenario, can be

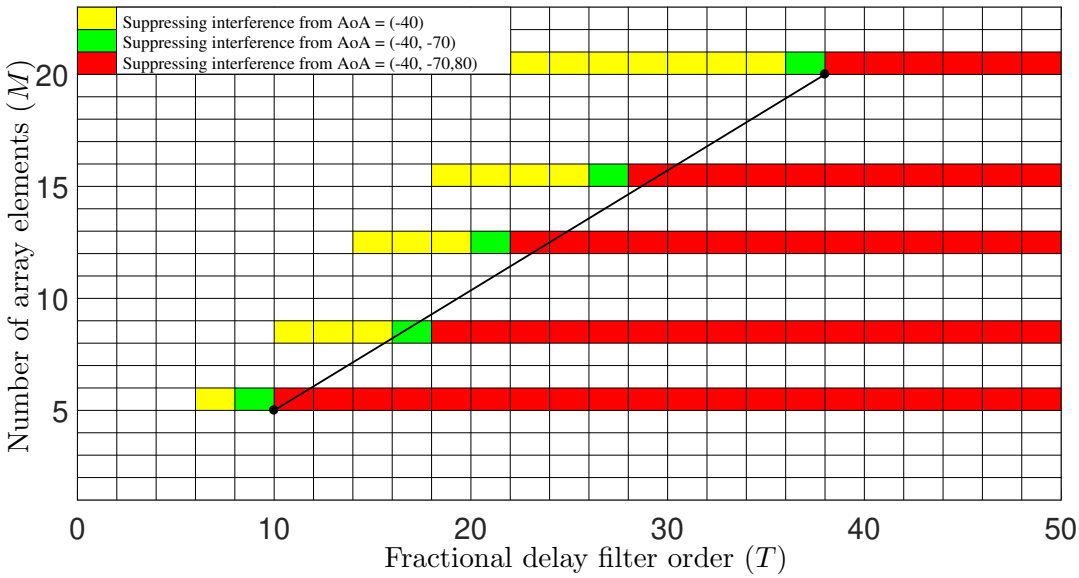


Figure 3.10: The relationship between $M, T$, and PBBF performance, for a number of ULA elements $M = \{5, 8, 12, 15, 20\}$ and AoAs' $\vartheta_{i=1,2,3} = \{-40°, -70°, 80°\}$.

given as

$$T \geq 2 \times M. \tag{3.24}$$

Nonetheless, as the length is further increased,the performance degrades again. This degradation of the performance is associated with misalignment of estimating interference samples at the output of the multichannel adaptive filter in relation to the interference samples in the desired signal path in Fig. 2.6 and Fig. 3.3.

A solution, to this misalignment, can be provided by applying a suitable delay, let's say $D$, to the desired signal path. In [133] this delay is reported to be related to the half of the adaptive filter channels' length. Nonetheless for the PBBF, in addition to that, the length of the FDFs, $T$, and blocking matrix entries,$N$, are also influence this delay. Thus, before defining the delay $D$, we are defining two intermediate parameters. The first is a reference point, which is the midpoint of the multi-channels length in the adaptive process, and it is defined as

$$j_r = \begin{cases} \frac{(J-1)}{2} & \text{when} \quad J \quad \text{is odd}\,, \\ \frac{J}{2} \quad \text{or} \quad (\frac{J}{2}) - 1 & \text{when} \quad J \quad \text{is even}\,, \end{cases} \tag{3.25}$$

we recall that $J$ is the length of the individual channel of the adaptive processor. The second is $\Delta$ which represents the shift from the reference point, $j_r$, with an aim to retain the filters' impulse responses, in average, nearly centralised around the reference point,

$$\Delta = \frac{N-T}{2} \, . \tag{3.26}$$

This, in turn, helps in providing better estimate of the interference signals and align it with its exist copy in the GSC's upper path. Then, the required delay is given by

$$D = j_r + \Delta. \tag{3.27}$$

However, for (3.27) to be valid, the relationship between blocking matrix order and the FDF order must satisfy, $\frac{N}{T/2}$ is greater than or approximately 1, otherwise the multi-channel order,$J$, must be increased.

## 3.5 Performance Metrics

In this section, metrics to measure and evaluate the performance of the proposed beamformer are described and examined, and will be used in the subsequent Sec. 3.6 to compare the proposed polynomial approach to a standard time domain broadband beamformer.

### 3.5.1 Directivity Pattern

The directivity or beam pattern $A(\vartheta, \Omega)$ measures the gain response of a broadband beamformer with respect to AoA $\vartheta$ and normalised angular frequency $\Omega$. With a broadband source at angle $\vartheta$ characterised by the broadband steering vector $\boldsymbol{a}(\vartheta, z)$, the overall transfer function of the beamformer is

$$\boldsymbol{w}(z) = \boldsymbol{w}_{\mathrm{q}}(z) - \boldsymbol{B}^{\mathrm{P}}(z)\boldsymbol{w}_{\mathrm{a}}(z) \, . \tag{3.28}$$

The directivity pattern is the magnitude of the response $A(\vartheta, e^{j\Omega})$,

$$A(\vartheta, z) = \boldsymbol{w}^{\mathrm{P}}(z) \cdot \boldsymbol{a}(\vartheta, z) \ , \tag{3.29}$$

which is obtained by probing (3.29) with a series of steering vectors $\boldsymbol{a}(\vartheta, z)$ that scan over a range of different angles $\vartheta$, and evaluating it on the unit circle, such that

$$A(\vartheta, \Omega) = \left| A(\vartheta, z)|_{z=(e^{j\Omega})} \right| \tag{3.30}$$

defines the directivity pattern.

### 3.5.2 Residual Error

To assess convergence of the optimisation methods for $\boldsymbol{w}_{\mathrm{a}}(z)$, a useful metric is to assess the mean square of the residual error $e_{\mathrm{r}}[n]$, obtained by subtracting the source signal projected through the quiescent vector from the error $e[n]$. If $s[n]$ is the SOI at the reference element, i.e. $x_1[n] = s[n]$ in the absence of any noise and interferers, then the residual error is defined as

$$e_{\mathrm{r}}[n] = e[n] - s[n - \Delta T]; , \tag{3.31}$$

where $\Delta T$ is the delay imposed to make the broadband steering vector in the quiescent beamformer causal. Thus the mean square residual error metric becomes

$$\xi_{\mathrm{r}} = \mathcal{E}\big\{|e_{\mathrm{r}}[n]|^2\big\} \ , \tag{3.32}$$

which provides an accurate assessment of how well the adaptive filter $\boldsymbol{w}_{\mathrm{a}}(z)$ is adapted. In the optimal case $\mathcal{E}\big\{|e[n]|^2\big\} \longrightarrow \sigma_r^2$, where $\sigma_r^2$ is the power of any residual noise and interference at the beamformer output. While $\xi_{\mathrm{r}} \longrightarrow 0$ even in the presence of noise and interferers and hence easier to assess than $\mathcal{E}\big\{|e[n]|^2\big\}$, particularly when displayed on a logarithmic scale. This metric is similar to the echo return loss enhancement (ERLE) in the adaptive noise cancellation literature for acoustic echo control [134, 135].

### 3.5.3 Computational Cost

The computational complexity is a key metric to determine whether a beamformer can be realistically implemented, and how much processing power a particular design requires. Also, high computational complexity may lead to processing latency and increase power consumption that are usually regarded as undesirable consequences.

The computational complexity of the various polynomial GSC components in Sec. 3.2 is listed in Tab. 3.1. For recollection, the parameters $M, T, N$ and $J$ are the number of sensors in the array, the FDF order, the order of polynomials in the blocking matrix's elements, and the adaptive filter's coefficients order respectively. For comparison, the costs for a time domain broadband beamformer are also stated [25]. An off-broadside look direction can be enforced through point constraints in the frequency domain, but prevents simplifications to the blocking matrix, which has to be applied to the full spatio-temporal data vector of dimension $ML$, with $L$ represents the FIR filter order as in Fig. 2.8 and 3.1. The independence of the blocking matrix from the steering vector length in the polynomial approach has reduced the overall computation complexity and outperformed the standard approach in this aspect among others as we will see in Sec. 3.6.

Table 3.1: Computational complexity of different broadband beamformer realisations in multiply accumulates (MACs).

| component | GSC cost | |
|---|---|---|
| | polynomial | standard |
| quiescent beamformer | $M(T+1)$ | $M(L+1)$ |
| blocking matrix | $M(M-1)(N+1)$ | $M(M-1)(L+1)^2$ |
| adaptive filter (NLMS) | $2(M-1)(J+1)$ | $2(M-1)(J+1)$ |

## 3.6 Simulations and Results

This section provides an example for designing a polynomial GSC, and compares its result to standard broadband beamforming as a benchmark. As an example scenario, a uniform linear array captures plane waves that propagate in free space from four wide-

sense stationary and zero mean wideband sources at different locations in the far field. A signal of interest from $\vartheta_\mathrm{s} = 30°$, and three interferers from angles $\vartheta_i \in \{-40°, -10°, 80°\}$ are assumed, which are active over the frequency range $\Omega = 2\pi \cdot [0.1;\ 0.45]$ at a signal to interference power ratio of -40 dB. The $M = 8$ element linear uniform array, with sensor spacing such that spatial sampling is just satisfied at the maximum frequency of $\Omega = \pi$, is also corrupted by spatially and temporally white additive Gaussian noise at 20 dB SNR. . The simulation parameters are summarised in Tab. 3.2.

An example for the directivity pattern of only the quiescent beamformer $\boldsymbol{w}_\mathrm{q}(z) = \boldsymbol{a}(30°, z)$ with $T = 50$, and $\boldsymbol{w}_\mathrm{a}(z) = \underline{0}$ is shown in Fig. 3.11. For comparison, a time domain broadband quiescent beamformer designed from $T + 1$ point constraints in the frequency domain is provided as a benchmark in Fig. 3.12. Both beamformers are similar and provide an approximate gain of one in direction of the SoI. Interestingly, while the polynomial version in Fig. 3.11 has inaccuracies in look direction towards $\Omega = \pi$ due to the broadband steering vectors lacking precision, the standard approach in Fig. 3.12 has inaccuracies particularly at the lower end of the spectrum. This will be further explored below and investigated in the discussion of Fig. 3.16 later.

With a quiescent design of $T = 50$ as shown previously and a blocking matrix via PEVD completion with order $N = 140$, an NLMS algorithm optimises $\boldsymbol{w}_\mathrm{a}(z)$ with order $J$. The convergence curve for the mean square residual error $\xi_\mathrm{r}$ as defined in (3.32) is shown in Fig. 3.13, together with that of a standard time domain broadband GSC of same dimension $J$. The directivity patterns with converged $\boldsymbol{w}_\mathrm{a}(z)$ are in Fig. 3.14 for the proposed polynomial approach and Fig. 3.15 for the benchmark. Both beamformers have placed nulls towards the three interferers, but the polynomial approach protects the constraint better — an example for the gain in look direction, which is constrained to 0 dB, is shown in Fig. 3.16 for $T = L = 50$ before and after adaptation. While the standard approach oscillates strongly between its point constraints, the polynomial approach is much better behaved.

With the design parameters in Tab. 3.2 and the cost as listed in Tab. 3.1, the proposed beamformer requires 10.7 kMACs, while the standard broadband beamformer takes 1.72 MMACs per iteration step. The difference in MACs between the two ap-

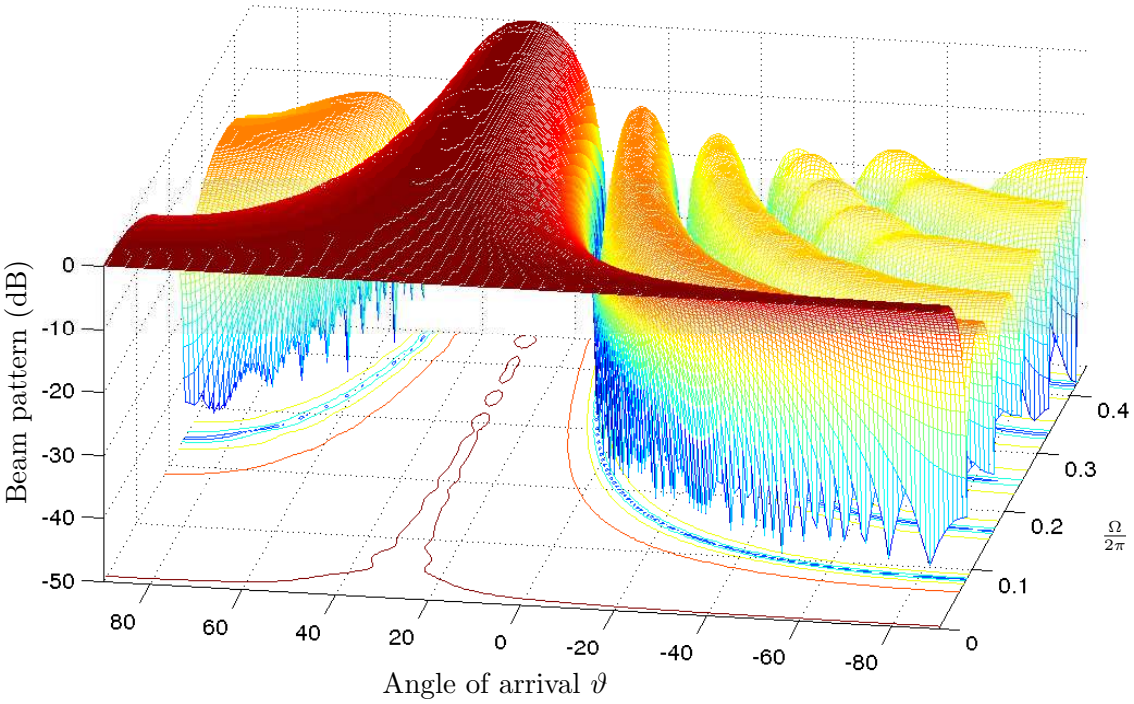


Figure 3.11: Directivity pattern of polynomial quiescent beamformer with look direction $\vartheta_s = 30°$.

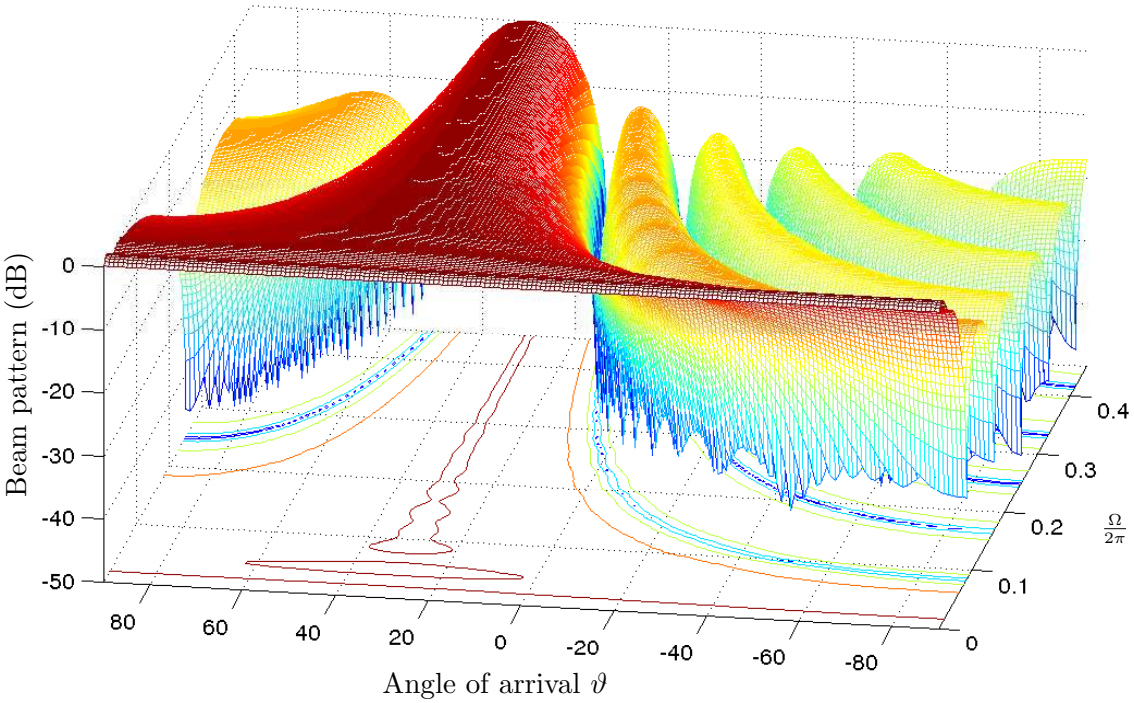


Figure 3.12: Directivity pattern of standard broadband quiescent beamformer with look direction $\vartheta_s = 30°$.

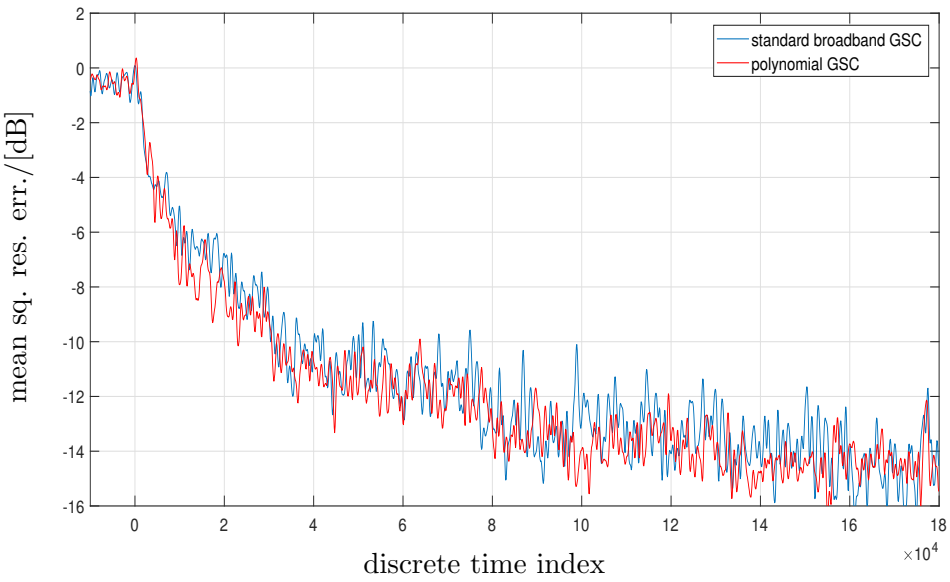


Figure 3.13: Mean square residual error for proposed polynomial GSC and standard time domain GSC using the NLMS.

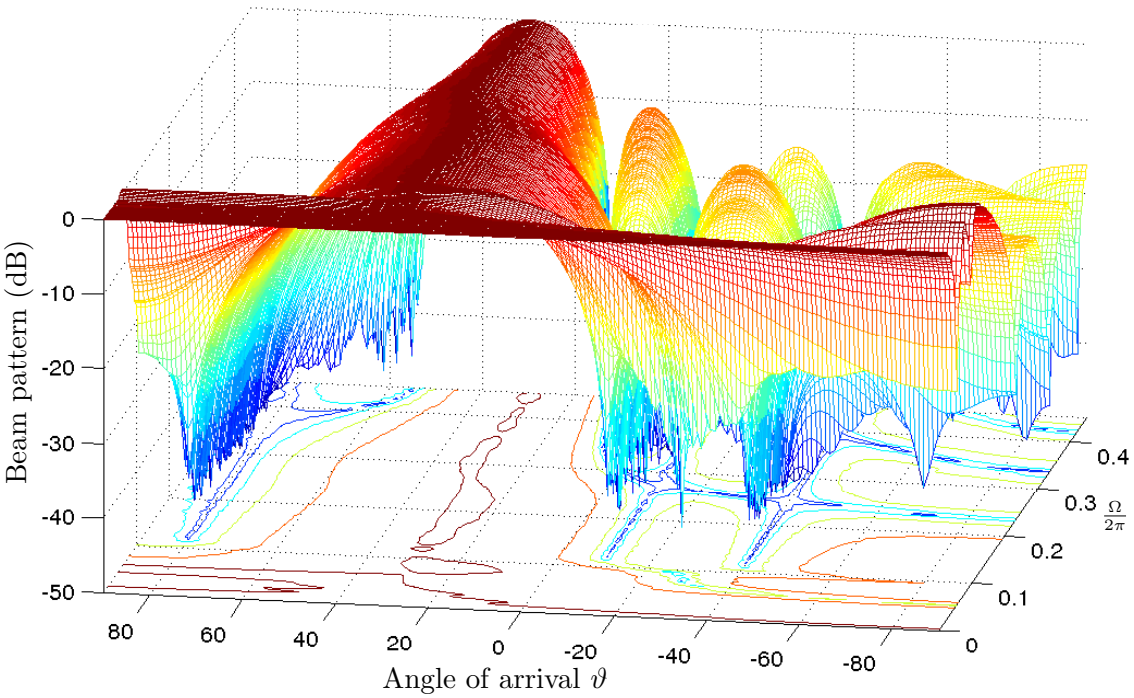


Figure 3.14: Directivity pattern of adapted polynomial GSC.

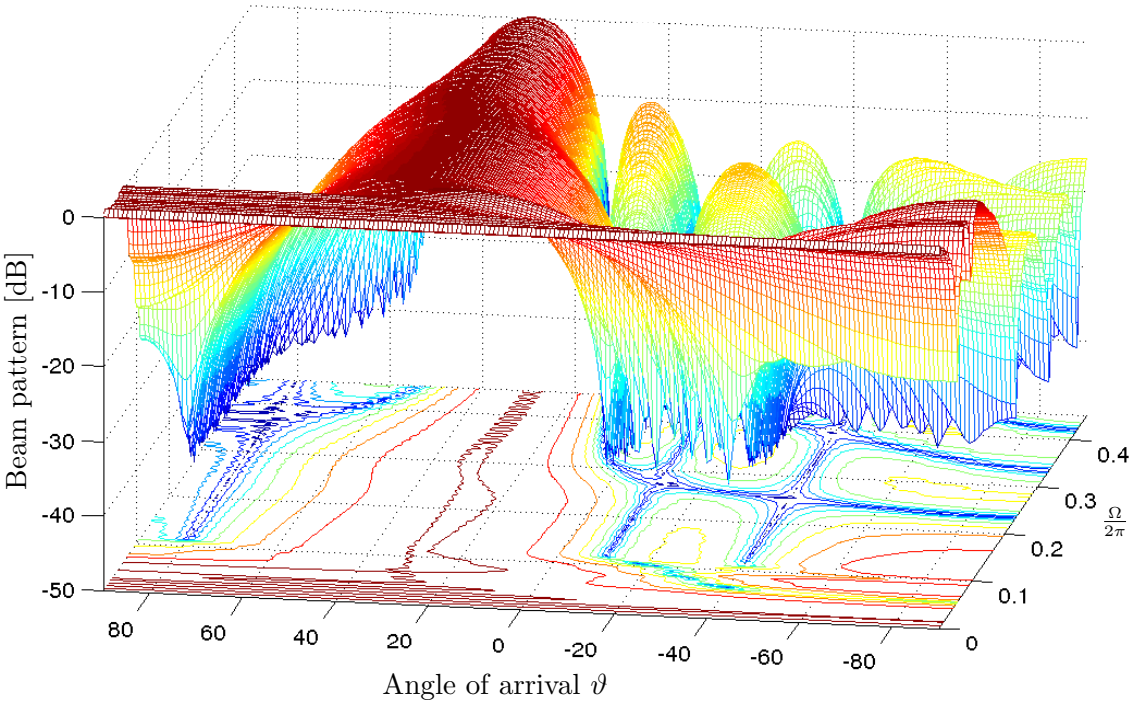


Figure 3.15: Directivity pattern of adapted standard GSC.

Table 3.2: Simulation design parameters summary.

| Parameter | Characteristic or value |
|---|---|
| Antenna geometry | ULA |
| Number of elements | 8 |
| sec:SF$_a nd_F DF$Sampling frequency $f_s$ | $2f_{\max}$ |
| SOI spectral | Low pass |
| SOI bandwidth | $[0,\ 0.5]f_s(Hz)$ |
| SOI AoA | $30°$ |
| Int1 AoA | $-10°$ |
| Int2 AoA | $-40°$ |
| Int3 AoA | $80°$ |
| Int-s spectral | Bandpass |
| Int-s bandwidths | $[0.1,\ 0.45]f_s(Hz)$ |
| FD filter order, $T$ | 50 |
| Temporal dimension, $L$ | 50 |
| NLMS temporal dimension $J$ | 175 |
| NLMS initial step size $\mu$ | 1 |

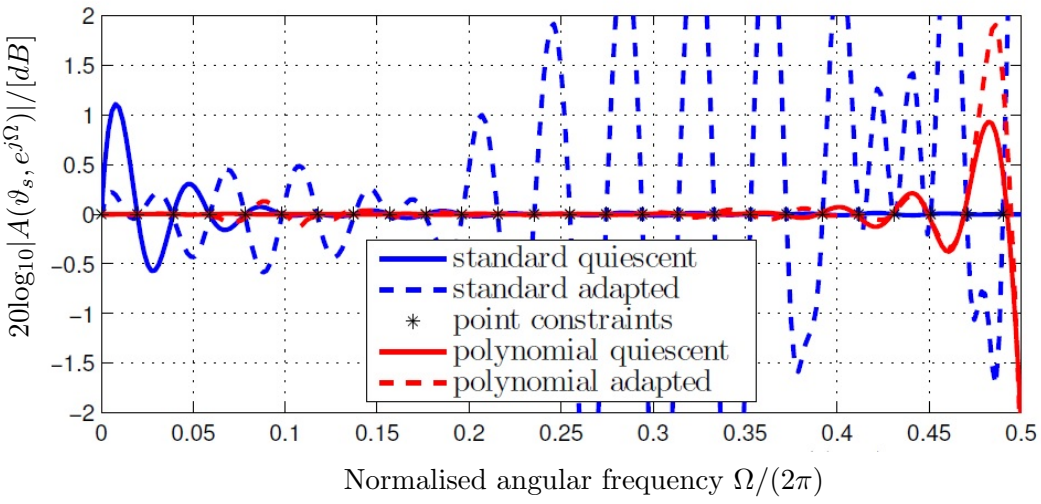


Figure 3.16: Gain in look direction $\vartheta_s = 30°$ before and after adaptation.

proaches comes from the high complexity of the blocking matrix required in the standard beamformer, since it non-linearly increases as a function of the square of the FIR filter length. However, the blocking matrix of the PBBF is decoupled from this factor and its computational complexity depends linearly on its order after PEVD and truncation processes.

One more factor that impacts on the performance of the proposed beamformer, as was explained in Sec. 3.4, is the length of the FDFs. Fig. 3.17 and Fig. 3.18 illustrate cross sections at $0.25f_s$ for an antenna array with 8 and 20 elements respectively. In Fig. 3.19, the response of PBBF over the entire simulated bandwidth and for various FDF length is depicted. Simulations indicate that the FDF order needs to increase with $M$. The length of the FDF has a significant impact on the beamformer response, particularly, to the interference signals. For a different length of FDF the beamformer behaviour changes which can be seen from the beam-pattern in Fig. 3.17, Fig. 3.18 and Fig. 3.19. When the FDF has a length equal to $T - 1 = M = 20$, the beamformer perfectly nulls the interference that has an AoA $= 10^\circ$ but not the others at $-40^\circ$ and $80^\circ$. However, when its length is a double or Quadruple of the number of antenna array elements, the entire interferers were suppressed and the main beam steered to the direction of SoI.

As the length is further increased, deviation from complete null of the interferers, along the specified frequency band, occurs, but the main beam towards the SoI is still protected by the constraints and has a unity power, this can be observed from the beam-pattern in Fig. 3.18 and Fig. 3.19.

Applying a proper delay on the desired signal path, as it was discussed in Sec. 3.4 retains the performance of the PBBF. An example of the impulse response of a length 175 adaptive filter, and for a number of sensors $M = 8$ and FDFs length $T = 51$ the polynomial blocking matrix has a length of 87. Hence the resulting delay based on (3.27) will be $D = 124$, and the impulse responses of the multichannel adaptive filter is directed in Fig. 3.20. As it can be seen that the impulse response of the channels, apart from $w_{a,5}[n]$, are nearly allocated about $j_r = 88$, this renders the estimation of the interference signal samples more accurate, thereby improves the attenuation of the

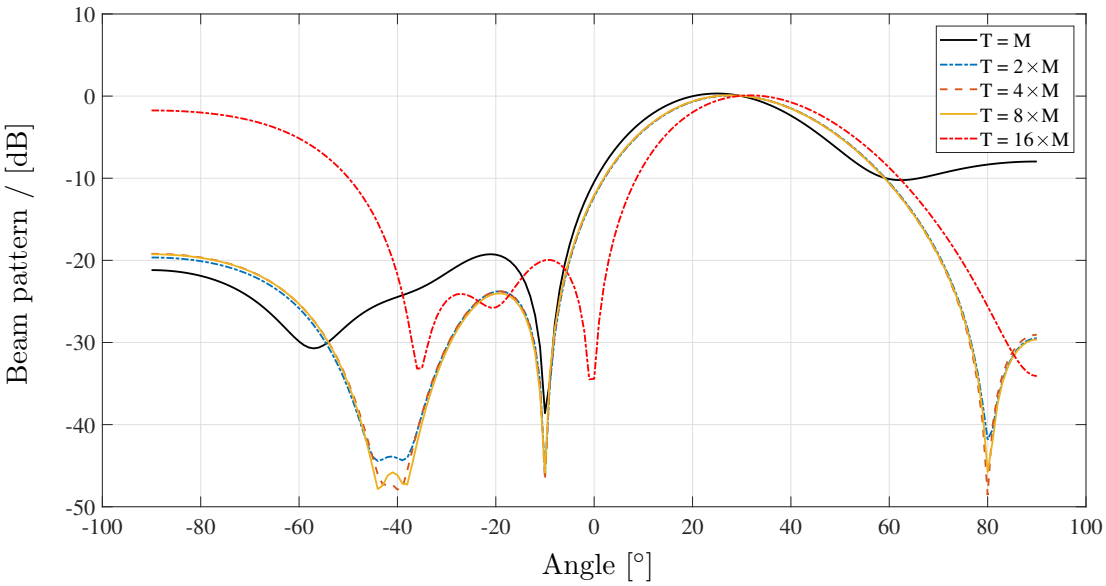


Figure 3.17: A cross section of the beam patterns at $\Omega = \pi/2$ and for different length of FDFs with M = 8.

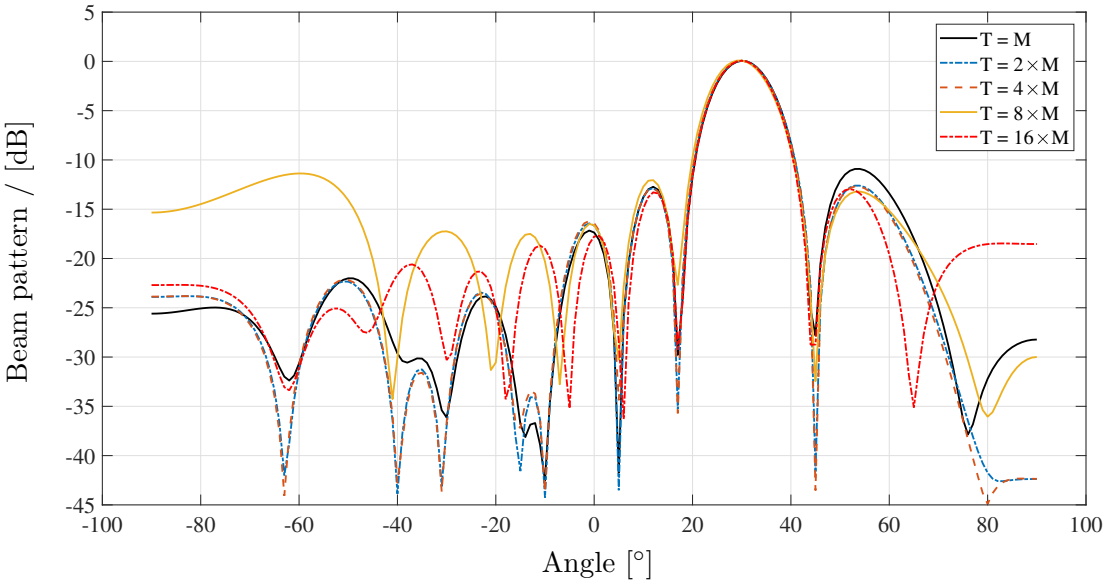


Figure 3.18: A cross section of the beam patterns at $\Omega = \pi/2$ and for different length of FDFs with M = 20.

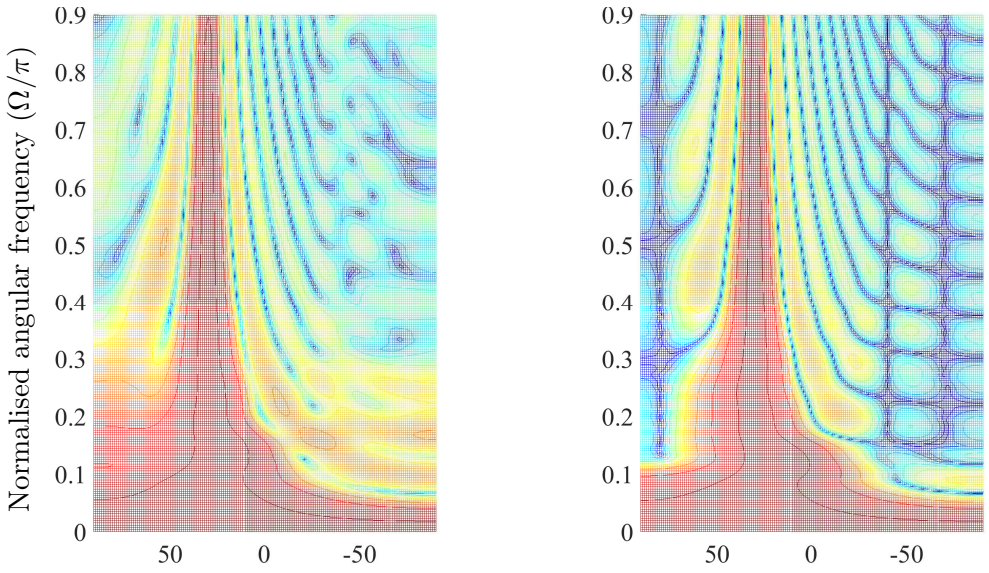


(a) FDF order = 20

(b) FDF order = 40

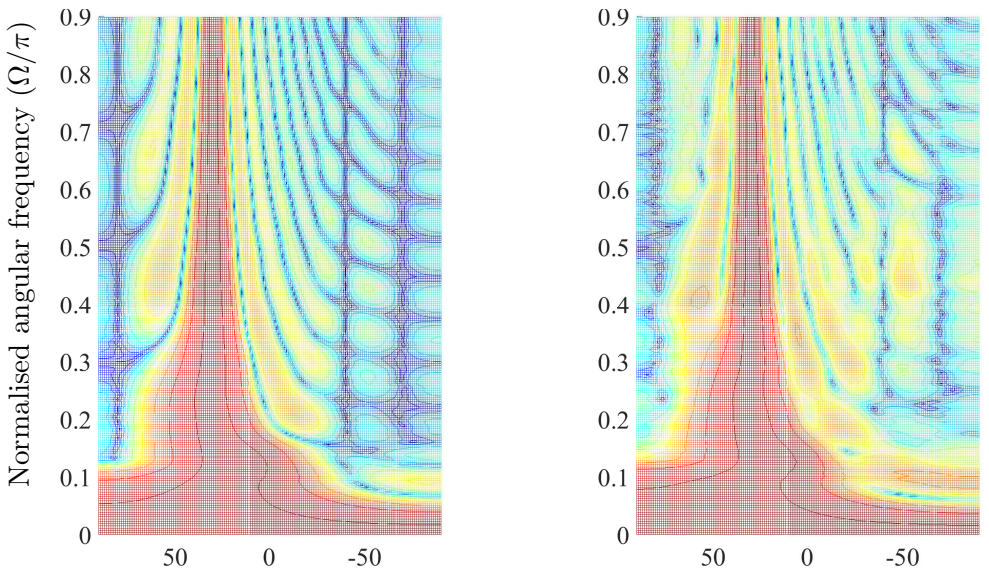


(c) FDF order = 80

(d) FDF order = 120

Figure 3.19: Beam-patterns of PBBF with antenna array elements number $M = 20$ and various FDF order, for $\vartheta_s = 30°$ and $\vartheta_i = [-40° - 70°, 80°]$.

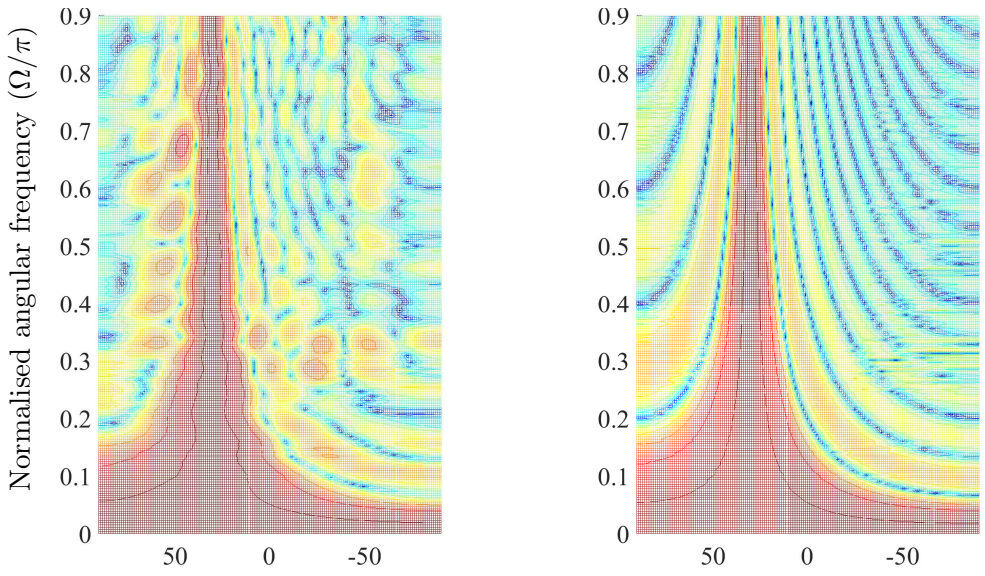


(a) FDF order =160

(b) FDF order = 320

Figure 3.19: *Continued*: Beam-patterns of PBBF with antenna array elements number $M = 20$ and various FDF order, for $\vartheta_s = 30°$ and $\vartheta_i = [-40°, -70°, 80°]$.

interfering signals.

## 3.7 Conclusions

A polynomial matrix formulation of a GSC structure of MVDR beamformer has been introduced, which requires the definition of constraints via broadband steering vectors. For the construction of the blocking matrix, a paraunitary matrix completion has been defined. The proposed method can elegantly and compactly incorporate off-broadside constraints and define metrics such as the directivity pattern. It can also lead to accurate beamformers of considerably lower complexity compared to the standard time domain counterpart.

Since the beamformer gain depends on steering and the weight vectors as well as the number of antenna array elements. The accuracy of the first two factors was examined, the result shows that the steering vector handles the spatial characteristics of the broadband signal up to around the half sampling rate with a satisfactory behaviour, and the polynomial broadband beamformer performance outperformed its standard time domain counterpart at lower frequencies.

Here only a single constraint —for the SoI — had been included. The more general case, where some interferers are known to arrive from a specific AoA, will be addressed as part of the Capon beamformer in the next chapter.

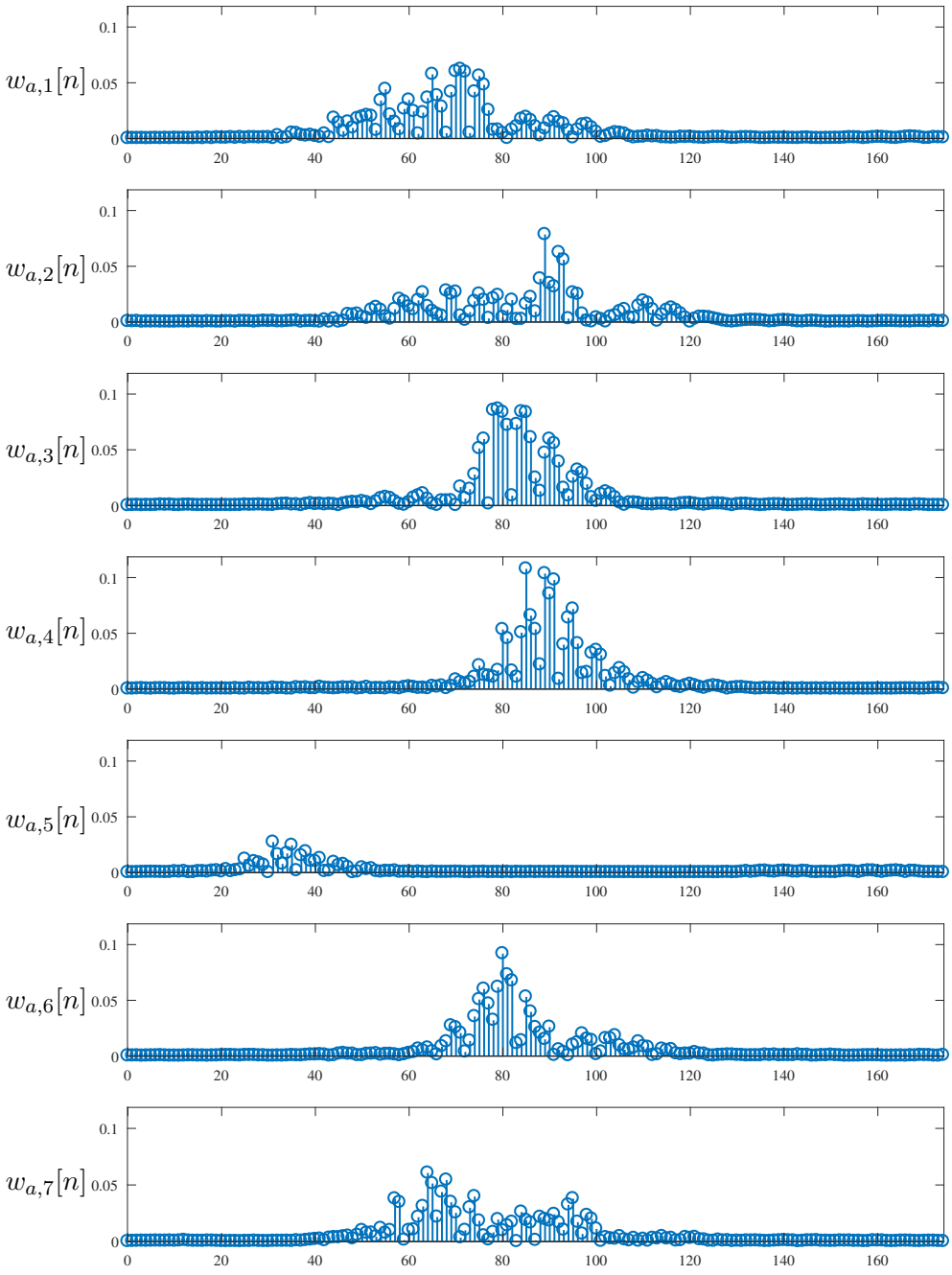


Figure 3.20: Multi-channel adaptive filters' impulse responses $w_a[n]$ for $M = 8$ and $J = 175$.

# Chapter 4

# Polynomial Matrix Formulation-Based Capon Beamformer

## 4.1 Introduction

The Capon solution to find the optimal coefficients of a beamformer is a constrained method that represents an alternative to the unconstrained procedure based on the GSC structure presented in Chap. 3. In the case of errors in the constraints, the leakage of the signal components through the blocking matrix, presented in Fig. 3.9 in the lower part of the GSC beamformer, could lead to the desired signal being eliminated by the adaptive noise canceller at the beamformer output. This could be, for example, due to non-stationarity of the source of interest or the change of sensor characteristics, which in turn, might lead to the change of signals characteristics, and hence will impact on the design of the blocking matrix. This leads to degradation of the system performance. In applications where computational complicity is less of an issue, the constrained Capon beamformer could offer a solution to overcome this problem. This beamforming solution is well-known in the narrowband case.

Consequently, this chapter demonstrates the ease with which broadband array problems can be generalised from their well-known narrowband equivalents when using

polynomial matrix formulations. This is exemplified for the Capon beamformer, which presents a solution to the MVDR problem. Based on the space-time covariance matrix of the array and the definition of a broadband steering vector, we formulate a polynomial MVDR problem. Results from its solution in the polynomial matrix domain are presented.

Narrowband array processing methods are well established and rely in their computation on optimal tools such as the eigenvalue decomposition to the covariance matrix. However, when addressing broadband problems, the extension of these classical narrowband algorithms is generally not straightforward. The inclusion of tap-delay-line processors to manipulate explicit delays instead of narrowband gain factors to adjust the phase of signals can complicate matters. Often the covariance matrix has to be inflated to include a temporal dimension of a fixed, a-priori defined order [136].

In this chapter, we demonstrate how polynomial matrix formulations can be used to easily generalise and calculate broadband beamforming solutions from narrowband ones. We here extend work from Chap. 3 and address the definition and calculation of a Capon beamformer such as discussed in e.g. [16, 38]. Based on broadband definitions of steering vectors and the data covariance matrix in Sec. 4.2, we review the narrowband Capon beamformer in Sec. 4.3 followed our broadband extension in Sec. 4.4. Some implementation aspects are highlighted in Sec. 4.5. Sec. 4.6 gives details about the inversion of the polynomial space-time covariance matrix. Implementation approaches are exemplified in Sec. 4.7, and numerical evaluation of each of the approaches is reported in Sec. 4.8. Finally, Sec. 4.9 presents conclusions.

## 4.2 Steering Vectors and Space-Time Covariance Matrix

For an $M$-element array receiving signals $x_m[n]$, $m = 1 \dots M$, we define a data vector $\mathbf{x}[n] \in \mathbb{C}^M$. If a source illuminates the array, its signal will be received with different

time delays $\tau_m \in \mathbb{R}$, and omitting any attenuation, we have

$$\mathbf{x}[n] = \begin{bmatrix} s[n-\tau_1] \\ \vdots \\ s[n-\tau_M] \end{bmatrix} = \begin{bmatrix} d[n-\tau_1] \\ \vdots \\ d[n-\tau_M] \end{bmatrix} * s[n] = \mathbf{a}[n] * s[n] \; . \tag{4.1}$$

The vector $\mathbf{a}[n] \in \mathbb{R}^M$ contains fractional delay filters (see e.g. [137]), and characterises the direction of the source. Its $z$-transform $\boldsymbol{a}(z) = \sum_n \mathbf{a}[n] z^{-n}$, or short $\boldsymbol{a}(z) \bullet\!\!-\!\!\circ\, \mathbf{a}[n]$, was explained in Sec. 3.2.2.

If the array signal measures a superposition of $K$ source signals $s_k[n]$, each characterised by a steering vector $\boldsymbol{a}_k(z)$, $k = 1 \dots K$, then

$$\mathbf{x}[n] = \sum_{k=1}^{K} \mathbf{a}_k[n] * s_k[n] + \mathbf{v}[n] \tag{4.2}$$

with $\mathbf{v}[n]$ containing independent and identically distributed Gaussian noise. The space-time covariance matrix $\mathbf{R}[\tau] = \mathcal{E}\{\mathbf{x}[n]\mathbf{x}^{\mathrm{H}}[n-\tau]\}$ of the array vector is

$$\mathbf{R}[\tau] = \begin{bmatrix} r_{11}[\tau] & r_{12}[\tau] & \dots & r_{1M}[\tau] \\ r_{21}[\tau] & r_{22}[\tau] & \dots & r_{2M}[\tau] \\ \vdots & \vdots & \ddots & \vdots \\ r_{M1}[\tau]\} & r_{M2}[\tau] & \dots & r_{MM}[\tau] \end{bmatrix}, \tag{4.3}$$

where its elements are auto- and cross-correlation sequences

$$r_{ij}[\tau] = \mathcal{E}\{x_i[n] x_j^*[n-\tau]\} \; . \tag{4.4}$$

The $z$-transform of $\mathbf{R}[\tau]$ gives the cross spectral density (CSD) matrix $\boldsymbol{R}(z) \bullet\!\!-\!\!\circ\, \mathbf{R}[\tau]$,

$$\boldsymbol{R}(z) = \sum_{k=1}^{K} \boldsymbol{a}_k(z) \boldsymbol{a}_k(z) S_k(z) + \mathbf{I}\sigma_v^2 \; , \tag{4.5}$$

where $S_k(z)$ is the power spectral density (PSD) of the $k$th source and $\sigma_v^2$ the noise power due to $\mathbf{v}[n]$ experienced at any array element.

The resulting CSD matrix, $\boldsymbol{R}(z)$ , contains polynomials in its entries

$$\boldsymbol{R}(z) = \begin{bmatrix} R_{11}(z) & R_{12}(z) & \dots & R_{1M}(z) \\ R_{21}(z) & R_{22}(z) & \dots & R_{2M}(z) \\ \vdots & \vdots & \ddots & \vdots \\ R_{M1}(z) & R_{M2}(z) & \dots & R_{MM}(z) \end{bmatrix} \tag{4.6}$$

where

$$R_{ij}(z) = \sum_{\tau=-T_a}^{T_a} r_{ij} z^{-\tau} \tag{4.7}$$

where $T_a \in \mathbb{Z}, T_a \geq 0$ is the support over which auto- and cross-correlation sequences take on finite values.

The type of matrix structure in (4.6) is involved in designing broadband Capon beamformer as will be discussed later in this chapter. Prior to this, let us introduce briefly the Capon solution for the narrowband scenario, before we generalise this formula to the broadband signal processing case using polynomial matrix techniques.

## 4.3 Narrowband Capon Beamformer

In the narrowband case, the above definitions for steering vectors and space-time covariance matrices are evaluated on the unit circle, $z = e^{j\Omega}$, and for a particular normalised angular frequency $\Omega_0$. With this evaluation, the steering vector $\mathbf{a}_k = \boldsymbol{a}_k(e^{j\Omega_0})$ collapses delays to scalar entries implementing phase shifts, and $\mathbf{R} = \boldsymbol{R}(e^{j\Omega_0})$ also contains only constant entries rather than polynomials.

If the array elements are followed by complex weight $w_m$ organised in a vector $\mathbf{w} \in \mathbb{C}^M$, then the LCMV problem minimises the output power

$$\mathbf{w}_{\text{opt}} = \arg\min_{\mathbf{w}} \mathbf{w}^{\text{H}} \mathbf{R} \mathbf{w} \tag{4.8}$$

$$\text{s.t.} \quad \mathbf{C}^{\text{H}} \mathbf{w} = \mathbf{f} \tag{4.9}$$

subject to constraints. Without loss of generality, if the beamformer receives source $k = 1$ as the signal of interest, then in the simplest case, $\mathbf{C} = \mathbf{a}_1$, and $\mathbf{f} = 1$ ensures unit

(i.e. distortionless) gain. If the steering vectors $\mathbf{a}_k$, $k = 2 \dots L \leq K$ of $L$ interfering sources are known, then this knowledge can be embedded as

$$\mathbf{C} = [\mathbf{a}_1,\ \mathbf{a}_2\ \dots\ \mathbf{a}_L] \quad , \qquad \mathbf{f} = \begin{bmatrix} 1 & \underbrace{0\ \dots\ 0}_{L-1} \end{bmatrix} \tag{4.10}$$

in the constraint equation of (4.9).

In order to find the closed form solution to the optimisation problem in (4.8) and (4.9), the Lagrange multiplier method is utilised. Solving the problem based on this method for a single source, with assumption that the constraint is a scalar with unit gain, gives

$$\frac{\partial(\mathbf{w}^{\mathrm{H}}\mathcal{E}\{\mathbf{x}^{\mathrm{H}}\mathbf{x}\} - \mathbf{w} - \beta(\mathbf{w}^{\mathrm{H}}\mathbf{a} - 1))}{\partial \mathbf{w}^{\mathrm{H}}} = \mathbf{R}\mathbf{w} - \beta\mathbf{a} = \mathbf{0} \tag{4.11}$$

where $\beta$ is the Lagrange multiplier. The solution then becomes

$$\mathbf{w} = \beta\mathbf{R}^{-1}\mathbf{a}, \tag{4.12}$$

which is inserted into (4.9) in order to determine $\beta$. Hence

$$\beta = (\mathbf{a}^{\mathrm{H}}\mathbf{R}^{-1}\mathbf{a})^{-1} \tag{4.13}$$

and

$$\mathbf{w}_{\mathrm{opt}} = (\mathbf{a}^{\mathrm{H}}\mathbf{R}^{-1}\mathbf{a})^{-1}\mathbf{R}^{-1}\mathbf{a}. \tag{4.14}$$

If this solution is generalised to more than one source, then

$$\mathbf{w}_{\mathrm{opt}} = \left(\mathbf{C}^{\mathrm{H}}\mathbf{R}^{-1}\mathbf{C}\right)^{-1}\mathbf{R}^{-1}\mathbf{C}\ \mathbf{f}\ , \tag{4.15}$$

which is known as the Capon beamformer. Since the covariance matrix $\mathbf{R}$ can be ill-conditioned, the inversion can be regularised in a number of fashions, see e.g. [16]. Unless the constraint only embraces the look direction $\mathbf{a}_1$, the term $\mathbf{C}^{\mathrm{H}}\mathbf{R}^{-1}\mathbf{C}$ may also be poorly conditioned.

As was mentioned, this beamformer is not sufficient to handle the process of band-

limited or broadband signals, and some amendments and extensions are required. These amendments are considered to deal with the cross-spectral density matrix using polynomial signal processing in the following section.

## 4.4 Polynomial Broadband Capon Beamformer

In the previous chapter, the MVDR optimization problem was discussed, and the design of the GSC broadband beamformer based on this problem formulation was introduced. There, the adaptive filtering technique is manipulated to implicitly satisfy constraints while calculating the weights using some polynomial matrix algebra operations. In this section, the linearly constrained beamformer, also known as the Capon beamformer [138], is used to solve the broadband MVDR problem.

For the definition of the broadband problem, we follow the narrowband formulation in Sec. 4.3 but use broadband instead of narrowband quantities. The beamformer now has to implement a tap-delay-line with impulse responses $w_m[n]$ following every sensor, leading to a filter vector $\mathbf{w}[n] \circ\!\!-\!\!\bullet\, \boldsymbol{w}(z)$, whose aim is to minimise the output power.

The latter can be obtained by integrating over the output PSD, such that the broadband MVDR formulation takes the form

$$\boldsymbol{w}_{\text{opt}}(z) = \arg\min_{\mathbf{w}(z)} \oint_{|z|=1} \boldsymbol{w}^{\text{P}}(z)\boldsymbol{R}(z)\boldsymbol{w}(z)\frac{dz}{z} \tag{4.16}$$

$$\text{s.t.} \quad \boldsymbol{C}^{\text{P}}(z)\boldsymbol{w}(z) = \boldsymbol{f}(z)\ . \tag{4.17}$$

The polynomial constraint matrix $\boldsymbol{C}(z)$ contains in its columns the broadband steering vectors $\boldsymbol{a}_k(z)$, $k = 1 \ldots L$,

$$\boldsymbol{C}(z) = [\boldsymbol{a}_1(z)\ \boldsymbol{a}_2(z)\ \ldots\ \boldsymbol{a}_L(z)]\ . \tag{4.18}$$

It is assumed that $\boldsymbol{a}_1(z)$ points in look direction, and that the remaining columns define

interferers. In this case, the constraining vector takes the form

$$\boldsymbol{f}(z) = \left[F(z) \underbrace{0 \ \ldots \ 0}_{L-1}\right]^{\mathrm{P}}, \tag{4.19}$$

where $F(z)$ is the desired array transfer function in look direction.

In order to verify the performance of the beamformer, in Sec. 4.7, two different simulation scenarios are considered. In the first, ideal case, the space-time covariance matrix $\boldsymbol{R}(z)$ in the algorithm is built based on actual data by using steering vectors, or the true covariance matrix. In contrast, in practical applications, the space-time covariance matrix must be estimated, leading to estimation errors and a perturbation from the true space-time covariance matrix [139].

As a result, the proposed beamformer, on the basis of the true space-time covariance matrix, is implemented in three different ways, based on the parameters that being used to calculate the optimum weight vector. The first relies on the use of SoI's steering vector as constraint, whereas the second additionally uses the steering vectors of interferers. Fig. **??** shows the block diagram associated with this approach. Before looking in depth into details and analysis of implementation procedures, some information that is used to assist in the implementation are discussed in Sec. 4.5 and 4.6 .

## 4.5 Special Considerations

In this section two concerns with the design of the Capon beamformer will be discussed. The first is diagonal loading in order to enhance the numerical stability of a subsequent matrix inversion. The second is specific to the broadband case and consists of forming steering vectors for signals with highpass characteristic for the interferers in order to create a solvable problem, noting that a beamformer possesses no spatial discrimination at DC, which we assume to be occupied by the SoI.

### 4.5.1 Diagonal Loading

For matrix inversion, diagonal loading or regularisation plays an important role. It provides a remedy to the inversion of a matrix that is either poorly conditioned or even

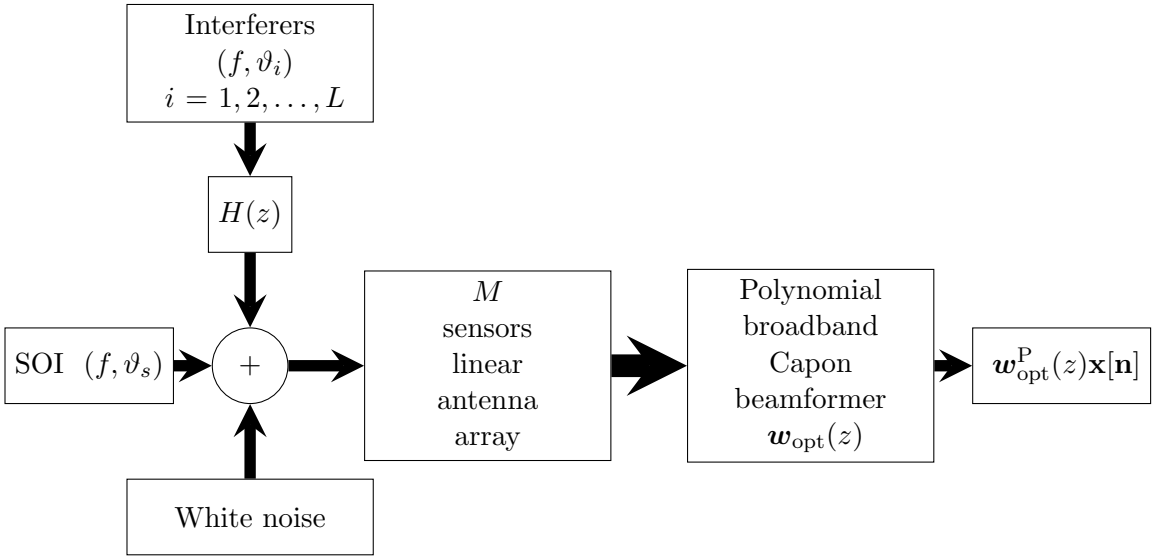


Figure 4.1: The block diagram associated with the design of the polynomial Capon beamformer.

singular otherwise.

In array processing, diagonal loading can be applied for LCMV beamformer computation, since it enhances the beamformer robustness against AoA mismatch, for example, due to inaccuracy of the steering vector, and also helps to achieve better control over the sidelobe response [140, 141].

This concept involves adding a scaled identity matrix $\sigma\mathbf{I}$ to the space-time covariance or CSD matrix, where the value of the scaling parameter $\sigma^2$ is small compared to the received signal variance,

$$\boldsymbol{R}_L(z) = \boldsymbol{R}(z) + \sigma^2\mathbf{I}. \tag{4.20}$$

The scaled identity matrix transfers itself to the para-Hermitian matrix eigenvalue decomposition of the CSD matrix $\boldsymbol{R}_L(z)$,

$$\boldsymbol{R}_L(z) = \boldsymbol{U}(z)\boldsymbol{\Lambda}(z)\boldsymbol{U}^{\text{P}}(z)\ . \tag{4.21}$$

The result will be the addition of $\sigma$ to eigenvalues without impacting the eigenvectors,

$$\boldsymbol{\Lambda}(z) = \text{diag}\{\lambda_1(z) + \sigma, \lambda_2(z) + \sigma, \ldots, \lambda_M(z) + \sigma\} \; . \tag{4.22}$$

The value of $\sigma_L^2$ depends on available information about noise power, where it is bounded by its value as follows [18]

$$\sigma_w^2 \leq \sigma_L^2 < 10\sigma_w^2, \tag{4.23}$$

however, the upper bound might vary from the one in (4.23) since it is application dependent [18].

Hence the LCMV problem becomes

$$\boldsymbol{w}_{\text{opt}}(z) = \arg\min_{\boldsymbol{w}} \boldsymbol{w}^{\text{P}}(z)\boldsymbol{R}_L(z)\boldsymbol{w}(z) \tag{4.24}$$

$$\text{s.t.} \quad \boldsymbol{C}^{\text{P}}(z)\boldsymbol{w}(z) = \boldsymbol{f}(z) \; , \tag{4.25}$$

and the optimum weight vector as a solution to this optimisation problem is

$$\boldsymbol{w}_{\text{opt}}(z) = \boldsymbol{R}_L(z)^{-1}\boldsymbol{C}(z)\left(\boldsymbol{C}^{\text{P}}(z)\boldsymbol{R}_L(z)^{-1}\boldsymbol{C}(z)\right)^{-1}\boldsymbol{f}(z) \; . \tag{4.26}$$

The regularisation introduces a bias term compared to a solution with $\sigma_L = 0$, but will stabilise the inverse operations in (4.26), as will be further explored in Sec. 4.6.

### 4.5.2 Bandpass Interferers

Different from a narrowband beamformer, the broadband formulation may include components at DC. While this may be suppressed in an implementation, at DC the general constraint matrix $\boldsymbol{C}(z)$ becomes rank one as $z \longrightarrow 1$, whereas $\mathbf{f}(z)$ imposes two inconsistent equations in the case $L > 1$. One solution to this is to modify the broadband steering vectors of interferering sources, $\boldsymbol{a}_k(z)$, $k = 2 \ldots L$, to have a bandpass characteristic. As an example, we may impose a bandpass transfer function $H(z)$ which extends over, say, around 70% of the normalised frequency band, from 0.2 to 0.9. Such

that

$$\bar{\boldsymbol{a}}_k(z) = H(z)\boldsymbol{a}_k(z), k = 2 \dots L \tag{4.27}$$

and (4.18) which then becomes

$$\bar{\boldsymbol{C}}(z) = [\boldsymbol{a}_1(z)\ \bar{\boldsymbol{a}}_2(z)\ \dots\ \bar{\boldsymbol{a}}_L(z)]\ . \tag{4.28}$$

The MVDR problem is obtained by extending (4.15) to a polynomial notation

$$\boldsymbol{w}_{\text{opt}}(z) = \boldsymbol{R}^{-1}(z)\bar{\boldsymbol{C}}(z)\boldsymbol{\beta}(z) \tag{4.29}$$

with $\boldsymbol{\beta}(z)$ a normalisation factor that is defined as

$$\boldsymbol{\beta}(z) = \left(\bar{\boldsymbol{C}}^{\text{P}}(z)\boldsymbol{R}^{-1}(z)\bar{\boldsymbol{C}}(z)\right)^{-1}\boldsymbol{f}(z)\ . \tag{4.30}$$

As stated in Sec. 4.3 this is known as the Capon beamformer, but it is now represented in its polynomial format to be adequate for a broadband beamformer application.

The inversions in (4.29) and (4.30) are performed on para-Hermitian matrix terms $\boldsymbol{R}(z)$ and $\boldsymbol{C}^{\text{P}}(z)\boldsymbol{R}^{-1}(z)\boldsymbol{C}(z)$, which is addressed in the following section, extending work in [142].

## 4.6 Inversion of the Space-Time Covariance Matrix

From (4.17) the power spectrum of the array output is a result of multiplication between the weight vector and a space-time covariance matrix, which in this case has entries in polynomial form. Also, from (4.29) the optimum weight vector in the minimum mean square error sense requires the inversion of this space-time covariance matrix.

The space-time covariance matrix is, in general term, either symmetric or Hermitian for real or complex-valued array signals $\mathbf{x}[n]$, respectively. Because it is built form broadband signals, the autocorrelation and the cross-correlation sequences constituting the space time covariance matrix force this symmetry. In the $z$-domain, this symmetry of the space time covariance matrix translates into a para-Hermitian property, where

$\boldsymbol{R}^{\mathrm{P}}(z) = \boldsymbol{R}^{\mathrm{H}}(1/z^*) = \boldsymbol{R}(z)$ [80] holds in analogy to the Hermitian property of narrowband, instantaneous covariance matrices.

The inversion of such a matrix was attempted in [142] based on the polynomial eigenvalue decomposition (PEVD) algorithm to approximate the inversion of the para-Hermitian matrix such that

$$\boldsymbol{R}(z)\boldsymbol{R}^{-1}(z) \approx \mathbf{I}\,. \tag{4.31}$$

The PEVD decomposes the para-Hermitian matrix into a product of a diagonal matrix and two para-unitary matrices. Such that

$$\boldsymbol{R}(z) \approx \boldsymbol{Q}(z)\boldsymbol{\Lambda}(z)\boldsymbol{Q}^{\mathrm{P}}(z)\,. \tag{4.32}$$

The columns of a para-unitary matrix are orthogonal vectors with unit length, or in other words they are orthonormal, such that

$$\boldsymbol{Q}(z)\cdot\boldsymbol{Q}^{\mathrm{P}}(z) = \boldsymbol{Q}^{\mathrm{P}}(z)\boldsymbol{Q}(z) = \mathbf{I} \tag{4.33}$$

or

$$\boldsymbol{Q}^{-1}(z) = \boldsymbol{Q}^{\mathrm{P}}(z). \tag{4.34}$$

Taking these properties into consideration facilitates the inversion of $\boldsymbol{R}(z)$ simply via the inversion of a diagonal matrix

$$\boldsymbol{R}(z)^{-1} \approx \boldsymbol{Q}(z)\boldsymbol{\Lambda}^{-1}(z)\boldsymbol{Q}^{\mathrm{P}}(z)\,. \tag{4.35}$$

where

$$\boldsymbol{\Lambda}(z) \cong \mathrm{diag}[\lambda_1(z),\ \ldots,\ \lambda_M(z)]\,, \tag{4.36}$$

contains the spectrally majorised polynomial eigenvalues of $\boldsymbol{R}(z)$. Thus, the inversion of the cross-spectral density matrix $\boldsymbol{R}(z)$ requires the inversion of its polynomial eigenvalues $\lambda_m(z)$, $m = 1, \cdots, M$.

The inversion of the polynomial eigenvalues can be accomplished by means of spectral factorisation. Since $\boldsymbol{\Lambda}(z)$ is a para-Hermitian matrix with $\boldsymbol{\Lambda}(z) = \boldsymbol{\Lambda}^{\mathrm{P}}(z)$, the same

holds for the polynomial eigenvalues, such that $\lambda_m(z) = \lambda_m^{\mathrm{P}}(z)$, $m = 1 \dots M$, i.e. they are identical to their complex-conjugated and time-reversed copies. In fact, the eigenvalues therefore are Laurent polynomials (i.e. they contain both positive and negative powers of $z$), such that

$$\lambda_m(z) = \sum_{\tau=-N}^{N} \lambda_m[\tau] z^{-\tau} \tag{4.37}$$

with $\lambda_m[\tau] = \lambda_m^*[-\tau]$ fulfilling the properties of an auto-correlation sequence. Because of its symmetry in (4.37), $\lambda_m(z)$ is a zero-phase system that permits a spectral factorisation

$$\lambda_m(z) = \lambda_{m,\min}(z)\lambda_{m,\max}(z) = \lambda_{m,\min}(z)\lambda_{m,\min}^{\mathrm{P}}(z) \; . \tag{4.38}$$

where $\lambda_{m,\min}(z)$ and $\lambda_{m,\max}(z)$ are the minimum and the maximum phase components of $\lambda_m(z)$, respectively.

The direct inverse of the maximum phase component $\lambda_{m,\max}(z)$ leads to a causal but unstable system. Since, as intimated in (4.38),

$$\lambda_{m,\max}(z) = \lambda_{m,\min}^{\mathrm{P}}(z) \; , \tag{4.39}$$

and therefore $\left(\lambda_{m,\min}^{\mathrm{P}}(z)\right)^{-1} = \left(\lambda_{m,\min}^{-1}(z)\right)^{\mathrm{P}}$, the inverse of $\lambda_m(z)$ turns into the inversion of the time-reversed and therefore anti-causal minimum phase system terms only, such that

$$\lambda_m^{-1}(z) = \lambda_{m,\min}^{-1}(z) \left(\lambda_{m,\min}^{-1}(z)\right)^{\mathrm{P}} \; . \tag{4.40}$$

By assuming $N < \infty$ and writing $\lambda_{m,\min}(z)$ in terms of its $N$ roots,

$$\lambda_{m,\min}(z) = \prod_{n=1}^{N} (1 - \alpha_n z^{-1}) \; , \tag{4.41}$$

the first order sections of each term $(1 - \alpha_n z^{-1})$ on the right hand side can be inverted separately, such that

$$\lambda_{m,\min}^{-1}(z) = \prod_{n=1}^{N} \frac{1}{1 - \alpha_n z^{-1}} \; . \tag{4.42}$$

This inversion can be accomplished using the geometric series expansions, since $|\alpha_n| <$

1, $n = 1 \dots N$ because of $\lambda_{m,\min}(z)$ being minimum phase. With adequate lengths $L$ in time domain,

$$\frac{1}{1-\alpha_n z^{-1}} \approx \sum_{\ell=0}^{L} \alpha_n^{\ell} z^{-\ell} \,. \tag{4.43}$$

Therefore, as proposed in [142], the overall inverse can be approximated as

$$\lambda_m^{-1}(z) \approx \prod_{n=1}^{N} \sum_{\ell=0}^{L} \alpha_n^{\ell} z^{-\ell} \prod_{n=1}^{N} \sum_{\ell=0}^{L} (\frac{1}{\alpha_n})^{\ell} z^{\ell} \,. \tag{4.44}$$

The evaluation of (4.44) is performed in the time domain, with the coefficients of the geometric series convolved for each of the first order sections. Noting that the geometric series of the different terms $\alpha_n$, $n = 1 \dots N$ decay at different rates, truncating every first order term after $L$ coefficients is suboptimal. Therefore, this thesis proposes an enhanced approach below.

An alternative approach to (4.44) relies also on the spectral factorisation of $\lambda_{m,\min}(z)$, but facilitates the process of computing its inverse via a partial fraction expansion based on the residue theorem [46], such that (assuming that there is no multiplicity of roots)

$$\lambda_{m,\min}^{-1}(z) = \prod_{n=1}^{N} \frac{1}{1-\alpha_n z^{-1}} = \sum_{n=1}^{N} \frac{\rho_n}{1-\alpha_n z^{-1}} \tag{4.45}$$

Therefore,

$$\hat{\lambda}_{m,\min}^{-1}(z) \approx \sum_{n=1}^{N} \rho_n \sum_{\ell=0}^{L} \alpha_n^{\ell} z^{-\ell} \tag{4.46}$$

is a better length-$L$ approximation of $\lambda_{m,\min}^{-1}(z)$, and

$$\lambda_m^{-1}(z) = \left( \sum_{n=1}^{N} \rho_n \sum_{\ell=0}^{L} \alpha_n^{\ell} z^{-\ell} \right) \left( \sum_{n=1}^{N} \rho_n^{*} \sum_{\ell=0}^{L} (\alpha_n^{*})^{\ell} z^{-\ell} \right) \tag{4.47}$$

will possess a better accuracy than (4.44) for the same support.

For example, let us consider an eigenvalue with power spectral density

$$\lambda_m(z) = \frac{1}{5} z^2 - 1\frac{4}{25} z + 2 - 1\frac{4}{25} z^{-1} + \frac{1}{5} z^{-2} \,,$$

which is depicted in Fig. 4.2. This eigenvalue can be factored into multiplication of first order terms as in (4.38), which produces

$$\lambda_m(z) = (1 - \frac{1}{5}z^{-1})(1 - \frac{4}{5}z^{-1})(1 - 5z^{-1})(1 - \frac{5}{4}z^{-1})$$

that consists of minimum and maximum phase terms. By referring to (4.39), the maximum phase component can be replaced by its reciprocal which relates to the complex conjugate and time reverse of the minimum phase term

$$\lambda_{m,\max\_1}(z) = (1 - \frac{1}{5}z),$$

and

$$\lambda_{m,\max\_2}(z) = (1 - \frac{4}{5}z).$$

Consequently, the inverse of $\lambda_m(z)$ based on (4.43) and (4.44) is a multiplication of polynomials as

$$\lambda_m^{-1}(z) \approx \left(\sum_{l=0}^{40}(-\frac{1}{5})^l z^{-l} \sum_{l=0}^{40}(-\frac{4}{5})^l z^{-l}\right)\left(\sum_{l=0}^{40}(-\frac{1}{5})^l z^{l} \sum_{l=0}^{40}(-\frac{4}{5})^l z^{l}\right) , \tag{4.48}$$

with $L = 40$ the selected approximation order. The ultimate result of the inverse of $\lambda_m(z)$, when convolution is used can be seen in Fig. 4.3.

We now move to the residue method to find the polynomial inverse based on (4.47). The partial fraction expansion is employed to obtain the coefficient $\rho_n$ associated with $\lambda_{m,min}^{-1}(z)$ . For this example $\rho_n = \{-\frac{5}{3}, \frac{5}{3}\}$, $n = 1, 2$, therefore

$$\lambda_m^{-1}(z) = \left(-\frac{5}{3}\sum_{l=0}^{40}(-\frac{1}{5})^l z^{-l} + \frac{5}{3}\sum_{l=0}^{40}(-\frac{4}{5})^l z^{-l}\right)^2 , \tag{4.49}$$

which is plotted in Fig. 4.4.

An assessment to the inversion process of $\lambda_m(z)$ can be accomplished by multiplying the eigenvalue by its inverse, which ideally results in an impulse. For the above example, the results for both approximation approaches are shown in Fig. 4.5, which demonstrates a closer match to an impulse and hence a lower estimation error when

applying the residue method.

## 4.7 Implementation Methods

In the LCMV beamformer, based on the available information about the direction and statistics of the SoI, interferences and noise, the optimum weight vector can be obtained in several ways as explained in the following experiments.

### Experiment-1

If AoAs of any interferences are unknown and the desired response in look direction is unity, then the constraint in (4.17) simplifies to

$$\boldsymbol{a}_1^{\mathrm{P}}(z)\boldsymbol{w}(z) = 1\ . \tag{4.50}$$

However, in this case, since $\boldsymbol{a}_1(z)$ contains — potentially fractional — delays, a $\boldsymbol{w}(z)$ satisfying (4.50) is likely non-causal, and the inclusion of a delay will be required to force a viable solution $\boldsymbol{w}_{\mathrm{opt}}(z)$ in (4.26). In this case, the space time covariance matrix is

$$\boldsymbol{R}(z) = \boldsymbol{a}_1(z)\boldsymbol{a}_1^{\mathrm{P}}(z) + \sum_{l=2}^{L} \bar{\boldsymbol{a}}_l(z)\bar{\boldsymbol{a}}_l^{\mathrm{P}}(z) + \sigma_v\mathbf{I};\,, \tag{4.51}$$

and the desired weight vector of the MVDR problem can be found by substituting the constraints matrix, $\mathbf{C}(z)$, in (4.26) by the steering vector of the direction of interest,$\boldsymbol{a}_1(z)$. Hence, the LMVDR weights are

$$\boldsymbol{w}_{\mathrm{opt}}(z) = \boldsymbol{R}(z)^{-1}\boldsymbol{a}_1(z)\left(\boldsymbol{a}_1^{\mathrm{P}}(z)\boldsymbol{R}(z)^{-1}\boldsymbol{a}_1(z)\right)^{-1}\boldsymbol{f}(z)\ . \tag{4.52}$$

### Experiment-2

The generalisation of experiment-1 is when the beamformer vector is computed by using (4.29), then the constraint matrix $\bar{\boldsymbol{C}}(z)$ in (4.28) consist of steering vectors of the signals that illuminate the antenna array, and the space time covariance matrix is

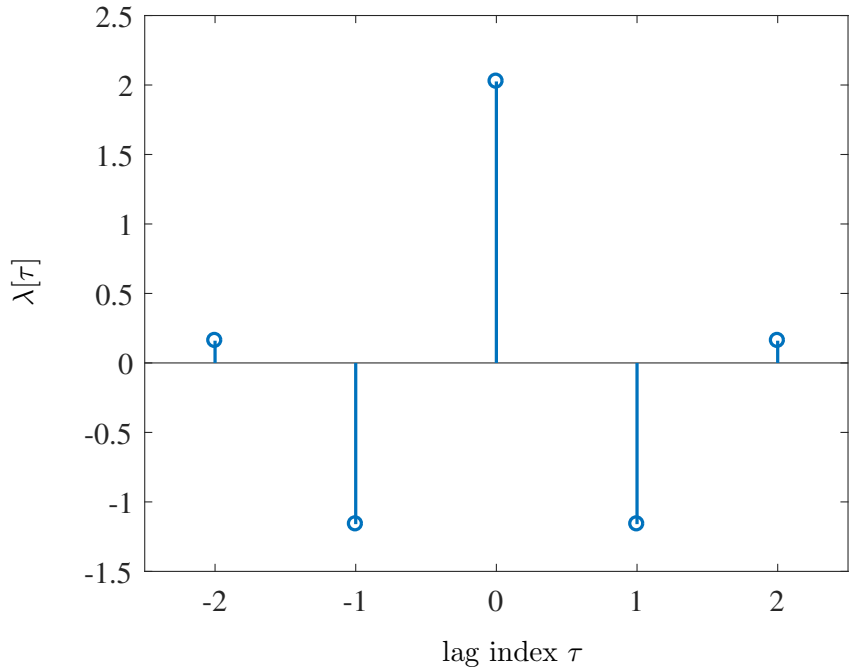


Figure 4.2: Example for a Laurent polynomial eigenvalue $\lambda_m^{-1}[\tau]$

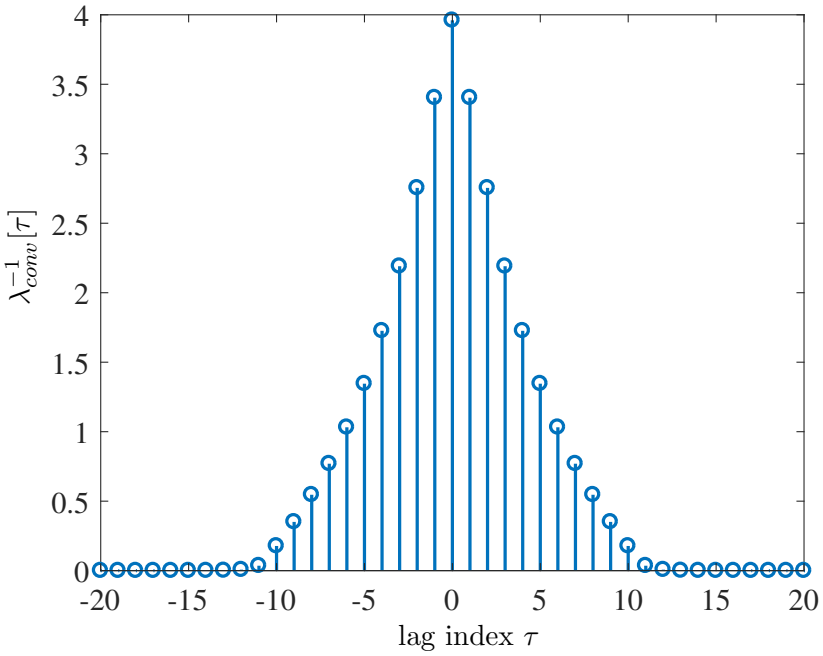


Figure 4.3: Inverse of $\lambda_m^{-1}[\tau]$ in (4.48)

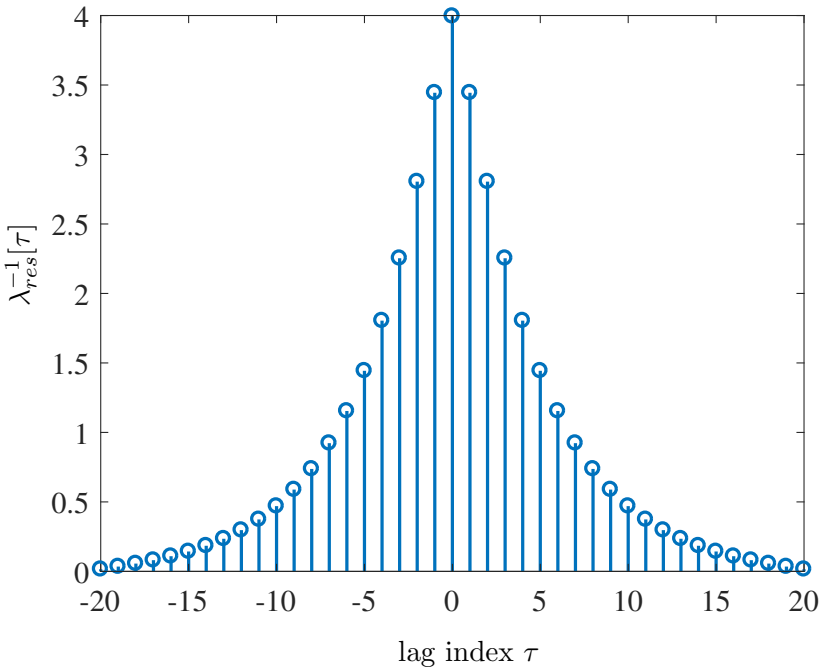


Figure 4.4: Inverse of $\lambda_m^{-1}[\tau]$ in (4.49)

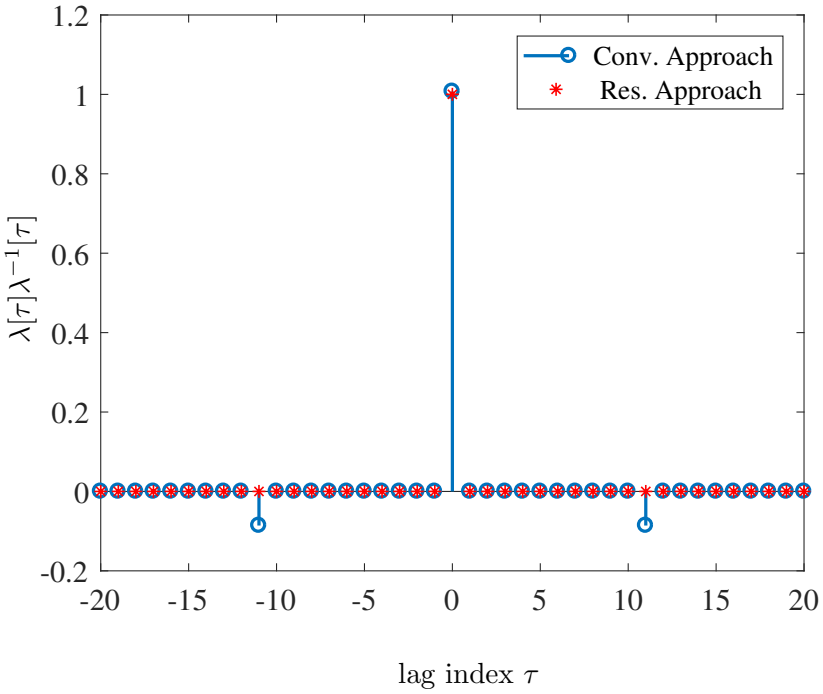


Figure 4.5: The result of multiplying $\lambda_m[\tau]$ with its inverse.

the same as defined in (4.51). thereby

$$\boldsymbol{w}_{\text{opt}}(z) = \boldsymbol{R}^{-1}(z)\bar{\boldsymbol{C}}(z)\left(\bar{\boldsymbol{C}}^{\text{P}}(z)\boldsymbol{R}^{-1}(z)\bar{\boldsymbol{C}}(z)\right)^{-1}\boldsymbol{f}(z)\ .$$

In above examples, the space-time covariance matrix constructed from the combination of SOI with interference and noise. However, this might not be the case on every occasion as the next example demonstrates.

### Experiment-3

Within the same framework, in contrast to the method that depends on the knowledge of signal of interest, the optimum weight vector can also be implemented even with the absence of SOI but with knowledge of its steering vector. In this case $\boldsymbol{R}(z)$ is only a result from interference and noise as [18]

$$\boldsymbol{R}_{i+n}(z) = \sum_{l=2}^{L} \bar{\boldsymbol{a}}_l(z)\bar{\boldsymbol{a}}_l^{\text{P}}(z) + \sigma_v\mathbf{I}. \tag{4.53}$$

Hence,the consequent weight vector, with analogy to the concept in scenario 1, is

$$\boldsymbol{w}_{\text{opt}}(z) = \boldsymbol{R}_{i+n}^{-1}(z)\boldsymbol{a}_1(z)\left(\boldsymbol{a}_1^{\text{P}}(z)\boldsymbol{R}_{i+n}^{-1}(z)\boldsymbol{a}_1(z)\right)^{-1}\boldsymbol{f}(z)\ , \tag{4.54}$$

or in general as in (4.29) and (4.30) with $\boldsymbol{R}(z)$ substituted by $\boldsymbol{R}_{i+n}(z)$ in both equation, and the constraint is the steering vector of the desired source, $\boldsymbol{a}_1(z)$. The simulation results of each of these experiments are going to be discussed in Sec. 4.8.

## 4.8 Numerical Examples

To provide some examples for the polynomial Capon beamformer based on the experiments in Sec. 4.7, we assume that four sources illuminate an $M = 8$ element linear equispaced sensor array. The signal of interest is located at 30° off broadside with unit variance ($\sigma_s = 1$) , and interferers with -20dB SIR are located at angles $\vartheta = \{-40°, -10°, 70°\}$. These interferers have a highpass PSD with a lower passband

edge at $\Omega = \frac{\pi}{10}$. Additionally, the array data is corrupted by additive white Gaussian noise (AWGN) with 30dB SNR.

In these examples we assumed precise knowledge of the true space-time covariance matrix, $\boldsymbol{R}(z)$, in (4.25). The LCMV beamformer involves the inverse $\boldsymbol{R}^{-1}(z)$, which, herein, is calculated via the SMD algorithm in [89] following the procedure in [142] but enhanced using the residue method in Sec. 4.6. helps to regularise the inversion of $\boldsymbol{R}(z)$. The broadband steering vectors that are used to construct the space-time covariance matrix have an order of 50. The simulation procedures are described in the flow chart depicted in Fig. 4.6.

### Numerical Evaluation of Experiment-1:

The PBBF in (4.29) is simulated in which the interfering sources are omitted from the problem formulation, and the Capon beamformer only requires a correction by the scalar term, which we refer to as a correction term in later sections, $\boldsymbol{a}_1^{\mathrm{P}}(z)\boldsymbol{R}^{-1}(z)\boldsymbol{a}_1(z)$, which is shown in Fig. 4.7. The beamformer has a polynomial order of 200, and a gain response as shown in Fig. 4.8, with a gain to look direction shown in Fig. 4.10 indicating a distortion-less response across almost the entire spectrum, and the interferers are appropriately attenuated. However, additional diagonal loading $\sigma_L^2$ with a value of 16 dB above the AWGN level, to the space-time covariance matrix, $\boldsymbol{R}(z) + \sigma_t^2\mathbf{I}$ where $\sigma_t^2 = \sigma_L^2 + \sigma_w^2$, produces a PBBF with a polynomial order of 206, and a beam pattern as shown in Fig. 4.9 with a correction term in Fig.4.7.

### Numerical Evaluation of Experiment-2:

For our second scenario the same calculation in (4.29) is applied for more extensive constraints with $L = 3$, which requires an additional regularisation to evaluate

$$(\boldsymbol{C}^{\mathrm{P}}(z)\boldsymbol{R}^{-1}(z)\boldsymbol{C}(z) + \epsilon\mathbf{I})^{-1}, \tag{4.55}$$

with $\epsilon \ll 1$, with a value of "$\epsilon$" as it is defined in *Matlab*. The result is a Capon beamformer of polynomial order 260. Fig. 4.11 shows the gain response of this beam-

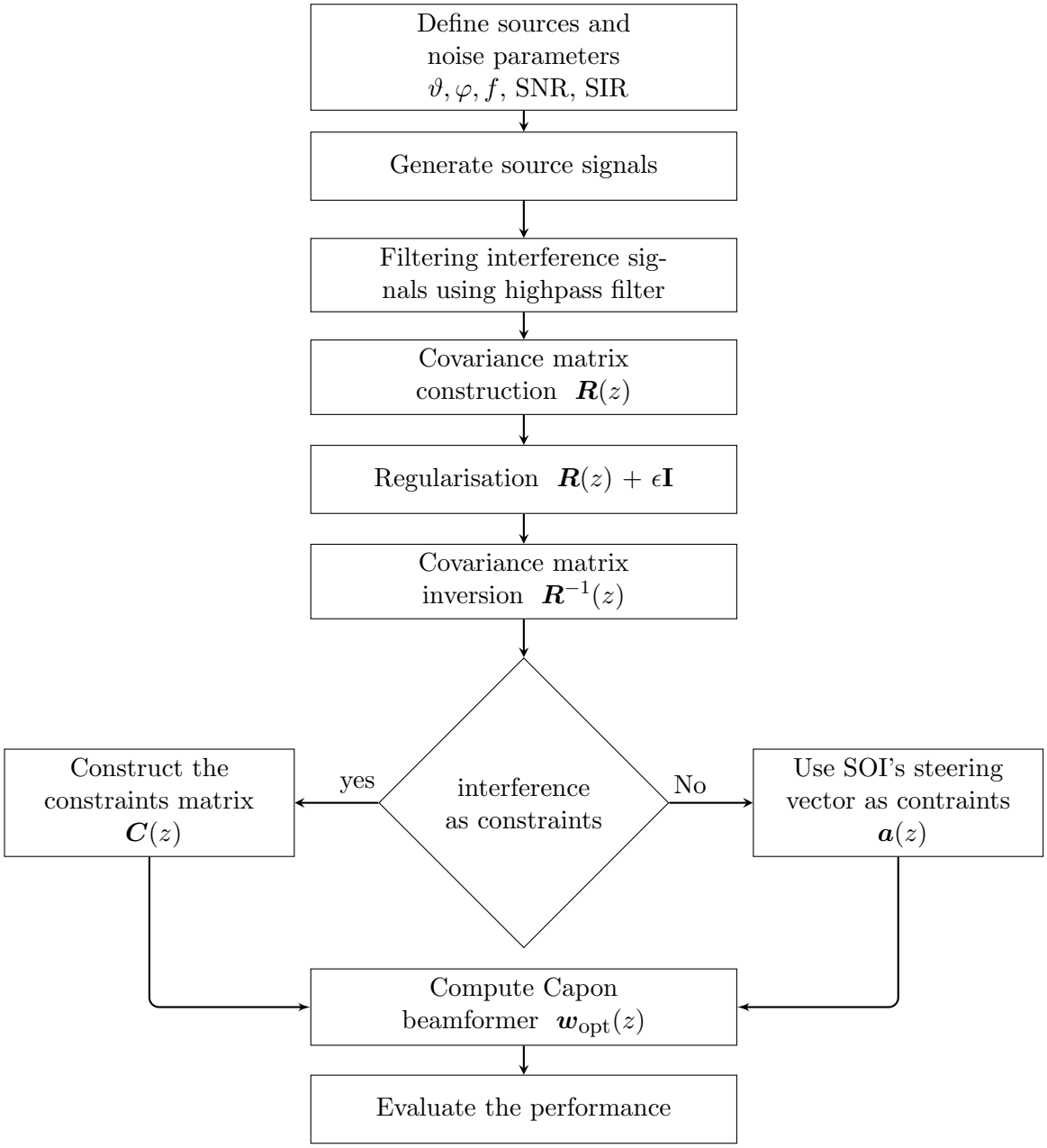


Figure 4.6: Polynomial Capon Beamformer simulation flowchart.

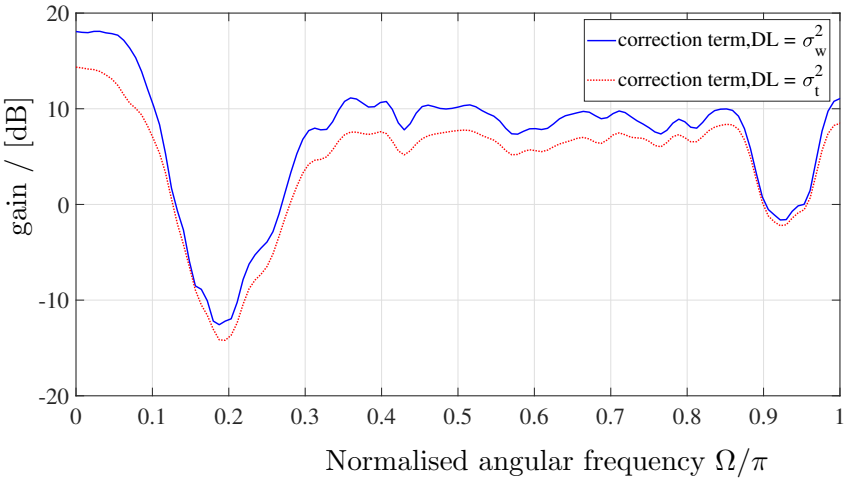


Figure 4.7: Gain of correction term.

former when the covariance matrix is diagonally loaded $\sigma_t^2$ with the same value as in the previous scenario, a suitable suppression of the highpass interferers and a lower sidelobe level is obtained from this approach with comparison to the PBBF in scenario 1, as it can be seen from Fig. 4.13 (a) .

### Numerical Evaluation of Experiment-3:

In the third experiment where the interference and noise signals used for space time covariance matrix $\boldsymbol{R}_{i+n}(z)$, and the beamformer achieved by (4.54). The beamformer in this case has a polynomial order of 189 and 186 with DL = $\sigma_w^2$ and with DL = $\sigma_t^2$ respectively, and its gain response for DL = $\sigma_t^2$ is shown in Fig. 4.12.

Fig. 4.13 shows a comparison among the beam patterns, at 0.5 of the normalised frequency, for scenarios in Sec. 4.7. This for regularising $\boldsymbol{R}(z)$ by $\sigma_w^2$ = -30 dB and also with additional diagonal loading with a value of $\sigma_L^2$. It can be seen that with an extra loading to the diagonal of the space-time covariance matrix using $\sigma_L^2$, an improvement fulfilled in the beamformer performance in terms of sidelobe level reduction. A numerical summary of this comparison is provided in Tab. 4.1.

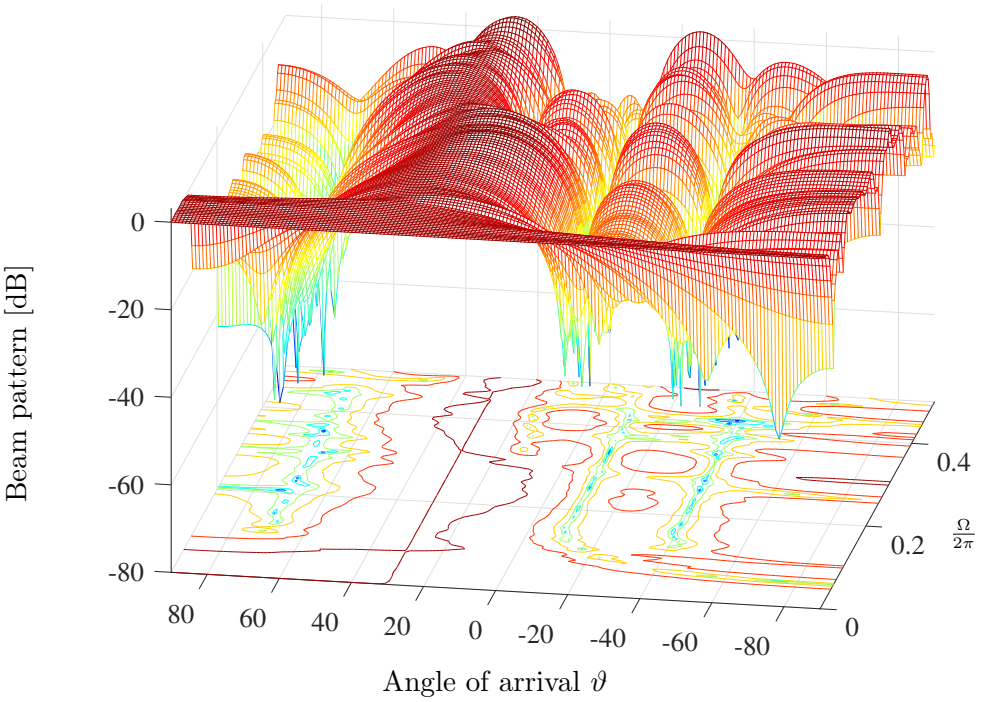


Figure 4.8: Directivity pattern of polynomial Capon beamformer, experiment (1) with DL = $\sigma_w$.

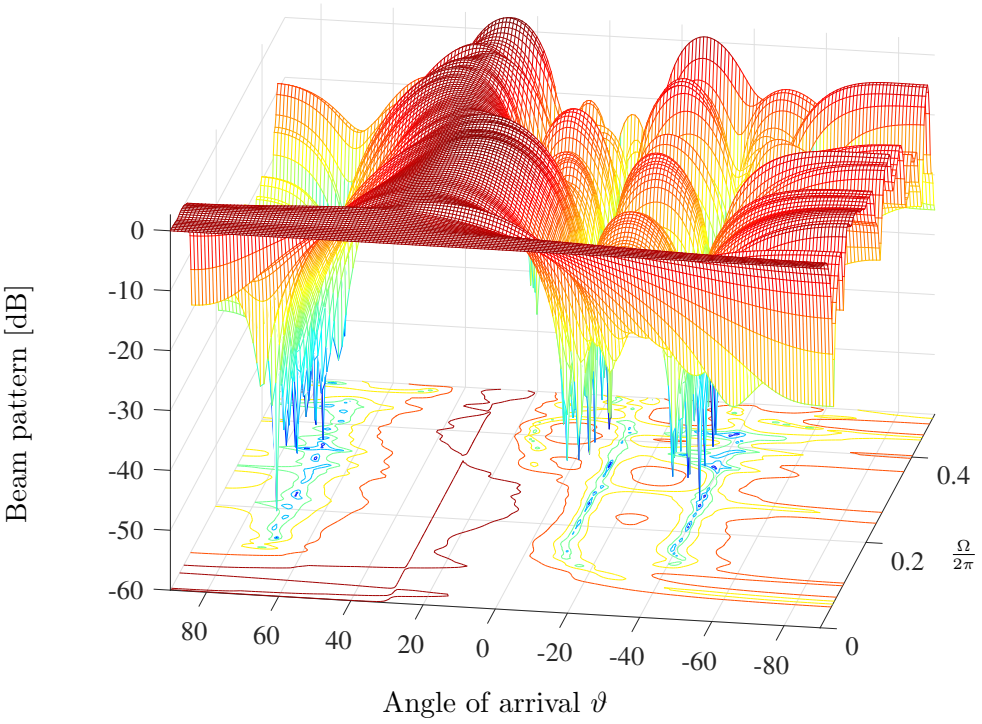


Figure 4.9: Directivity pattern of polynomial Capon beamformer, experiment (1) with DL = $\sigma_t$ .

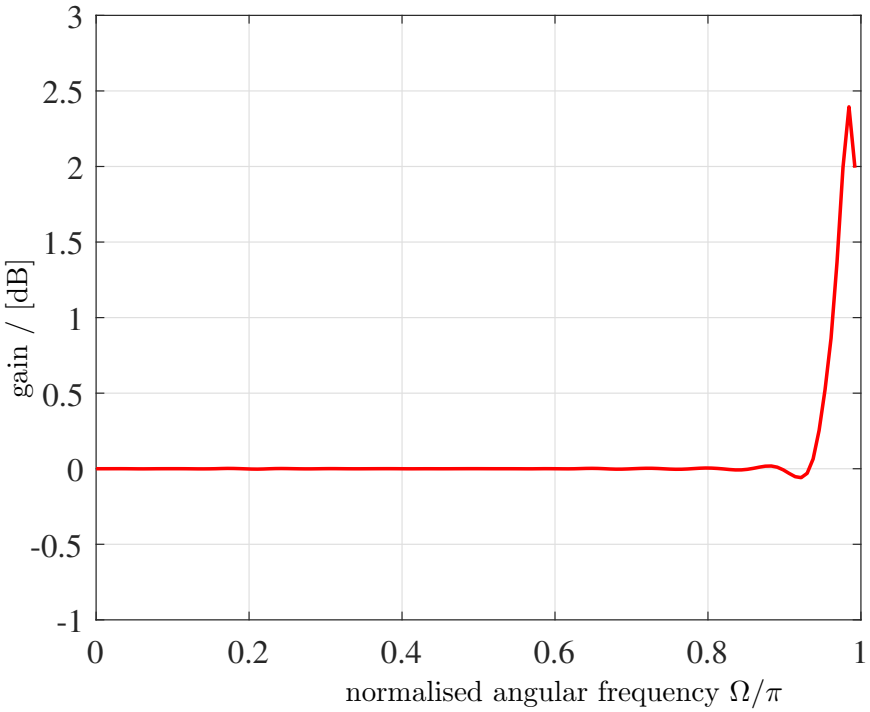


Figure 4.10: Gain in look direction for scenario (1) with DL = $\sigma_w$.

Table 4.1: A comparison of the performance of implementation methods based on their beam pattern.

| Example NO | DL | Constraints | STC matrix | SL suppression [dB]at $\vartheta = -25°$ | Null depth [dB] | | |
|---|---|---|---|---|---|---|---|
| | | | | | $-40°$ | $-10°$ | $70°$ |
| 1 | $\sigma_w^2$ | $\boldsymbol{a}_1(z)$ | $\boldsymbol{R}(z)$ | - | $-40$ | $-47$ | $-33$ |
| 3 | $\sigma_w^2$ | $\boldsymbol{a}_1(z)$ | $\boldsymbol{R}_{i+n}(z)$ | 9.84 | $-35$ | $-50$ | $-43$ |
| 1 | $\sigma_t^2$ | $\boldsymbol{a}_1(z)$ | $\boldsymbol{R}(z)$ | 1.9 | $-40$ | $-50$ | $-35$ |
| 2 | $\sigma_t^2$ | $\bar{\boldsymbol{C}}(z)$ | $\boldsymbol{R}(z)$ | 7.79 | $-53$ | $-47$ | $-62$ |
| 3 | $\sigma_t^2$ | $\boldsymbol{a}_1(z)$ | $\boldsymbol{R}_{i+n}(z)$ | 10.9 | $-35$ | $-47$ | $-43$ |

From Tab. 4.1 and Fig.4.13 it can be noticed that among the scenarios, the beamformer in the third case offers the best main-lobe resolution and side-lobe level, defined in Sec. 2.2, suppression but the lowest of null depth in both cases when DL = $\sigma_w^2$ and $\sigma_t^2$. But the beamformer with extensive constraints, as in the second example, when diagonally loaded with $\sigma_t^2$ attenuates the interference more which results in deeper nulls.

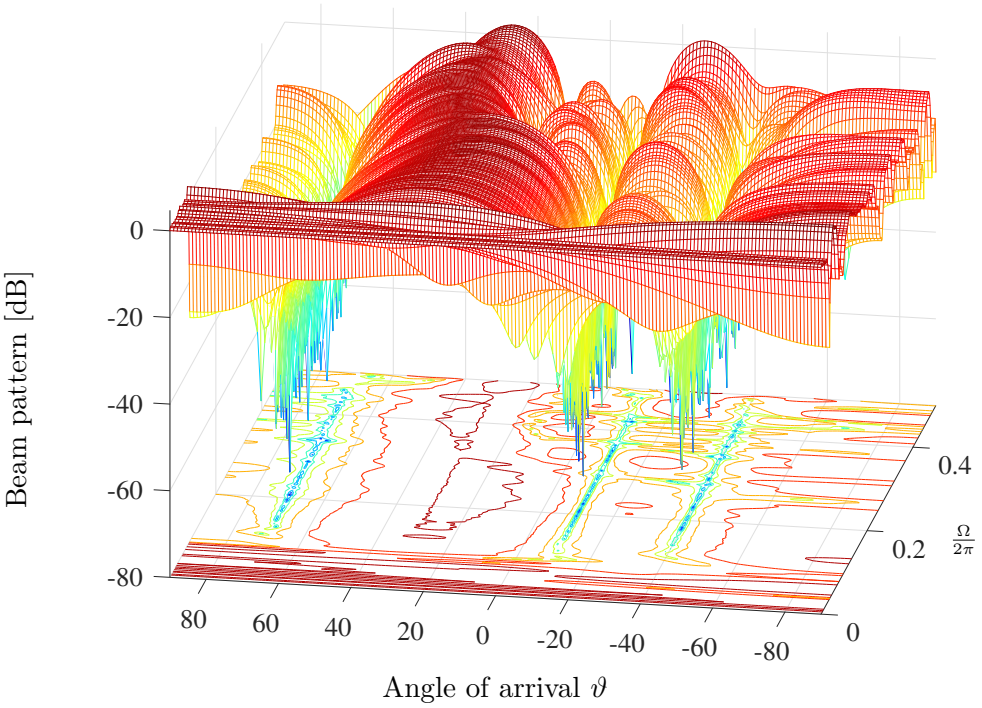


Figure 4.11: Directivity pattern of polynomial Capon beamformer, experiment (2) with DL = $\sigma_t$ .

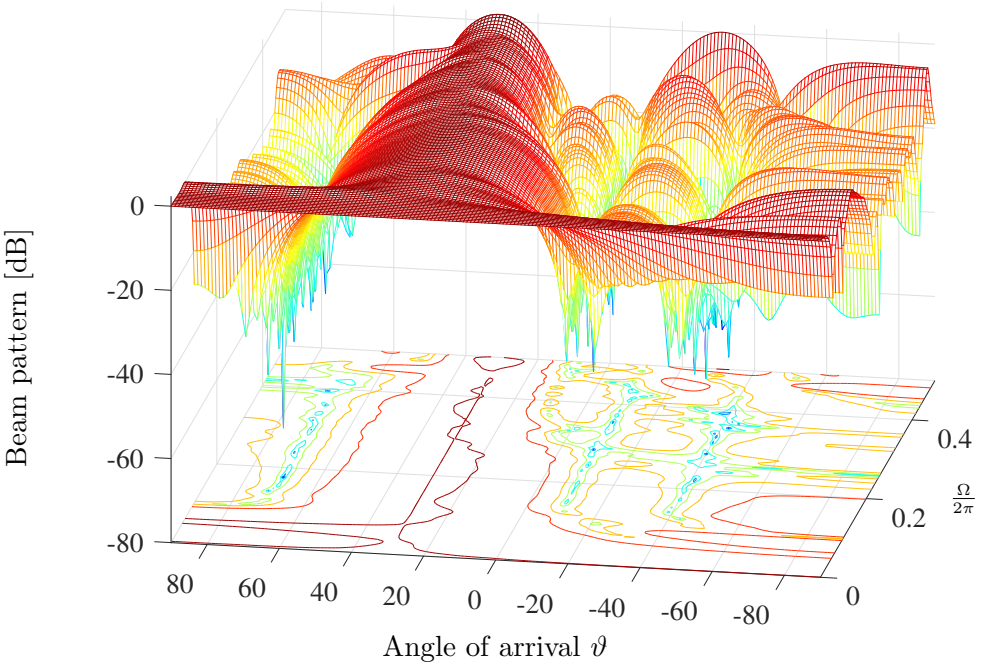


Figure 4.12: Directivity pattern of polynomial Capon beamformer, experiment (3) with DL = $\sigma_t$ .

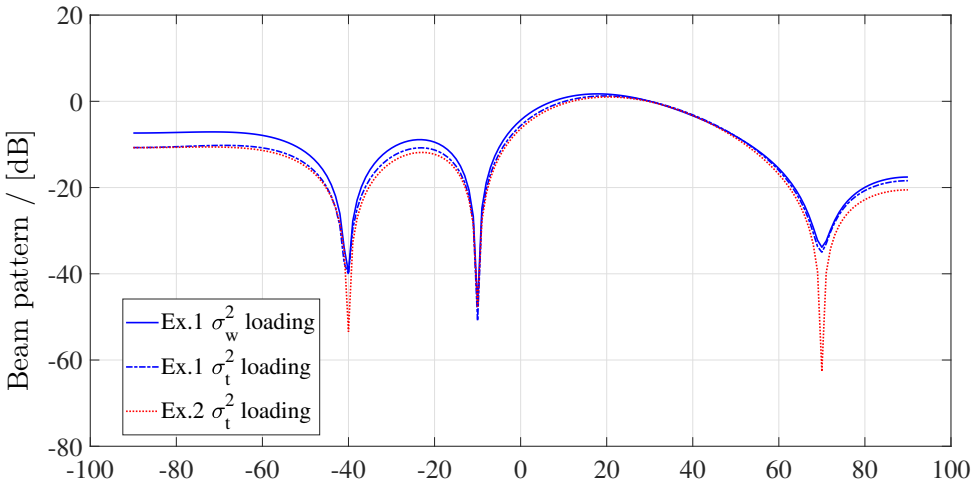


(a)

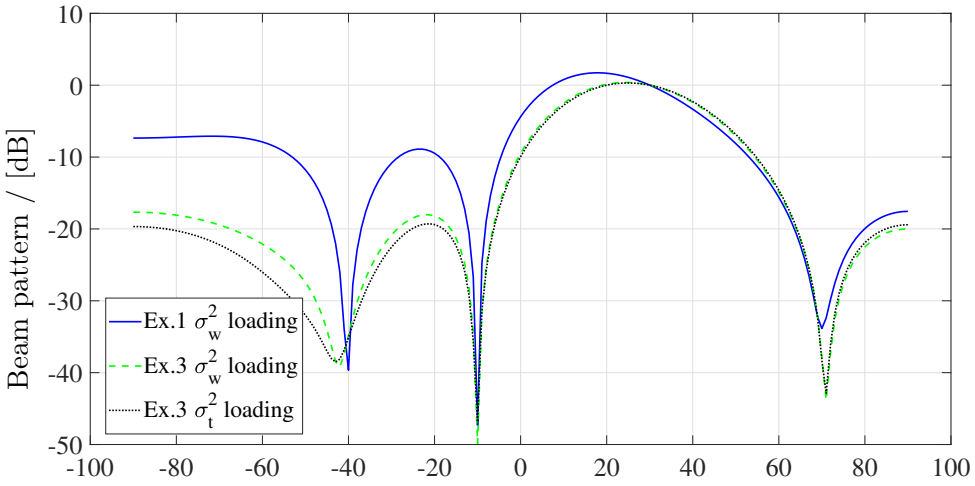


(b)

Figure 4.13: A comparison of a cross-section of the beam patterns among the examples in Sec.4.7 at $\Omega = \frac{\pi}{2}$.

## 4.9 Conclusions

Based on polynomial matrix formulations, exemplarily a broadband version of the classical narrowband Capon beamformer has been derived. Only the inclusion of DC requires some extra considerations, and can be addressed by treating either the signal of interest or the interferers as high-pass processes. Throughout the chapter, we assumed precise knowledge of the array space-time covariance matrix, and the inverse of this matrix is accomplished via the PEVD in combination with the residue method which with the latter providing an improvement over [82]. Within this context, a careful regularisation is required when inverting polynomial matrices that may be poorly conditioned in space and frequency, which examined for different regularisations that are applied to the space time covariance matrix. This has also led to a reduction in sidelobe peak levels, which enhances the overall performance of the PBBF.

# Chapter 5

# Adaptive Broadband Beamforming with Arbitrary Array Geometry

## 5.1 Introduction

As it has been shown in preceding chapters, the steering vector plays a very crucial rule in stating the time (or in the narrowband case the phase) difference with which a source signal arrives at the array elements relative to the reference one. The signal components at the element outputs then are coherently and incoherently combined for the desired and interfering signals respectively. This leads to an improved SNR for the desired signal.

Also previously, the difference between narrowband and broadband scenarios was highlighted. In the narrowband case, the above time delays collapse to simple phase shifts. In the broadband case however, time delays have to be explicitly incorporated, typically via tapped delay lines as suggested in [39]. This then permits to constructively or destructively combine the array signals via fractional delay filters [143]. Also, polynomial techniques have been applied to achieve the same objective in Chapter 3.

This chapter is specifically dedicated to demonstrate the constraint design and broadband beamformer implementation for an array with arbitrary configuration in

3-dimensional space. The array element locations have to be known, but the elements themselves can be randomly distributed as long as the spatial sampling theorem is satisfied by at least two array elements. We extend the definition of the broadband steering vector and metrics such as the directivity pattern to three dimensions, and show how this can be applied in a three dimensional example scenario.

The chapter is organised as follows. Sec. 5.2 highlights the shortcomings of ULA and the need for a 3D antenna rather than a ULA for some beamforming applications. Sec. 5.3 will define the extension of a steering vector to a three dimensional array setup. The implementation of broadband steering vectors and the blocking matrix required for a generalised sidelobe canceller implementation of the MVDR is addressed in Sec. 5.4. Finally, Sec. 5.5 presents some simulation results, followed by conclusions in Sec. 5.6.

## 5.2 Ambiguity Phenomena in Beam Steering Using ULA

So far in this thesis, beamformers have been derived for the case when the antenna array elements are linear and uniformly distributed, with element spacing related to the shortest wave length by factor of a half, $\frac{1}{2}\lambda_{\min}$. Nevertheless, this type of geometry will be unsuitable for some applications, for example, when the array needs to be fitted to a surface with a particular shape or distributed over a space such that regularity distribution of the elements is not practical. Also, a linear array cannot unambiguously resolve all angles-of-arrival, or blind areas as encountered in the ULA case of Fig. 5.1. The shortcomings of using a ULA in the three dimensional space is depicted in Fig. 5.2, 5.3, and 5.4. This demonstrates the ambiguity introduced by an 8 elements ULA as a response to a impinging signal arrives from azimuthal and elevation angles $\varphi = -70^\circ$ and $\vartheta = 60^\circ$ respectively. The beamformer, consequently, in this case is subject to cone ambiguities and might be considered in some applications as useless for beam-steering.

Therefore in this chapter, arbitrary, volumetric arrays will be considered, which inherently removes ambiguity, as going to be demonstrated later in Sec. 5.5.4. Such structure of an antenna array are widely used for source localisation [144], and acoustic

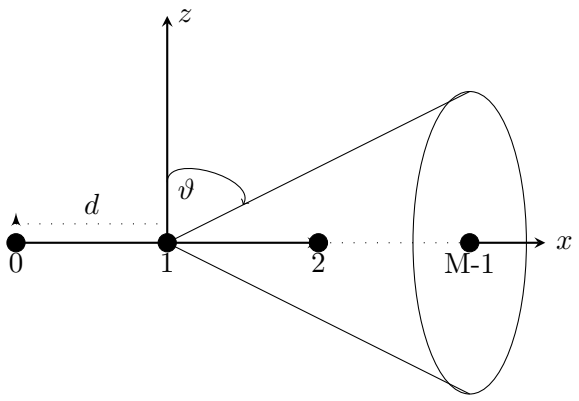


Figure 5.1: A uniform linear array and its ambiguity angle cone.

or sound applications [145] in order to improve the accuracy of parameter estimation.

## 5.3 3D Signal Model and Associated Steering Vectors

Let $\mathbf{x}[n]$ denotes a measurement vector at time instance $n$ at the output of an antenna array that consists of $M$ elements. The measurements result from a superposition of planar wave-fronts propagating from $L$ far field sources as well as white noise. The source contributions are arriving from directios described by angles $(\vartheta_1, \varphi_1) \dots (\vartheta_L, \varphi_L)$. The angles $\vartheta_\ell$ and $\varphi_\ell$ represents the azimuth and elevation angles of the $\ell$-th source respectively, with $\ell = 1, \dots, L$. In this case, the measurement vector is

$$\mathbf{x}[n] = \sum_{\ell=1}^{L} \mathbf{a}_{\varphi_\ell, \vartheta_\ell}[n] * s_\ell[n] + \mathbf{v}[n] = \mathbf{A}_{\boldsymbol{\Phi},\boldsymbol{\Theta}}[n] * \mathbf{s}[n] + \mathbf{v}[n] \tag{5.1}$$

The parameters $\boldsymbol{\Phi}$ and $\boldsymbol{\Theta} \in \mathbb{R}^L$ contain the above azimuth and elevation angle pairs

$$\boldsymbol{\Phi} = [\varphi_1, \varphi_2 \dots, \varphi_L]^{\mathrm{T}} \tag{5.2}$$

$$\boldsymbol{\Theta} = [\vartheta_1, \vartheta_2, \dots \vartheta_L]^{\mathrm{T}} . \tag{5.3}$$

Further in (5.1), $\mathbf{A}_{\boldsymbol{\Phi},\boldsymbol{\Theta}}[n] \in \mathbb{C}^{M \times L}$ is a matrix of broadband steering vectors, $\mathbf{s}[n] \in \mathbb{C}^L$ contains the $L$ source signals, and $\mathbf{v}[n]$ is an $M \times 1$ of additive white Gaussian noise

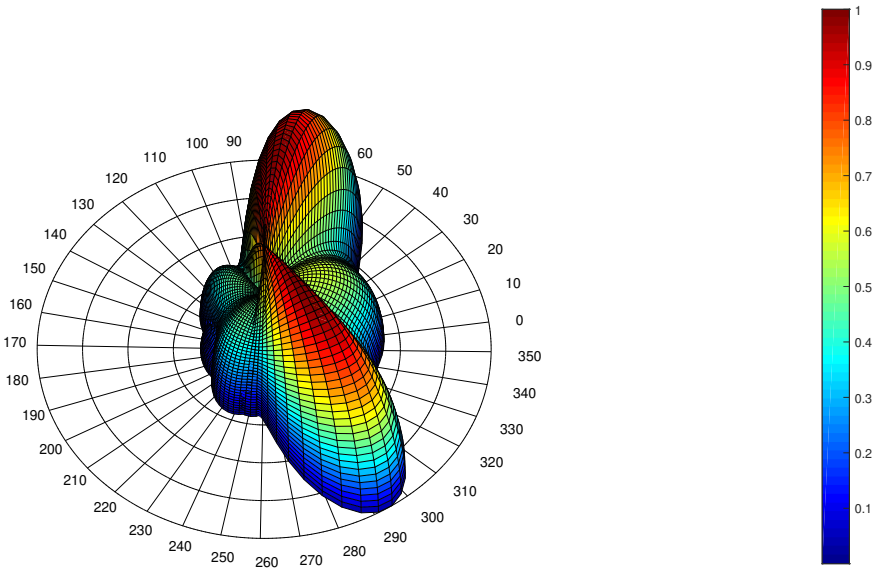


Figure 5.2: A ULA array beam-pattern for an azimuth and elevation angles $\varphi = -70^\circ$ and $\vartheta = 60^\circ$ respectively.

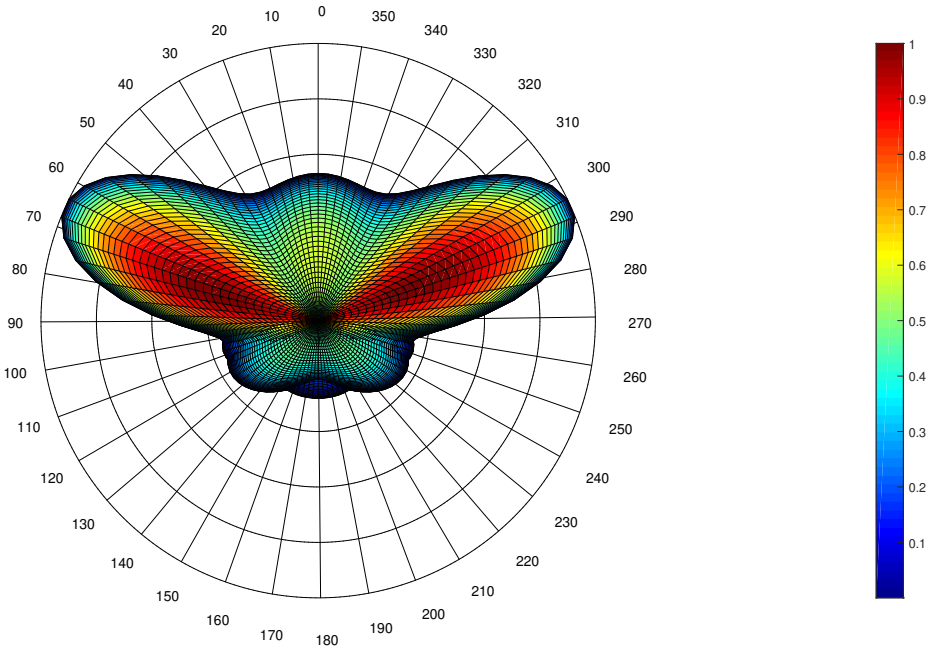


Figure 5.3: A top view of a ULA array beam-pattern for an azimuth and elevation angles $\varphi = -70^\circ$ and $\vartheta = 60^\circ$ respectively.

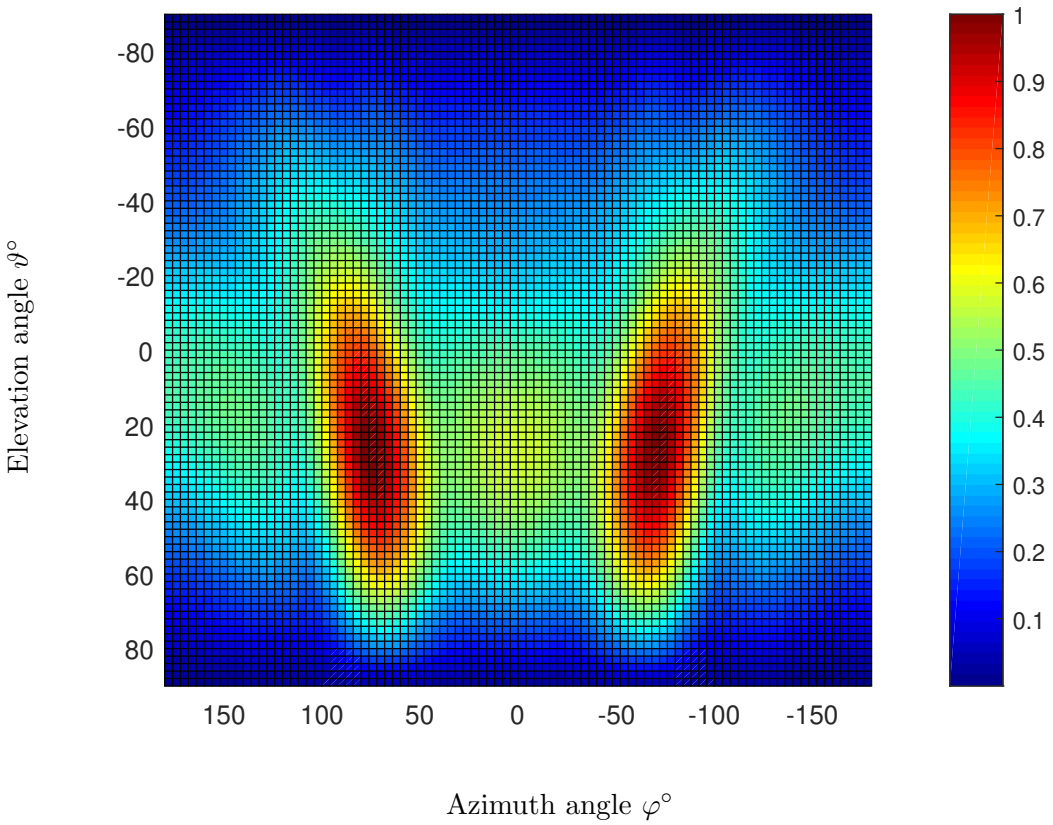


Figure 5.4: An arbitrary array beam-pattern for a source at azimuth and elevation angles $\varphi = -45^\circ$ and $\vartheta = 60^\circ$ respectively, in the azimuthal and elevation angles plane.

at each antenna element.

The steering vector is given in Sec. 3.2.2 by (3.7). However, it was derived for ULA array which is, in principle, a one dimensional array that considers the elevation angle for AoA, and does not account for azimuthal one. In the case of 2D or 3D array of sensors, the tow angles usually present, hence the steering vector in (3.7) becomes

$$\mathbf{a}_{\vartheta,\varphi}[n] = \frac{1}{\sqrt{M}} \begin{bmatrix} f[n - \tau_1(\vartheta,\varphi)] \\ f[n - \tau_2(\vartheta,\varphi)] \\ \vdots \\ f[n - \tau_M(\vartheta,\varphi)] \end{bmatrix}, \tag{5.4}$$

As it can be seen, it includes the lag values $\tau_m$, on the right hand side of (5.4), which depends on the elevation $\vartheta$ and azimuth $\varphi$ of the source, this is reflected by the subscript of the broadband steering vector, $\mathbf{a}_{\vartheta,\varphi}[n]$. Attenuation of the wavefront while travelling across the array is neglected. In order to highlight this dependency, let the position of the $m$th sensor in the Cartesian coordinate to be defined as

$$\mathbf{p}_m = \begin{bmatrix} x_m \\ y_m \\ z_m \end{bmatrix}, m = 1, 2, \ldots, M, \tag{5.5}$$

that specifies the distance relative to the array's centre of gravity $\mathbf{p}_0$, that can be given by

$$\mathbf{p}_0 = \frac{1}{M} \sum_{m=1}^{M} \mathbf{p}_m \tag{5.6}$$

The choice of the location of the array centre has a significant impact on the beamformer performance, more precisely, on the interference null depth [15, 54].

With the assumption of being the signals are propagated from far field sources, and with the definition of spherical coordinates, the normal vector of the wave-front related to the $l$-th source is

$$\mathbf{k}_{\vartheta_l,\varphi_l} = \begin{bmatrix} \sin\vartheta_l \cos\varphi_l \\ \sin\vartheta_l \sin\varphi_l \\ \cos\vartheta_l \end{bmatrix} \quad . \tag{5.7}$$

This planar wave-front travels across the array, and arrives at different array elements with different time delays. When the normal vector of this wave-front is normalised by the propagation speed $c$ in the medium, $\mathbf{k}_{\vartheta,\varphi}/c$, in this case, this parameter is also known as the source's slowness vector. Based on this, the time delay which the wave-front experiences at the $m$-th element relative to the origin is

$$t_m = \frac{1}{c}\mathbf{k}_{\vartheta,\varphi}^{\mathrm{T}}\mathbf{p}_m. \tag{5.8}$$

If the unit length in the Cartesian coordinate system is chosen as half the minimum wavelength, then

$$|\mathbf{k}_{\vartheta,\varphi}| = 1 = \lambda_{\min}/2 = c/(2f_{\max}) = cT_{\mathrm{s}} \ , \tag{5.9}$$

where $T_{\mathrm{s}}$ is the sampling period, assuming critical sampling.
Therefore,

$$t_m = \tau_m T_{\mathrm{s}} \ , \tag{5.10}$$

with

$$\tau_m(\vartheta,\varphi) = \mathbf{k}_{\vartheta,\varphi}^{\mathrm{T}}\mathbf{p}_m \tag{5.11}$$

is the time taken by a wave-front related to a source in direction $(\vartheta,\varphi)$ and measured by the $m$-th element relative to the origin in samples. It is also known as a lag or time lag. Since we are dealing with a broadband signal that, we assume, is propagating in a homogeneous medium, the propagation delay given in (5.11) as it is being directional dependent, it is also a function of frequency. This will have a role in representing the beamformer beampattern later.

Consequently, when the array is illuminated by a planar wave, the resulting signal

received by the $m$-th element is

$$x_m[n] = s[n - \tau_m(\vartheta_s, \varphi_s)] + \sum_{l=1}^{L-1} i_l[n - \tau_m(\vartheta_l, \varphi_l)] + v_m[n]. \tag{5.12}$$

The notation $x[n-\tau]$ with a fractional $\tau$ implied the convolution of $x[n]$ with a fractional delay filter implementing a delay by $\tau$ samples. The signal components are assumed to be zero mean stochastic processes with second order moments relationships as follows:

$$\mathcal{E}\{s[n - \tau_m(\vartheta_s, \varphi_s)]s[n]\} = r_m[\tau_m] \tag{5.13}$$

$$\mathcal{E}\{s[n - \tau_m(\vartheta_s, \varphi_s)]i_l[n]\} = 0 \tag{5.14}$$

$$\mathcal{E}\{i_l[n - \tau_m(\vartheta_s, \varphi_s)]i_b[n]\} = 0 \tag{5.15}$$

where $b \neq l$

$$\mathcal{E}\{s[n - \tau_m(\vartheta_s, \varphi_s)]v_m[n]\} = 0 \tag{5.16}$$

$$\mathcal{E}\{i_l[n - \tau_m(\vartheta_l, \varphi_l)]v_m[n]\} = 0 \tag{5.17}$$

where $\mathcal{E}\{.\}$ indicates the expected value. Then, the expected values in (5.13) to (5.17) denotes that the elemental signal components are mutually uncorrelated,and the directional discrete sources are expressed by their correlation function $r[\tau]$ which constitutes a Fourier transform pair with the source spectrum.

The signals measured by the array elements are stacked into a data vector

$$\mathbf{x}[n] = [x_1[n] \;\; x_2[n] \;\; \ldots \;\; x_M[n]]^{\mathrm{T}}. \tag{5.18}$$

This signal is processed by the beamformer, in either time, frequency, in order to produce the desired response. In the following section, will explain processing the array signal by the time domain beamformer based on the polynomial technique.

### 5.3.1 The Polynomial MVDR

Having established the signal model of a three dimensional antenna array, we are developing the PBBF to process such signal, and then evaluate its performance based on some criterion as in Sec. 5.5. Solutions to the MVDR problem using polynomial techniques have been derived in Chap. 3 and 4 in terms of unconstrained and constrained optimisation problem scenarios, respectively. The resulting beamformers based on these derivation are given in (3.6) and (4.16). From the concept of the MVDR beamforming, applying the signal defined in (5.18) might lead to distortion or even cancellation of the desired signal, since the constraint in (4.17) does not reflect the correct array geometry .

Because of the the widespread use of the unconstrained MVDR beamformer, the implementation of this beamformer in Sec. 3.2 is going to be extended in order to suit for processing 3D signals such as the one in (5.18). If we recall that the beamformer output is given by

$$y[n] = \mathbf{w}[n]^H \mathbf{x}[n] \tag{5.19}$$

where $\mathbf{w}[n]$ is $\in C^{(2T)M\times 1}$ and contains the spatial filter coefficients. Applying the $z$ transform on (5.19)

$$R_y(z) \bullet\!\!-\!\!\circ\, \mathcal{E}\{y[n]y^*[n-\tau]\}\,,$$

we get the power spectral density that is therefore given by

$$R_y(z) = \boldsymbol{w}^{\mathrm{P}}(z)\boldsymbol{R}(z)\boldsymbol{w}(z)\,. \tag{5.20}$$

Since the array signal model in (5.12) and (5.18) consists of a superposition of three terms that are assumed to interact based on equation (5.13) to (5.17), then (5.20) can be expressed as

$$R_y(z) = \boldsymbol{w}^{\mathrm{P}}(z)(\boldsymbol{R}_s(z) + \boldsymbol{R}_i(z) + \boldsymbol{R}_v(z))\boldsymbol{w}(z)\,, \tag{5.21}$$

where $\boldsymbol{R}_s(z), \boldsymbol{R}_i(z)$, and $\boldsymbol{R}_n(z)$ are, respectively, the power spectral density of the SoI, cross- and power spectral density of the interference, and the power spectral density of

the AWGN noise.

$$\boldsymbol{R}_s(z) \bullet\!\!-\!\!\circ\, \mathbf{R}_s[\tau] = \mathcal{E}\{\mathbf{s}[n]\mathbf{s}^{\mathrm{H}}[n-\tau]\} \tag{5.22}$$

$$\boldsymbol{R}_i(z) \bullet\!\!-\!\!\circ\, \mathbf{R}_i[\tau] = \mathcal{E}\{\mathbf{i}[n]\mathbf{i}^{\mathrm{H}}[n-\tau]\} \tag{5.23}$$

$$\boldsymbol{R}_v(z) \bullet\!\!-\!\!\circ\, \mathbf{R}_v[\tau] = \sigma_v^2\mathbf{I} \tag{5.24}$$

If the objective is to keep the output power as low as possible with maximisation of the desired signal power, this makes such beamformer in is not preferable and constraints need to be applied. From (5.21) we define

$$R_s(z) = \boldsymbol{w}^{\mathrm{P}}(z)\boldsymbol{R}_s(z)\boldsymbol{w}(z) \tag{5.25}$$

as the desired signal power spectral portion, and

$$R_i(z) = \boldsymbol{w}^{\mathrm{P}}(z)\boldsymbol{R}_i(z)\boldsymbol{w}(z) \tag{5.26}$$

is the contribution of interference in the beamformer output power spectral density, and

$$R_v(z) = \boldsymbol{w}^{\mathrm{P}}(z)\boldsymbol{R}_v(z)\boldsymbol{w}(z) \tag{5.27}$$

the noise power spectral density. Then, minimisation of the beamformer output power is equivalent to reducing the interference and noise power. Consequently, an appropriate filtering of the interference and averaging the AWGN noise fulfils the requirement, which means the design of the spatio-temporal filter is the key within this process.

The PBBF to solve the MVDR problem suggested in [36] helps to accomplish an estimation of the beamformer weights to achieve reduction in noise level and hence improvement in the mean power output. Sec. 5.4 will review the design procedures of the MVDR beamformer in its GSC structure based on polynomial techniques.

## 5.4 Implementation

In this section, the GSC version of the MVDR beamformer implementation is discussed, where the broadband steering vectors for (3.7) is expanded, and building a blocking matrix, $\boldsymbol{B}(z)$, from the constraint in (3.6) is presented. Also, for the completion of GSC components, a multichannel adaptive filter and the calculation of the optimum beamformer is considered.

### 5.4.1 Quiescent Vector and Blocking Matrix

From Sec. 3.2.2.2 we recall that the quiescent beamformer $\boldsymbol{w}_{\mathrm{q}}(z)$ is derived from the constraint, and in the absence of further constraints for the suppression of interferers, can be represented as a match filter of the SoI's steering vector

$$\boldsymbol{w}_{\mathrm{q}}(z) = \boldsymbol{a}(\varphi_{\mathrm{s}}, \vartheta_{\mathrm{s}}, z). \tag{5.28}$$

Also, we recall that, in view point of the desired signal's steering vector, the blocking matrix can be considered as a null beamformer. Hence, the blocking matrix has to be designed such that

$$\boldsymbol{B}(z)\boldsymbol{w}_{\mathrm{q}}(z) = \underline{0}\,, \tag{5.29}$$

which can therefore be achieved by completing $\boldsymbol{w}_{\mathrm{q}}(z)$ to a paraunitary matrix as suggested in [36]. The procedures are depicted schematically in Fig. 5.5 .

The proposition in this procedure is that, since the covariance matrix, which resulting from the outer product of the quiescent vector $\boldsymbol{w}_{\mathrm{q}}(z)\boldsymbol{w}_{\mathrm{q}}^{\mathrm{P}}(z)$, is para-Hermitian and positive definite, it can be diagonalised by means of a para-Unitary transformation matrix, for example, $\boldsymbol{Q}(z)$ . A polynomial eigenvalue decomposition (PEVD, [81]) is applied to the rank one matrix so that

$$\boldsymbol{w}_{\mathrm{q}}(z)\boldsymbol{w}_{\mathrm{q}}^{\mathrm{P}}(z) = \bar{\boldsymbol{Q}}(z)\boldsymbol{D}(z)\bar{\boldsymbol{Q}}^{\mathrm{P}}(z)\,, \tag{5.30}$$

where $\boldsymbol{D}(z)$ is a diagonal matrix of eigenvalues, and $\boldsymbol{Q}(z)$ is a modal square matrix for

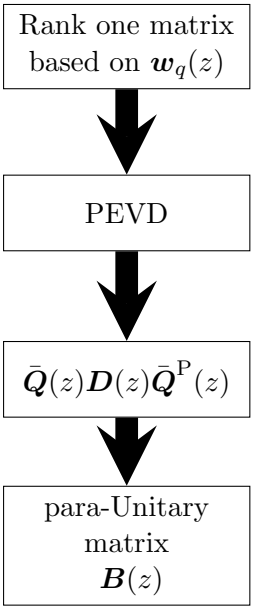


Figure 5.5: Construction of a paraunitary blocking matrix.

the covariance matrix, and consists of columns of eigenvectors. The PEVD is ordered in descending power of the eigenvectors and due to the definition of the steering vector, we have

$$\boldsymbol{D}(z) = \mathrm{diag}\{1 \;\; 0 \;\; \ldots \;\; 0\} \; . \tag{5.31}$$

The paraunitary matrix $\bar{\boldsymbol{Q}}(z)$ is not unique even in the case where (5.30) has full rank. Defining the column vectors of the paraunitary matrix

$$\bar{\boldsymbol{Q}}(z) = [\bar{\boldsymbol{q}}_1(z) \;\; \bar{\boldsymbol{q}}_2(z) \;\; \ldots \;\; \bar{\boldsymbol{q}}_M(z)] \; , \tag{5.32}$$

then e.g. $\bar{\boldsymbol{q}}_1(z)$ can be shifted with respect to $\boldsymbol{w}_{\mathrm{q}}(z)$,

$$\bar{\boldsymbol{q}}_1(z) = z^{-\Delta}\boldsymbol{w}_{\mathrm{q}}(z) \; , \tag{5.33}$$

and yet satisfy both (5.30) and (5.31). Similarly, the remaining columns $\bar{\boldsymbol{q}}_m(z)$ can be arbitrarily shifted without affecting the validity of the decomposition.

Therefore, if the blocking matrix

$$\boldsymbol{B}(z) = [\bar{\boldsymbol{q}}_2(z) \quad \dots \quad \bar{\boldsymbol{q}}_M(z)] \tag{5.34}$$

is selected, which defines an $M \times M-1$ polynomial matrix with (M-1) orthonormal columns. This choice of $\boldsymbol{B}^{\mathrm{P}}(z)$ implies that $\boldsymbol{B}^{\mathrm{P}}(z)\boldsymbol{w}_{\mathrm{q}}(z) = \underline{0}$ is guaranteed, in other word, the projection of $\boldsymbol{w}_{\mathrm{q}}(z)$ onto the subspace of columns of $\boldsymbol{B}(z)$ is zero. But $\boldsymbol{B}(z)$ could have a larger order than necessary. By appropriately shifting rows and truncation of small leading and trailing coefficients of $\boldsymbol{B}^{\mathrm{P}}(z)$ [**?** ], it is possible to reduce this order.

### 5.4.2 Adaptive Multichannel Filter

One necessary step in MVDR, besides steering the main beam towards a specific direction, is to minimise the output power. In the case of GSC this is done by estimating the noise at the output of the quiescent beamformer by using a multichannel adaptive filter as shown in Fig. 5.6.

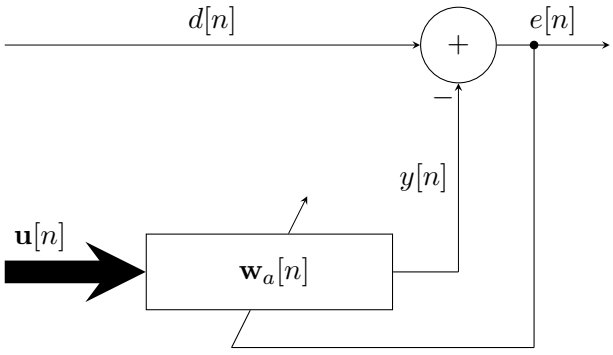


Figure 5.6: Multichannel adaptive filter.

The coefficients of the adaptive filter are obtained by NLMS algorithm [49], which can be viewed as an approximation to the minimum norm solution to the filter coefficient vector $\mathbf{w}_{\mathrm{a}}[n]$, that depends on the statistics of the data as a normalisation factor to adjust the coefficients during the recursion iterative calculation process. This

Table 5.1: The NLMS algorithm

| for each $n$ compute |
|---|
| $y[n] = \mathbf{w}_a^H \mathbf{u}[n]$<br>$e[n] = d[n] - y[n]$<br>$\mathbf{w}_{\mathrm{a}}[n+1] = \mathbf{w}_{\mathrm{a}}[n] + \frac{\mu}{\mathbf{u}^H[n]\mathbf{u}[n] + \epsilon} e^*[n]\mathbf{u}[n]$ |

process is expressed as

$$\mathbf{w}_{\mathrm{a}}[n+1] = \mathbf{w}_{\mathrm{a}}[n] + \frac{\mu}{\mathbf{u}^H[n]\mathbf{u}[n] + \epsilon} e^*[n]\mathbf{u}[n] \; . \tag{5.35}$$

The inner product provides the input signal power for each iteration, which makes the innovation vector of $\mathbf{w}_{\mathrm{a}}[n]$ less vulnerable to any change of the power at the input of the filter. The term $\epsilon \ll 1$ applies a regularisation to avoid numerical problems if the input power is zero. Table 5.1 describes the NLMS algorithm steps, where $d[n]$ represents the output of quiescent beamformer, and $\mathbf{u}[n]$ is a tap vector from the bocking matrix at time $n$ .

### 5.4.3 Overall GSC Optimum Weight

Consequently, the steady state optimum weight vector of MVDR beamformer based on GSC concept, from (3.28), is

$$\boldsymbol{w}_{gsc}(z) = \boldsymbol{w}_{\mathrm{q}}(z) - \boldsymbol{B}^{\mathrm{P}}(z)\boldsymbol{w}_{\mathrm{a}}(z), \tag{5.36}$$

which consists of both data independent weights from the upper path in Fig. 3.3, and the multiplication of the parameters in the lower path as interference filter.

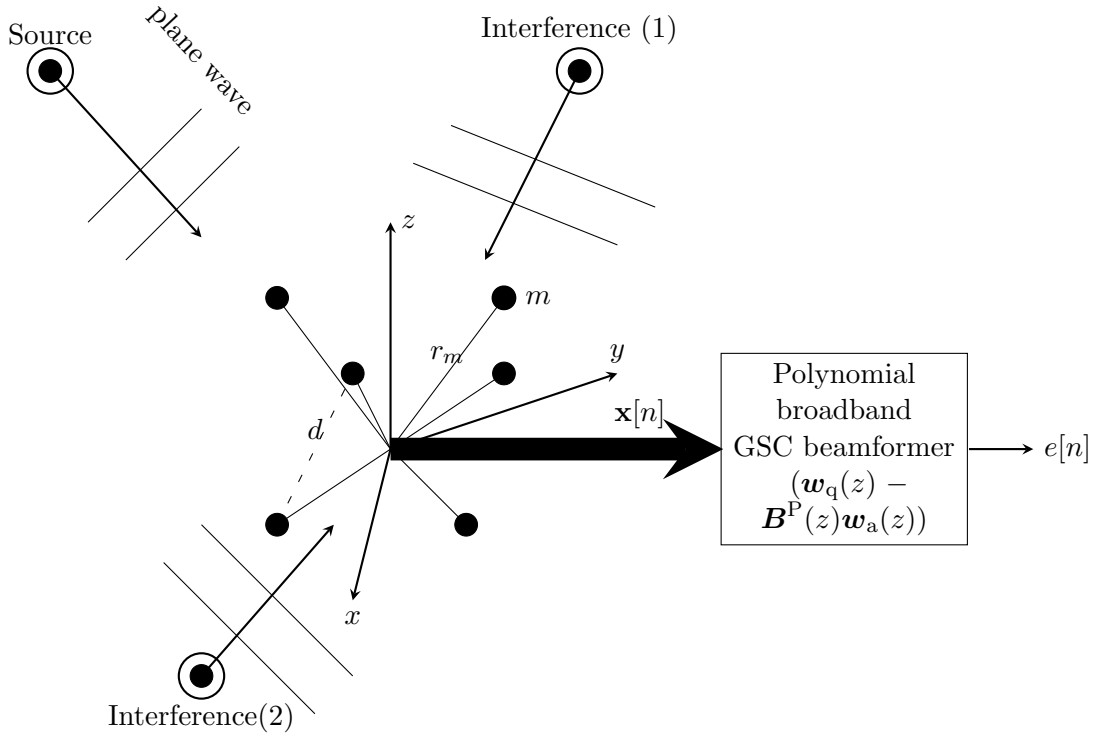


Figure 5.7: Polynomial broadband beamformer with arbitrary antenna array configuration. At least two elements are separate by no more than $\lambda_{\min}/2$ .

## 5.5 Simulations and Results

Based on performance metrics that were briefly mentioned in Sec. 2.2, in Sec. 5.5.1 broader explanations and definitions are given, followed by analysis of the PSV and techniques to enhance the visualisation of the PBBF's beam-pattern in Sec. 5.5.2. Sec. 5.5.3 explains the methods that are used to demonstrate 3D beam-pattern. Finally, simulation scenarios and results are in Sec. 5.5.4.

### 5.5.1 Performance Metrics

#### 5.5.1.1 Residual Error

To assess the performance of broadband GSC beamformer, the mean square of the residual error $e_{\mathrm{r}}[n]$ is a useful metric. Since the beamformer output $e[n]$ in (3.31) should contain the signal of interest plus residual error, subtracting out the desired source signal — appropriately delayed to compensate for propagation delays in $\boldsymbol{w}_{\mathrm{q}}(z)$ — provides a metric similar to echo return loss enhancement known in acoustic echo cancellation.

#### 5.5.1.2 Directivity Pattern

The directivity pattern represents the gain response of a broadband beamformer with respect to the angles of arrival and frequency. Assuming that a broadband source is located at $(\vartheta, \varphi)$ as characterised by the broadband steering vector $\boldsymbol{a}(\vartheta, \varphi, z)$, if we define the spatial Fourier transform the overall transfer function of the beamformer with respect to this excitation is

$$A(\vartheta, \varphi, z) = \left(\boldsymbol{w}_{\mathrm{q}}^{\mathrm{P}}(z) - \boldsymbol{w}_{\mathrm{a}}^{\mathrm{P}}(z)\boldsymbol{B}(z)\right) \cdot \boldsymbol{a}(\vartheta, \varphi, z)\ . \tag{5.37}$$

By probing (5.37) with a series of steering vectors, the directivity pattern is obtained evaluating it on the unit circle and taking the gain only.

The beam pattern of a broadband beamformer, as a spatio-temporal filter, is usually visualised as a function of space variables and temporal frequency. The space variables

can be expressed explicitly, as angles of the direction of arrival, or implicitly within the wave-number, whereas the temporal frequency extends over an octave or a frequency band between $f_{\text{low}}$ and $f_{\text{high}}$. This, in consequence, indicates that the shortest wave length within the band is $\lambda_{\min} = \frac{f_{\text{high}}}{c}$, in which $c$ is the propagation speed of the wave in the media.

For an arbitrary array that is assumed to be constructed with $M$ sensors in this study, the inter-element spacing should not be restricted to half of the shortest wave-length among the entire array elements, but it should be guaranteed for at least between two sensors in order to avoid spatial aliasing. The beam-pattern associated with such arrays, as a response to plane-waves in space, are analysed over three dimensional space. This space is specified by two dimensions that are related to azimuthal and elevation angles, and the third dimension represents the frequency. The azimuthal angle is $\varphi \in [-180^\circ, 180^\circ]$ whereas elevation angle is $\vartheta \in [-90^\circ, 90^\circ]$, and normalised angular frequency band extends between 0 and $\pi$.

#### 5.5.1.3 Modified MVDR Polynomial Weights

Before we proceed with the visualisation procedures of the beam-pattern, we need to improve the resolution of the beamformer over the temporal frequency to have higher resolution spectral, which in turn becomes adequate for better visualisation and assessment. By means of a longer DFT, the frequency resolution can be enhanced[146]. Mathematically, this can be expressed as

$$\hat{\boldsymbol{w}}(k) = \boldsymbol{w}_{gsc}(z)\big|_{z=e^{-j(\frac{2\pi}{Q})k}} \tag{5.38}$$

for the $k$-th frequency bin, where $Q \gg 2L$, and $2L$ is the filter length after each sensor. Alternatively, it can be interpreted as evaluating $\boldsymbol{w}(z)$ at $Q$ points on the unit circle which will be used as coefficients for the components of the broadband steering vector during the beam-pattern assessment, that will be described in Sec.5.5.2.

### 5.5.2 Analysis of the Polynomial Steering Vector

Since the broadband signals can be modelled as superposition of many narrowband signals spreads over limited band [10]. This also applies on the broadband steering vectors. From (3.7) and (5.4) the broadband steering vector in its Laurent polynomial form expressed as

$$\boldsymbol{a}(\vartheta, \varphi, z) = \sum_{n=-\infty}^{\infty} \mathbf{a}_{\vartheta,\varphi}[n] z^{-n}. \tag{5.39}$$

If this PSV is evaluated on the unit circle for $z = e^{\Omega_o}$, the result is a narrowband steering vector at frequency $\Omega_o$, which can be generalised to any frequency point. Then the PSV that relates to a source from AoA $(\vartheta, \varphi)$ can be analysed at frequency $f$ as

$$\mathbf{a}(\vartheta, \varphi, f) = \begin{bmatrix} e^{-j2\pi f/f_{\mathrm{s}}(x_1 \cos\vartheta \sin\varphi + y_1 \sin\vartheta \sin\varphi + z_1 \cos\vartheta)} \\ \vdots \\ e^{-j2\pi f/f_{\mathrm{s}}(x_M \cos\vartheta \sin\varphi + y_M \sin\vartheta \sin\varphi + z_M \cos\vartheta)} \end{bmatrix}. \tag{5.40}$$

where $j = \sqrt{-1}$, and $(x_m, y_m, z_m)$ refer to the Cartesian coordinates of the $m$-th sensor of the array. This now leads us to the beam-pattern representation of PBBF.

#### 5.5.2.1 3D PBBF's Beam-pattern

In general, the beampattern is defined as the response or the gain of the beamformer w.r.t. a specific direction and frequency of excitation. Hence, for the weights in (5.36), the beamformer gain is

$$A(\vartheta, \varphi, z) = \boldsymbol{w}^{\mathrm{P}}(z) \cdot \boldsymbol{a}(\vartheta, \varphi, z)\ . \tag{5.41}$$

By using equations (5.38) and (5.40) then (5.41) can be rewritten as

$$A(\vartheta, \varphi, f) = \hat{\boldsymbol{w}}^{\mathrm{H}}(e^{j2\pi f/f_s}) \cdot \boldsymbol{a}(\vartheta, \varphi, e^{j2\pi f/f_s}). \tag{5.42}$$

The equation (5.42) is used to illustrate the synthesis of the beam-pattern. However, considering the three variables at the same time leads to a cumbersome visualisation

process. For this reason, in Sec. 5.5.3 we will explain our approach to simplify the representation of the beam-pattern synthesis.

### 5.5.3 Partial Representation of the PBBF 3D Beam-pattern

In this section, we demonstrate the method and the considerations of visualising the beam-pattern of the GSC-PBBF with an arbitrary array geometry configuration.

For the array pattern in (5.41) it is possible to express $A(\vartheta, \varphi, z)$ as a function of two variables while the third is substituted by a constant value. To evaluate the beam-pattern based on elevation angle and the frequency, in this case, the beam-pattern it can be rewritten as

$$A(\vartheta, f) = \hat{\mathbf{w}}^{\mathrm{H}}(e^{j2\pi f/f_s}) \cdot \mathbf{a}(\vartheta, \varphi, e^{j2\pi f/f_s})|_{\varphi=const}. \tag{5.43}$$

This, then, can be examined in 3D plot with axes represent the elevation angle $\vartheta$, frequency , $f$, and the gain.

A similar procedures are repeated to represent the beamformer as a function of azimuthal angle, $\varphi$, and the frequency to become

$$A(\varphi, f) = \hat{\mathbf{w}}^{\mathrm{H}}(e^{j2\pi f/f_s}) \cdot \mathbf{a}(\vartheta, \varphi, e^{j2\pi f/f_s})|_{\vartheta=const}. \tag{5.44}$$

And, finally, for a specific frequency and variable angles it becomes

$$A(\vartheta, \varphi) = \hat{\mathbf{w}}^{\mathrm{H}}(e^{j2\pi f/f_s}) \cdot \mathbf{a}(\vartheta, \varphi, e^{j2\pi f/f_s})|_{f=const}. \tag{5.45}$$

### 5.5.4 Scenarios

The first performance of PBBF after amending PSV, to be adequate for 3D antenna arrays, and the other GSC components will now be illustrated for two scenarios. In a first scenario, we consider an arbitrary configuration of antenna array elements. For comparison, in the second scenario, we have chosen the location of antenna elements such that they are arranged symmetrically around the centre of the array.

Table 5.2: Sensor locations

| $i$ | $x_i$ | $y_i$ | $z_i$ |
|---|---|---|---|
| 1 | -1.1242 | -1.8617 | 0.7471 |
| 2 | -1.8118 | -1.7862 | 0.3559 |
| 3 | 0.7155 | 0.1188 | 1.7217 |
| 4 | 0.7172 | 0.6846 | 1.3847 |
| 5 | 1.7388 | -1.9692 | 0.1077 |
| 6 | -0.4660 | -0.4663 | -1.6321 |
| 7 | 0.0777 | -1.7326 | 0.6157 |
| 8 | 1.3239 | -0.3301 | -0.3360 |

#### 5.5.4.1 Scenario-1: Random antenna array configuration

The scenario simulates a polynomial adaptive beamformer with an arbitrary array as in Fig. 5.7. This array with $M = 8$ elements is generated by randomly drawing element locations from $\{x_m, y_m, z_m\} \in [-2; 2]$, i.e., all elements lie within a cube. The resulting coordinates are listed in Table 5.2. Note in Tab. 5.2 that the shortest inter-element distance among the array elements is occurring between the third and fourth elements, which are separated by $\lambda_{\min}/1.7$. This is slightly wider than the spatial Nyquist distance, and could potentially result in spatial aliasing for a number of 'unlucky' directions (e.g. perpendicular to the line defined by those two elements). For all simulations that we have performed, in particular the once reported below, spatial aliasing was not evident.

The uncorrelated source of interest is set to illuminate the array from an elevation $\vartheta_{\mathrm{s}} = 60^\circ$ and azimuth $\varphi_{\mathrm{s}} = -45^\circ$. A first interferer is located at $\{\vartheta_{\mathrm{i},1} = 0^\circ, \varphi_{\mathrm{i},1} = -45^\circ\}$, with a second at $\{\vartheta_{\mathrm{i},2} = 60^\circ, \varphi_{\mathrm{i},2} = 90^\circ\}$. Both interferers have a signal-to-interference noise ratio of $-30$ dB, and additive white Gaussian noise at a level of 20 dB relative to the signal of interest. Both interferers have a high-pass characteristic, with passband edge at $\Omega = \pi/4$. In the following we will look at and evaluate the beampattern of the PBBF for this particular case before and after adaptation.

**5.5.4.1.1 Quiescent Response:** The beam-pattern of the un-adapted beamformer, which means that $\boldsymbol{w}_{\mathrm{a}} = \underline{0}$, is the response of the quiescent beamformer only. The quiescent beamformer has been designed as a broadband steering vector consisting of fractional delay filters of order 40, which was found to provide sufficient accuracy.

Fig. 5.8 and Fig. 5.9 show the directivity patterns $|A(\vartheta, \varphi, e^{j\Omega})|$ for two fixed points. Firstly, for $\vartheta = \vartheta_{\mathrm{s}} = 60°$, the beamformer is pointing in the elevation direction of the source but with varying azimuth angle. Note that the gain response in Fig. 5.8 satisfies the constraint for $\varphi$, with a frequency-independent unit gain response in direction $\varphi = \varphi_{\mathrm{s}} = -45°$. Secondly, fixing the azimuth angle $\varphi = \varphi_{\mathrm{s}} = -45°$ but varying the elevation $\vartheta$ in Fig. 5.9, the constraint is fulfilled for $\vartheta = \vartheta_{\mathrm{s}} = 60°$.

**5.5.4.1.2 Adapted Beamformer:** Based on the quiescent beamformer, a blocking matrix was designed by paraunitary matrix completion, resulting in a blocking matrix of order 480 after appropriate truncation [113]. The adaptive filter $\boldsymbol{w}_{\mathrm{a}}(z)$ was chosen of order 140. Using a normalised LMS algorithm for unconstrained optimisation, the mean square residual error is depicted in Fig. 5.10.

Fig. 5.11 and 5.12 show the directivity patterns of the GSC beamformer after adaptation. In Fig. 5.11, the elevation angle is fixed at $\vartheta_{\mathrm{s}} = 60°$, such that the look direction of the array is observed for the flexible azimuth angle at $\varphi = \varphi_{\mathrm{s}} = -45°$. The directivity pattern differs from the one of the quiescent beamformer in Fig. 5.8 but fulfils the constraint.

As mentioned in Sec. 5.5.3, the beam-pattern of the PBBF can also be evaluated in the azimuthal and elevational plane for a fixed frequency. For an arbitrary array with $M = 8$ elements those are generated in a way similar to the current scenario, the obtained results are plotted in Fig. 5.13 to 5.17. At this point we should say that the values of the beam-pattern in theses plots are corresponding to the normalisation by the maximum gain either in azimuthal or elevation direction. This evaluation is based on the relationship between elevation angle, $\vartheta$, and azimuth angle, $\varphi$, for fixed frequency. Fig. 5.13 to Fig. 5.17 show this relationship when the look direction is $\{\vartheta_s = 60°,\ \varphi_s = -45°\}$ and the frequency at $\Omega = \pi/2$. These figures provide a broader

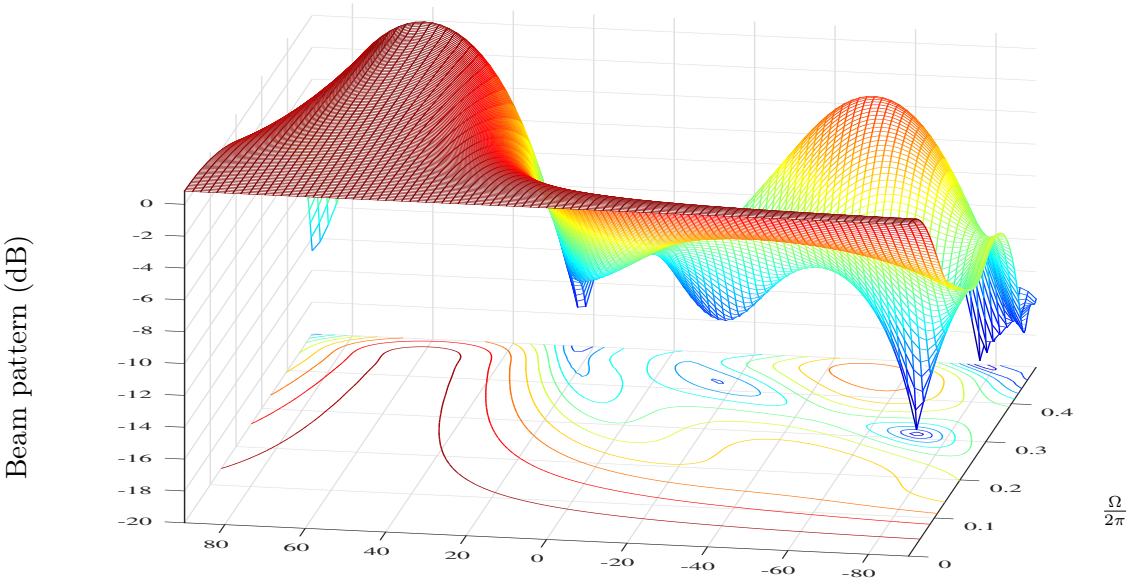


Figure 5.8: Directivity pattern of polynomial quiescent beamformer $\boldsymbol{w}_{\mathrm{q}}(z)$ in elevation look direction $\vartheta_{\mathrm{s}} = 60°$ for variable azimuth angle $\varphi$.

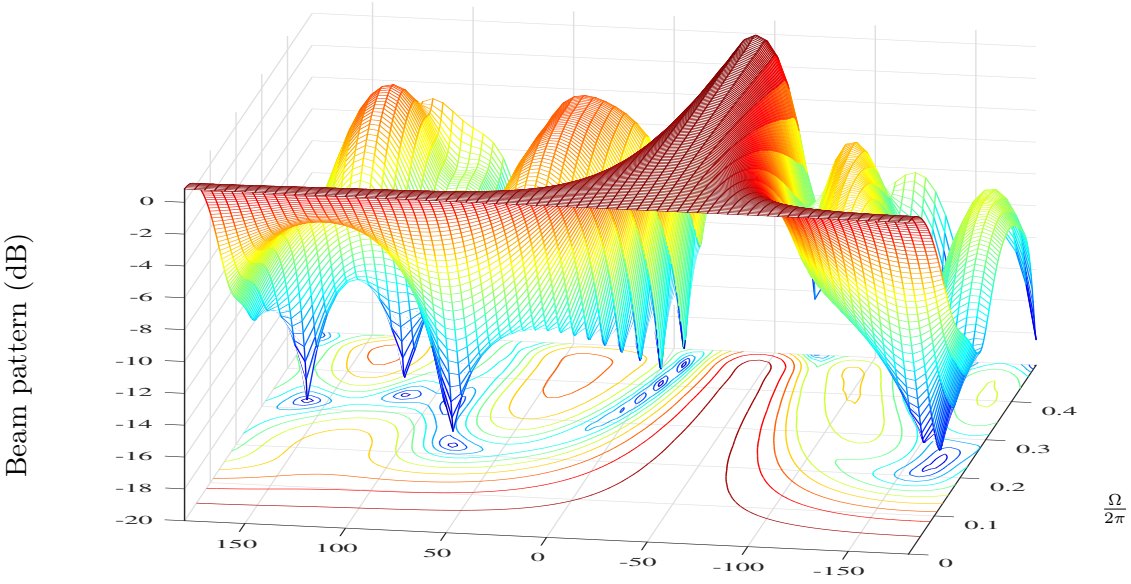


Figure 5.9: Directivity pattern of polynomial quiescent beamformer $\boldsymbol{w}_{\mathrm{q}}(z)$ in azimuth look direction $\varphi_{\mathrm{s}} = -45°$ for variable elevation angle $\vartheta$.

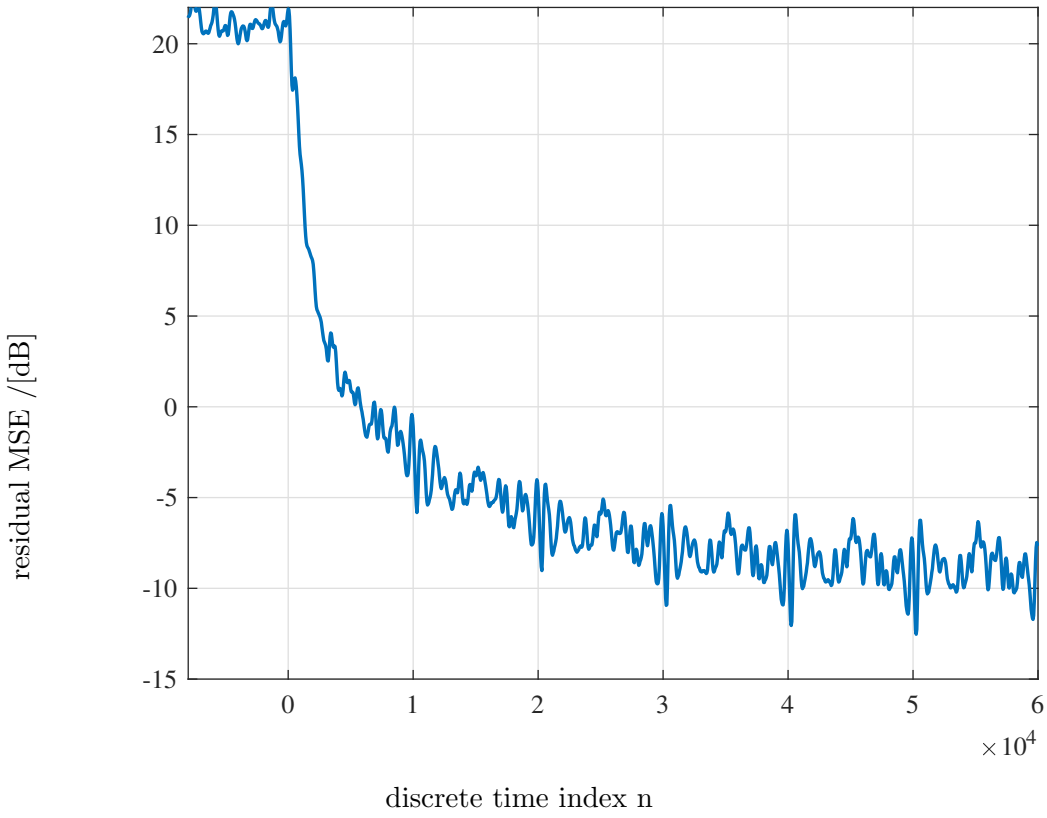


Figure 5.10: Mean square residual error after switching adaptation on at $n = 0$.

insight to evaluate the performance of the combination of the PBBF and the assumed antenna, in addition to beam steering and forming nulls towards interference we can see the back lobe and side lobes, this provide another measure that reflect the quality of the combination. It can be seen that the main beam is steered towards the SoI and nulls are formed at directions of arrival of interferers, also for this particular scenario only relatively small back and side lobes are observed. Consequently, the objective of deploying the beamformer is achieved, since it directs most of its gain towards the SoI and suppresses interference.

#### 5.5.4.2 Scenario-2: A Symmetric Antenna Array Configuration

The sensors' positions in Tab. 5.2 were generated randomly by using Matlab program command *rand*. Since the location of the reference element impacts the performance of the beamformer [15, 54], we have examined a different scenario of the array geometry, by which we can ensure that the centre of gravitation is located at the origin of the coordinate system. The position of the sensors are listed in Tab. 5.3, the first and second listed sensors are placed sufficiently apart so the minimum inter-element spacing is the same as in scenario-1, that in order for the impinging signal is spatially sampled with no aliasing, also the furthest antenna element has the same spacing distance from the origin as the furthest element in scenario-1. This is in order to maintain the same antenna aperture size in both cases. For illustrative purposes and for easy comparison with an asymmetric antenna array configuration, we will assume the same number of antenna elements, SNR, and AWGN level as in scenario-1.

However, two signals arrive at the array simultaneously, a desired signal and a single interference which arrive from angles $\{\vartheta_{\mathrm{s}} = 60^{\circ}, \varphi_{\mathrm{s}} = -45^{\circ}\}$ and $\{\vartheta_{\mathrm{i}} = 0^{\circ}, \varphi_{\mathrm{i}} = 90^{\circ}\}$, respectively. The performance of the PBBF is depicted in Fig. 5.18 in terms of the residual error for the two different sets up of the antenna array, Figs. 5.19 and 5.20 cross-sections of the beam-pattern at $\Omega = \pi/2$ as a function of the azimuthal and elevation angles, respectively. Fig. 5.18 shows faster convergence can be achieved when properly choose the reference sensor to be at the origin of the coordinate system. Also, from Fig. 5.19 and Fig. 5.20 the response of the beamformer to the interferes has

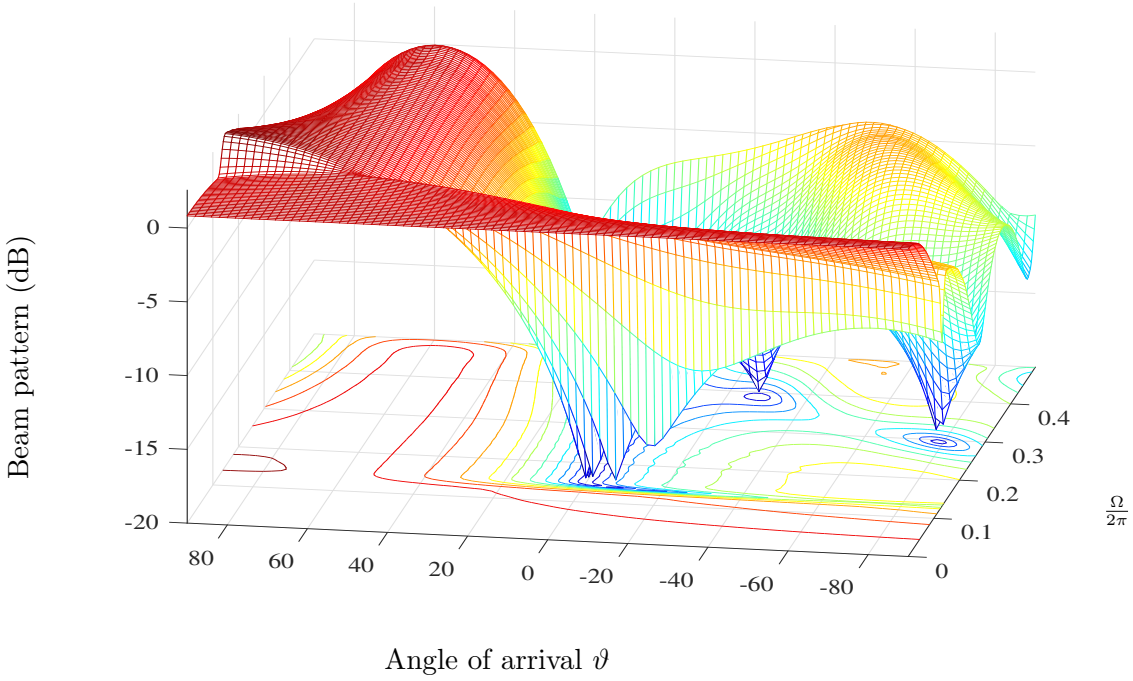


Figure 5.11: Directivity pattern of polynomial adapted beamformer $\boldsymbol{w}(z)$ in elevation look direction $\vartheta_s = 60°$ for variable azimuth angle $\varphi$.

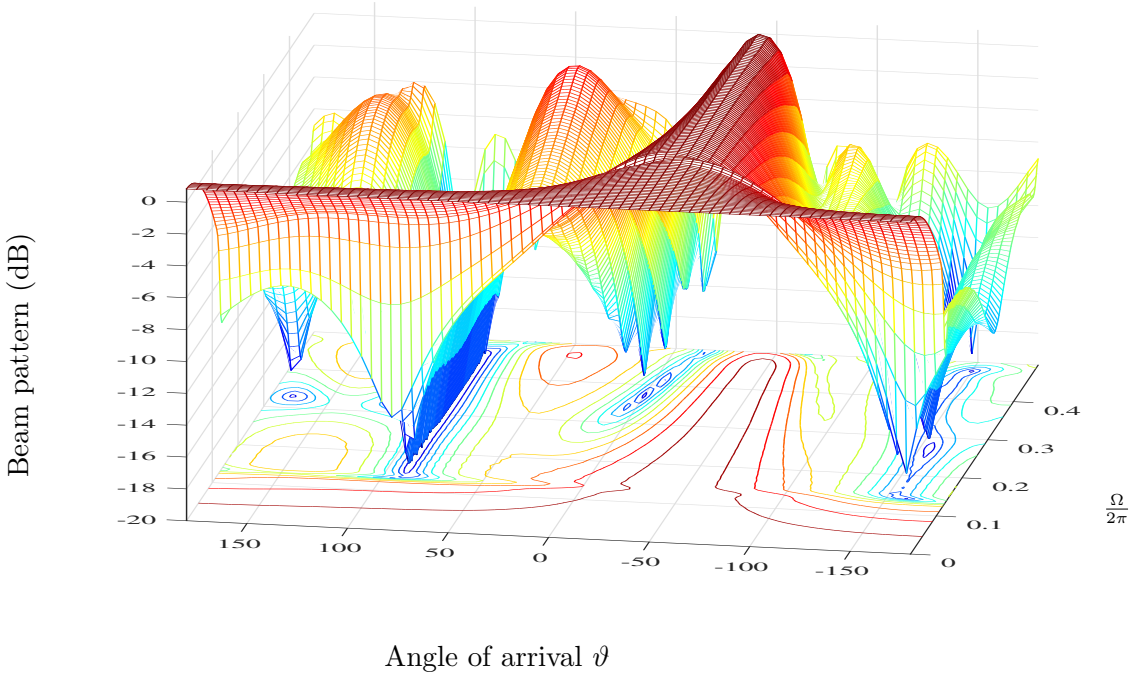


Figure 5.12: Directivity pattern of polynomial adapted beamformer $\boldsymbol{w}(z)$ in azimuth look direction $\varphi_s = -45°$ for variable elevation angle $\vartheta$.

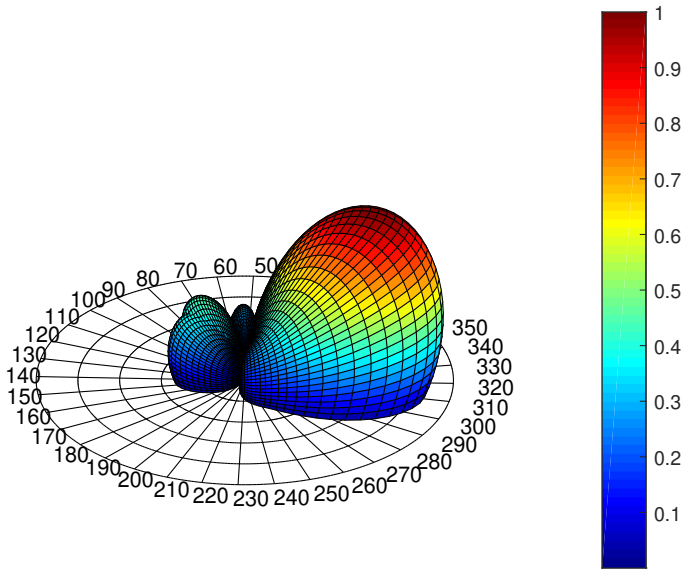


Figure 5.13: An arbitrary array beam-pattern for an azimuth and elevation angles $\varphi = -45°$ and $\vartheta = 60°$ respectively. Frequency is fixed at $\Omega = \pi/2$.

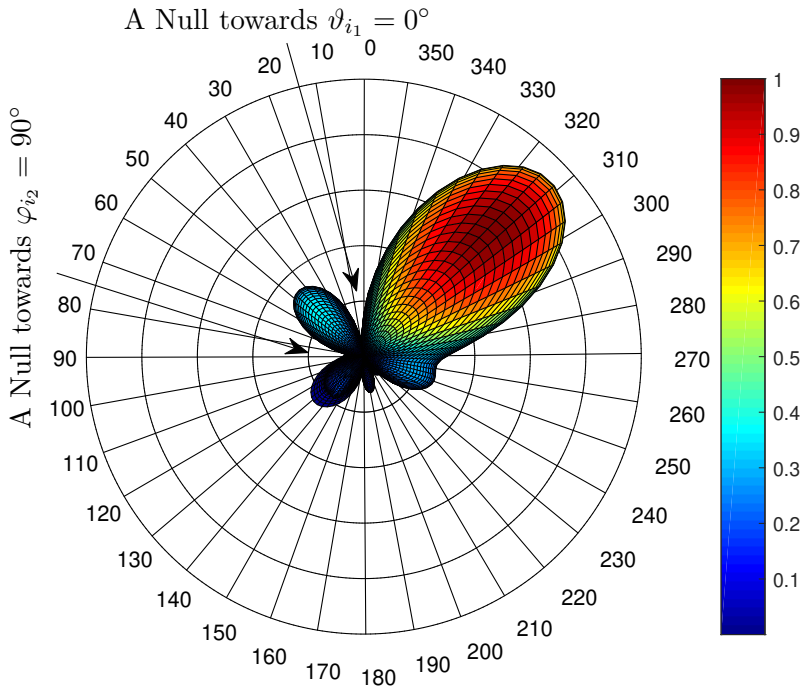


Figure 5.14: A top view of an arbitrary array beam-pattern for an azimuth and elevation angles $\varphi = -45°$ and $\vartheta = 60°$ respectively. Frequency is fixed at $\Omega = \pi/2$.

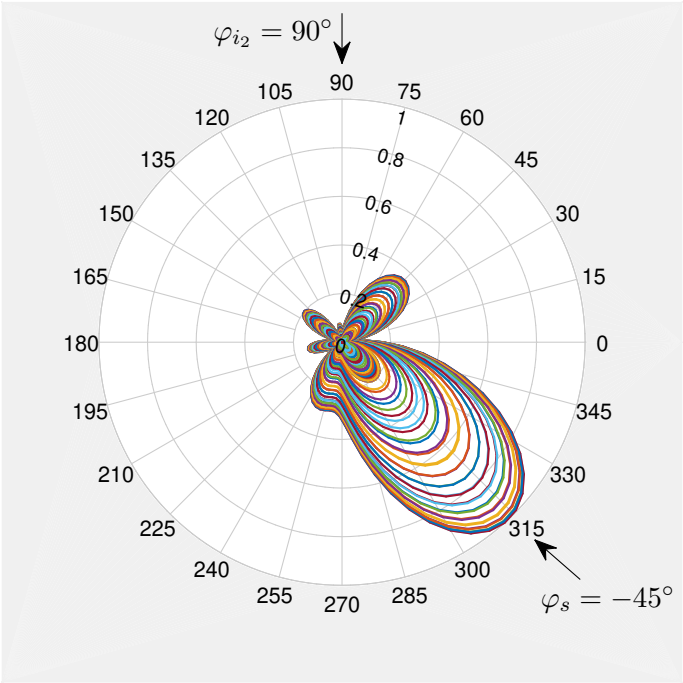


Figure 5.15: Polar plot of an arbitrary array beam-pattern for an azimuth angle $\varphi = -45°$, while frequency is fixed at $\Omega = \pi/2$. Different curves are for Different elevation angles.

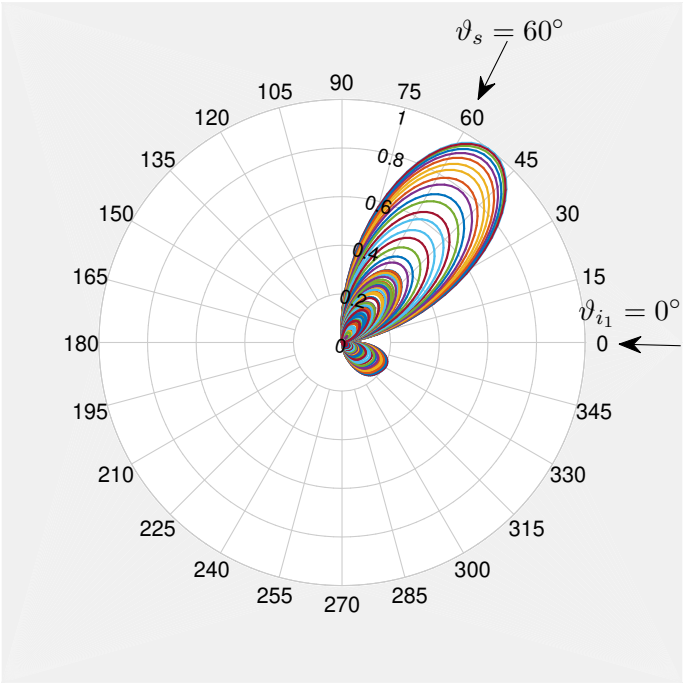


Figure 5.16: Polar plot of an arbitrary array beam-pattern for an elevation angle $\vartheta = 60°$, while frequency is fixed at $\Omega = \pi/2$. Different curves are for different azimuth angles.

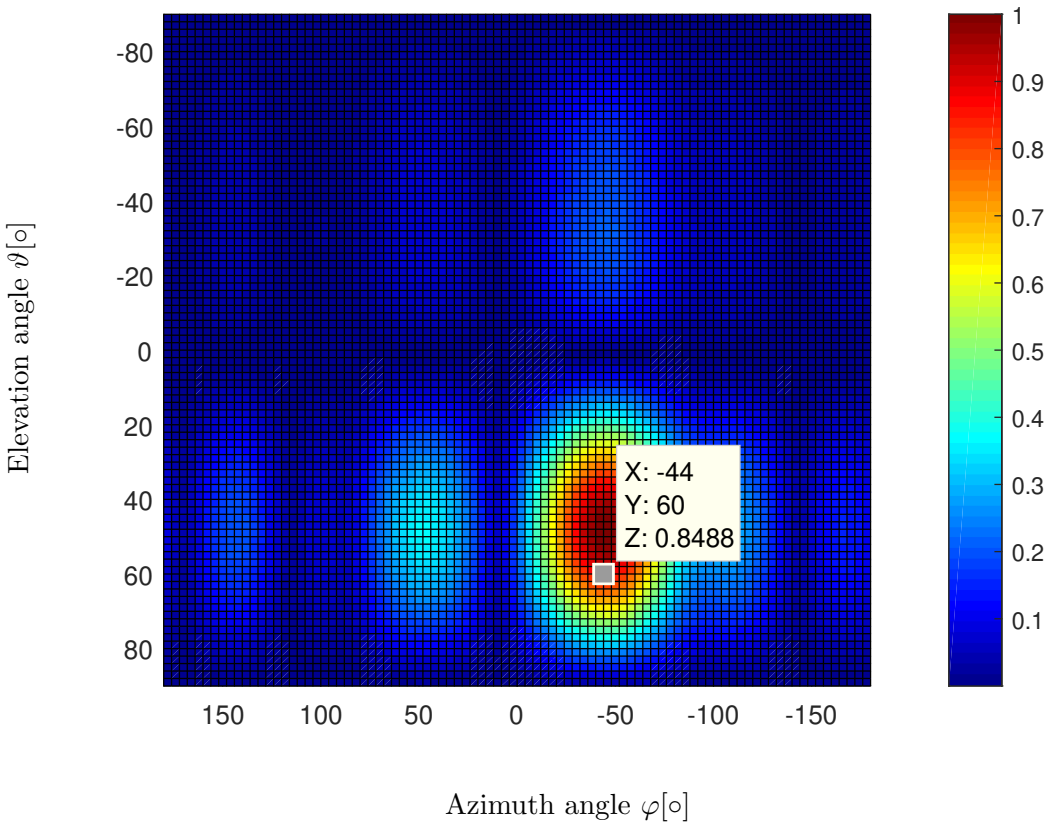


Figure 5.17: An arbitrary array beam-pattern for a source at azimuth and elevation angles $\varphi = -45^\circ$ and $\vartheta = 60^\circ$ respectively in the azimuthal and elevation plane. The frequency is set to $\Omega = \pi/2$.

Table 5.3: Sensor locations

| $i$ | $x_i$ | $y_i$ | $z_i$ |
|---|---|---|---|
| 1 | -0.2 | -0.2 | -0.2 |
| 2 | 0.2 | 0.2 | 0.2 |
| 3 | 0 | -1 | 0 |
| 4 | 0 | 1 | 0 |
| 5 | 0 | 0 | 1.5 |
| 6 | 0 | 0 | -1.5 |
| 7 | -1.8617 | -1.8617 | -1.8617 |
| 8 | 1.8617 | 1.8617 | 1.8617 |

improved in terms of the null depth, where in the second scenario the beamformer achieves a deeper null.

## 5.6 Conclusions

In Chap. 3 we have established some of the advantages of the proposed design, which includes the decoupling of orders in the quiescent beamformer, the blocking matrix, and the adaptive filter. Also, the proposed beamformer permits a simple handling of constraints. In this chapter, we have shown that for an arbitrary array configuration, constraints are straightforward to implement and are protected coherently across the spectrum. This is in contrast to state-of-the-art broadband beamformers, where off-broadside constraints or arbitrary array configurations generally require pre-steering before any processing can be performed. One more advantage of this modified version of polynomial broadband beamformer its ability to overcome direction ambiguity issue associated with this beamformer when it is merged with a uniform linear array antenna.

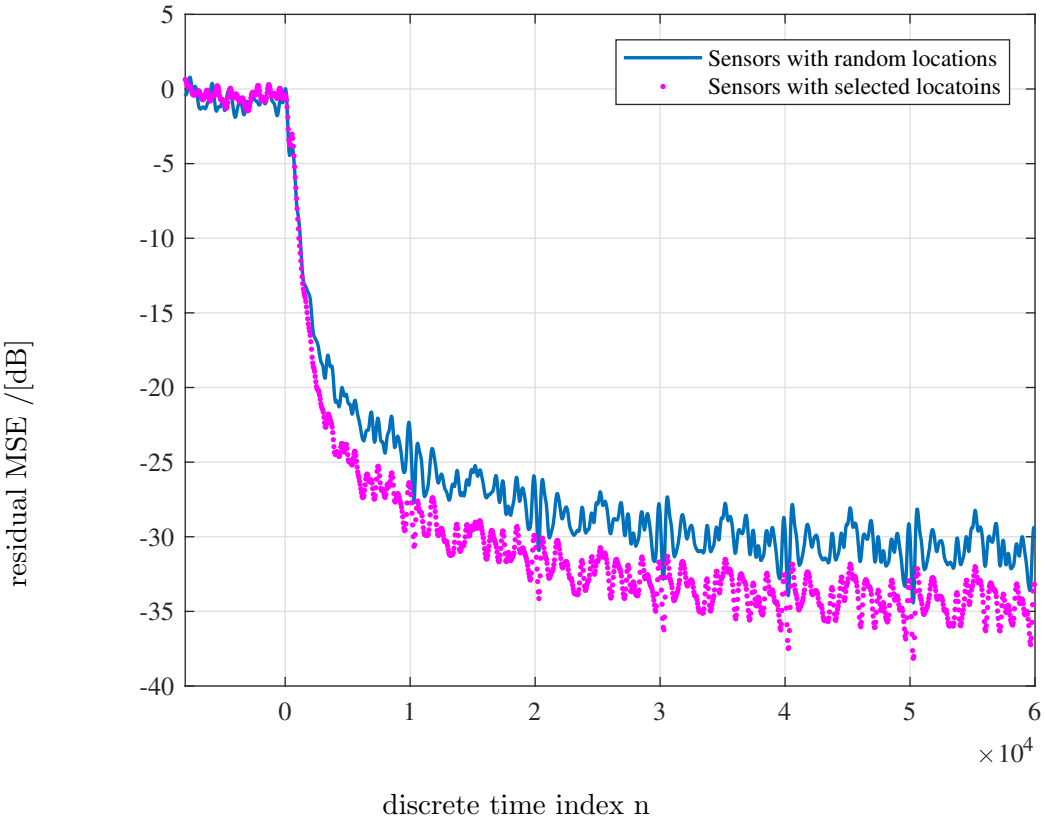


Figure 5.18: A comparison of the mean square residual error after switching adaptation on at $n = 0$ for randomly and selected sensors' locations.

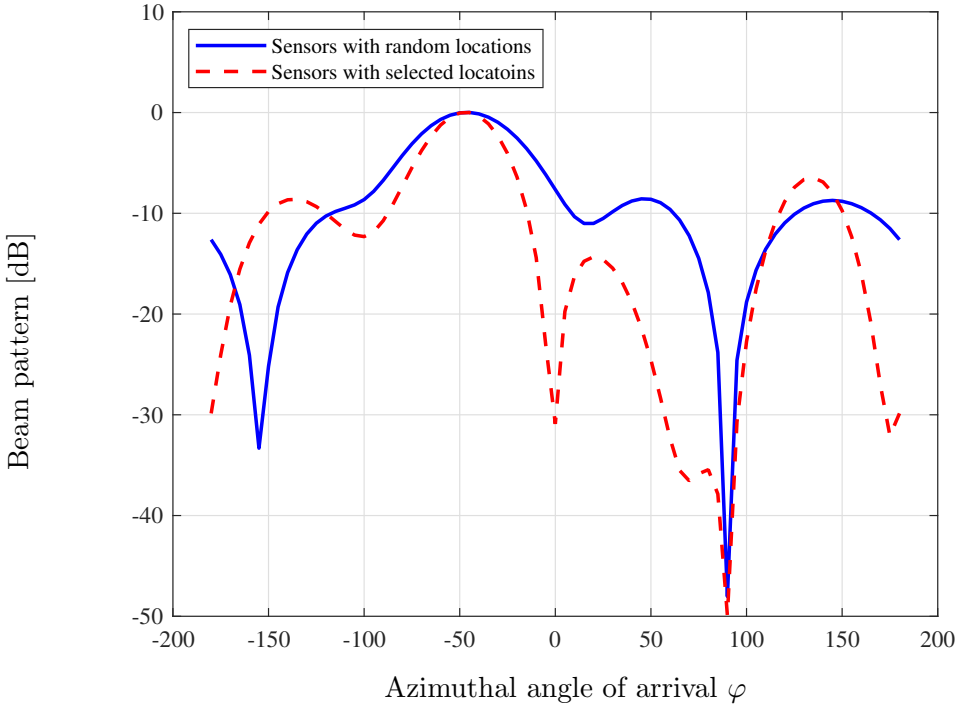


Figure 5.19: A cross-section of the directivity pattern of the elevation direction at $\Omega = \pi/2$ .

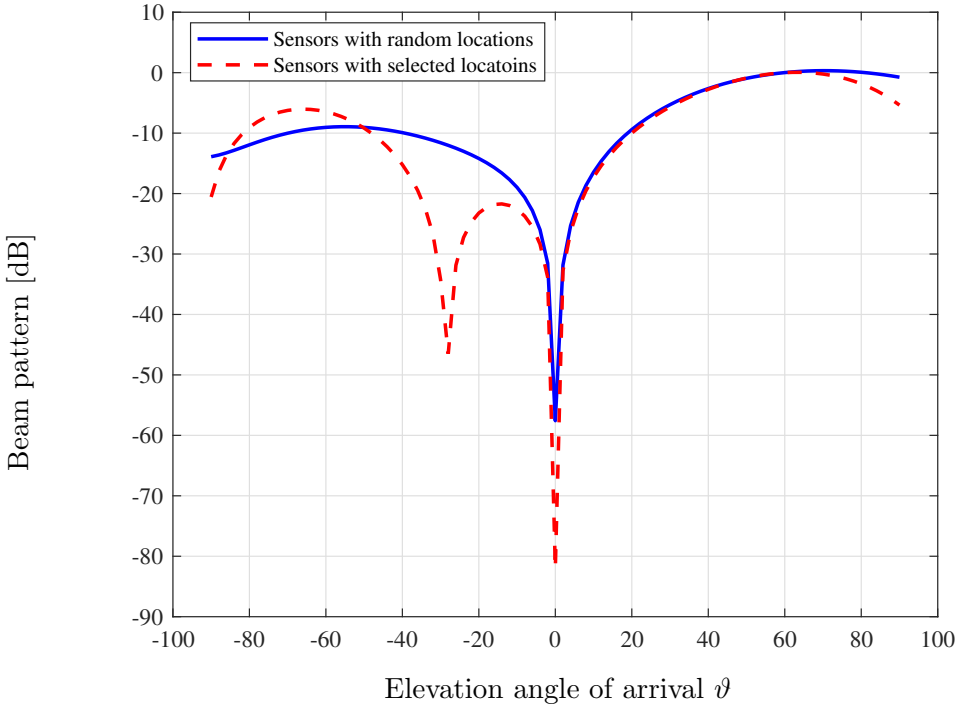


Figure 5.20: A cross-section of the directivity pattern of the elevation direction at $\Omega = \pi/2$ .

# Chapter 6

# Conclusion and Future Directions

In this chapter we first summarize the completed research work and then discuss the main results, findings, and potential future directions.

## 6.1 Summary

Chap. 1 and Chap. 2 have provided a motivation and some background into broadband beamforming, whereby spatial filtering is applied to array signals. These signals have a fractional bandwidth that can cover up to several octaves in frequency, such that simple narrowband processing is insufficient. As a standard, such broadband beamforming problems have been addressed by tap delay lines following each sensor, such that signals are processed in both space and time. Particularly Chap. 2 has provided some of the background on polynomial matrix methods, which is a useful linear algebraic tool to formulate and solve general broadband multichannel signal processing problems.

Chap. 3 has introduced a polynomial matrix notation to formulate the MVDR problem, including the minimisation of the beamformer's ouput power and the description of constraints via a broadband steering vector, and solved the broadband MVDR problem via a GSC. The GSC's quiescent beamformer is directly given by the constraint equation and hence the broadband steering vector, while we have introduced a paraunitary matrix completion to find a polynomial form for the blocking matrix. For a uniform linear array and off-broadside constraints, the polynomial form of the GSC

gave better protection for such constraints, and due to the decoupling of dimensions of the GSC components, provided a lower computational complexity compared to a standard tap-delay line implementation of a broadband GSC beamformer.

Chap. 4 has utilised the polynomial matrix formulation to solve the problem via a broadband extension of the Capon beamformer. This uses the same constraint formulation as in Chap. 3 but extends the constraints by potentially including the directions of known interference. Similar to the narrowband Capon solution, the broadband formulation requires the inversion of a – now polynomial – matrix for which an accurate residue-based approach has been proposed. The Capon beamformer is thus able to suppress interferers either via the constraints if their direction and frequency range are known, or via optimisation in case the interferers are unknown but contribute to the space-time covariance matrix.

Chap. 5 has provided some further analysis and metrics to assess beamformer performance, and expanded the broadband beamformer application from a uniform linear array to arbitrary array configurations. The visualisation of 3D array performance is difficult, and we have shown snapshots of the directivity pattern by fixing always one quantity within the parameter triplet of azimuth, elevation and frequency.

Chap. 6 has given a chapter-wise summary, and will continue with overall conclusions and some suggestions for future directions for research investigations.

## 6.2 Conclusions

Polynomial matrix techniques allow to generalise well-known narrowband concepts, such as MVDR beamformers. We have investigated both GSC and Capon approaches. Within this framework, we have shown the ease of applying the narrowband formulation concepts to the broadband case, which reveals practical advantages obtained by deploying this technique in designing a broadband beamformer with comparison to the standard approach. In the following, we conclude these procedures and highlight the main results, findings, and benefits.

The developed method is used to derive a solution to minimum variance distortionless response (MVDR) beamformer in its generalised sidelobe canceller (GSC) structure.

The fundamental components of the GSC are the quiescent beamformer, blocking matrix, and adaptive filter, these components are derived in an innovative way based on the polynomial matrix techniques. The broadband steering vector, for the constraint formulation, has been firstly implemented in polynomial form, then the quiescent beamformer derived from the constraints of MVDR problem, which includes the broadband steering vector. The quiescent vector, in turn, is used to define the blocking matrix and multichannel adaptive filter. Lastly, in order to obtain the blocking matrix, we proposed para-unitary matrix completion technique for this purpose, the procedures involves building a proper matrix from the quiescent vector and using polynomial matrix decomposition algorithm.

Each component of this structure is examined individually in order to assess its performance, where the quiescent vector is evaluated by means of its beam-pattern, the blocking matrix via the amount of the desired signal that leaks along with interference and noise to the adaptive filter, and the multichannel adaptive filter based on its convergence curve. The results show that the quiescent beamformer steers the beam towards the desired direction, a little amount of the desired signal leaks through the blocking matrix, and the multichannel adaptive filter converges and the contribution of interferers and noise in output power is minimised.

In addition, we investigated the characteristics of the beamformer's components and their influence on each other, specifically; we investigated the relationship among fractional delay filter length, blocking matrix order, and adaptive filter order. Based on this investigation, we have presented the specifications in which these components act collectively without causing the overall performance of the beamformer to degrade.

All in all, the proposed approach is tested under scenarios that assume a uniformly spaced linear array (ULA) ULAuniformly linear array and an environment without reverberation. The sole impairment that the desired signal encounters is due to interference and noise. The performance of the proposed design is compared with a standard beamformer by using MATLAB simulations. The metrics to assess the performance of the adaptive beamfomer are its directivity pattern, the mean square residual error, and its computational cost.

When the polynomial broadband beamformer is compared with the standard time domain one, the simulation results illustrated that the former can respond faster due to the reduction of complexity, and hence, in the processing time. The major complexity saving is obtained via decoupling of the blocking matrix design from the fractional filter length. Where the complexity associated to the standard form of the GSC is greater than the one of the polynomial form by a factor related to the tap delay line length, in our simulation the complexity is 1.72 MMAC versus 10.7 kMAC for the former and the later, respectively. Also the polynomial technique offers a a flexible approach to focusing the antenna array beam towards a specific direction with no need for pre-steering process.

We have further studied the Capon beamformer as an alternative form of addressing the MVDR problem. This form of formulation of the MVDR includes the inverse of the space-time covariance matrix, which is accomplished by a new polynomial matrix inversion technique based on the residue method. The polynomial extension requires the inversion of a polynomial matrix, for which we proposed a residue-based method as a novel approach that offers better accuracy compared to previously utilised convolution approach. Within this context, a regularisation factor or diagonal loading is applied to the polynomial matrix in order to mitigate poor conditioning in space and frequency. This is examined for a chosen regularisation parameter which indicates some control over the the directivity pattern side-lobe levels and has led to a reduction in sidelobe peak levels, hence can enhance the performance of the polynomial broadband beamformer.

The derivation procedures of the GSC components were revisited and adapted to become suitable to be incorporated with arbitrary layout of antenna array elements. In this context, we were successful in making the polynomial based broadband beamformer able to perform well, with performance evaluated via its beam-pattern, learning curve convergence. We – also – examined the impact of the geometry of the antenna array and the location of its elements on the beamformer behaviour; we considered, again, the beam-pattern and learning curve as measures. A comparison of results shows that when antenna array elements are arranged in a way that they are symmetric around

the origin of coordinate axis, the beamformer responses faster and produces deeper null at the interferes direction of arrival. One more advantage of this modified version of polynomial broadband beamformer its ability to overcome direction ambiguity issue associated with this beamformer when it is merged with a uniform linear array antenna. The beamformer is demonstrated to sufficiently steer the beam at the desired direction and nulls at unwanted signals directions.

## 6.3 Future Directions

Based on the work reported in this thesis, this last section provides a number of ideas that where beyond the scope of this research but may represent worthwhile starting points for further investigation.

As a first future step, it might be useful to design an algorithm to compute an optimal diagonal loading factor to enhance Capon beamformer performance in terms of null depth and side lobe levels reduction. This might be more significant, in the case, when an estimated space time covariance matrix used instead of the true space time covariance matrix that was used [139]. The estimation error in the sample space time covariance can be minimised by selection the optimum lag support [**?** ]. Nevertheless, this estimation error will perturb the eigenvalues and eigenspaces of the PEVD [**?** ]. The impact of subspace perturbation on angle of arrival estimation has been assessed in [112, 147], and could be similarly investigated in the context of beamforming.

Secondly, this thesis has assumed ideal far-field propagation characteristics, such that source signals illuminate the array from exactly a single direction. It would therefore be advantageous to evaluate for non-ideal propagation scenarios, for instance, with multipath signals and mutual coupling among antenna elements. This would include the case of near-field propagation, and particularly affect the constraint design in order to protect the signal of interest, that may now arrive from several directions or over a range of angles.

Another point is examining the beamformer response sensitivity to look direction errors [148]. The error in the look direction leads to mismatch between the actual and presumed steering vectors. In consequence, the space time covariance matrix cannot be

accurately estimated, which in turn effects on the adaptive beamformer and degrades its performance.

A family of DFT based polynomial EVD algorithms is currently emerging [114, 149, 150, 151], which aims to extract analytic functions rather than spectrally majorised ones in case of SBR2/SMD. These algorithm are based on a smoothness metric [115, 116, 152, 153, 154] to extract analytic solutions, which therefore offer smoother subspaces and yield significantly lower-order polynomial factors compared to the factorisations provided by SBR2 and SMD. Therefore, the already enhanced computation cost of polynomial beamformers could be further reduced.

# References


[1] Eli Brookner. Radar and phased array breakthroughs. *Microwave Journal*, 58(11):20, 2015.

[2] Eli Brookner. Phased-array radars. *Scientific American*, 252(2):94–103, 1985.

[3] William C Knight, Roger G Pridham, and Steven M Kay. Digital signal processing for sonar. *Proceedings of the IEEE*, 69(11):1451–1506, 1981.

[4] Simon Haykin. Array signal processing. *Englewood Cliffs, NJ, Prentice-Hall, Inc., 493 p*, 1985.

[5] Michael Brandstein and Darren Ward. *Microphone arrays: signal processing techniques and applications*. Springer Science & Business Media, 2001.

[6] Anthony CS Readhead. Radio astronomy by very-long-baseline interferometry. *Scientific American*, 246(6):52–61, 1982.

[7] Teodora Szasz, Adrian Basarab, and Denis Kouamé. Beamforming through regularized inverse problems in ultrasound medical imaging. *IEEE transactions on ultrasonics, ferroelectrics, and frequency control*, 63(12):2031–2044, 2016.

[8] R.T. Compton. An adaptive array in a spread-spectrum communication system. *Proceedings of the IEEE*, 66(3):289–298, 1978.

[9] Joseph Mayhan. Nulling limitations for a multiple-beam antenna. *IEEE Transactions on Antennas and Propagation*, 24(6):769–779, 1976.

[10] Simon Haykin. *Advances in spectrum analysis and array processing (vol. III)*. Prentice-Hall, Inc., 1995.

[11] Wolfgang Herbordt and Walter Kellermann. Adaptive beamforming for audio signal acquisition. In *Adaptive Signal Processing*, pages 155–194. Springer, 2003.

[12] Harry L Van Trees. *Optimum array processing: Part IV of detection, estimation, and modulation theory*. John Wiley & Sons, 2004.

[13] B. D. Van Veen and K. M. Buckley. Beamforming: A Versatile Approach to Spatial Filtering. *IEEE Acoustics, Speech, and Signal Processing Magazine*, 5(2):4–24, April 1988.

[14] Seung-Jean Kim, Alessandro Magnani, Almir Mutapcic, Stephen P Boyd, and Zhi-Quan Luo. Robust beamforming via worst-case sinr maximization. *IEEE Transactions on Signal Processing*, 56(4):1539–1547, 2008.

[15] Kevin M Buckley and Lloyd J Griffiths. Linearly-constrained beamforming: A relationship between phase center location and beampattern. In *IEEE 9th Asilomar Conference on Circuits, Systems and Computers*, pages 234–238, 1985.

[16] Robert G Lorenz and Stephen P Boyd. Robust minimum variance beamforming. *IEEE Transactions on Signal Processing*, 53(5):1684–1696, 2005.

[17] Irving S Reed, John D Mallett, and Lawrence E Brennan. Rapid convergence rate in adaptive arrays. *IEEE Transactions on Aerospace and Electronic Systems*, (6):853–863, 1974.

[18] Dimitris G Manolakis, Vinay K Ingle, and Stephen M Kogon. *Statistical and adaptive signal processing: spectral estimation, signal modeling, adaptive filtering, and array processing*. McGraw-Hill Boston, 2000.

[19] Otis Lamont Frost. An algorithm for linearly constrained adaptive array processing. *Proceedings of the IEEE*, 60(8):926–935, 1972.

[20] K. M. Buckley. Spatial/Spectral Filtering with Linearly Constrained Minimum Variance Beamformers. *IEEE Transactions on Acoustics, Speech, and Signal Processing*, ASSP-35(3):249–266, March 1987.

[21] Michael W. Hoffman and Kevin M. Buckley. Robust Time-Domain Processing of Broadband Microphone Array Data. *IEEE Transactions on Speech and Audio Processing*, 3(3):193–203, May 1995.

[22] Stephan Weiss, Wei Liu, Robert. W. Stewart, and Ian K. Proudler. A Generalised Sidelobe Canceller Architecture based on Oversampled Subband Decompositions. In *5th International Conference on Mathematics in Signal Processing*, Warwick, December 2000.

[23] Wei Liu, Stephan Weiss, and L. Hanzo. Subband Adaptive Generalized Sidelobe Canceller for Broadband Beamforming. In *11th IEEE Signal Processing Workshop on Statistical Signal Processing*, volume 1, pages 591–594, Singapore, August 2001.

[24] Stephan Weiss. Broadband Beamforming Structures. final project report for qinetiq ltd under contract cu016-012628, Dept. of ECS, University of Southampton, Southampton, UK, February 2002.

[25] Wei Liu and Stephan Weiss. *Wideband beamforming: concepts and techniques*, volume 17. John Wiley & Sons, 2010.

[26] Lal Chand Godara. Application of antenna arrays to mobile communications. ii. beam-forming and direction-of-arrival considerations. *Proceedings of the IEEE*, 85(8):1195–1245, 1997.

[27] Lal Chand Godara and Mohammad R Sayyah Jahromi. Limitations and capabilities of frequency domain broadband constrained beamforming schemes. *IEEE transactions on signal processing*, 47(9):2386–2395, 1999.

[28] Olaf Jaeckel. Strengths and weaknesses of calculating beamforming in the time domain. *Proceedings of the 1st Berlin Beamforming Conference (BeBeC)*, 2006.

[29] S. Weiss and I. K. Proudler. Comparing Efficient Broadband Beamforming Architectures and Their Performance Trade-Offs. In *14th International Conference*

*on Digital Signal Processing*, volume I, pages 417–422, Santorini, Greece, July 1–3 2002. (invited paper).

[30] Lal Chand Godara and Mohammad Reza Sayyah Jahromi. Presteering broadband antenna arrays without using steering delays. In *IEEE International Conference on Communications (ICC)*, pages 2562–2567, 2007.

[31] Mohamed Abubaker Alrmah. *Broadband angle of arrival estimation using polynomial matrix decompositions*. PhD thesis, University of Strathclyde, 2015.

[32] Wei Liu, Stephan Weiss, and Lajos Hanzo. A subband-selective broadband gsc with cosine-modulated blocking matrix. *IEEE Transactions on Antennas and Propagation*, 52(3):813–820, 2004.

[33] Ching-Yih Tseng and Lloyd J Griffiths. A systematic procedure for implementing the blocking matrix in decomposed form. In *Twenty-Second Asilomar Conference on Signals, Systems and Computers*, volume 2, pages 808–812. IEEE, 1988.

[34] Sven Nordebo, Ingvar Claesson, and Sven Nordholm. Adaptive beamforming: spatial filter designed blocking matrix. *IEEE Journal of Oceanic Engineering*, 19(4):583–590, 1994.

[35] Choo Leng Koh, Soydan Redif, and Stephan Weiss. Broadband gsc beamformer with spatial and temporal decorrelation. In *17th European Signal Processing Conference (EUSPCO)*, pages 889–893, 2009.

[36] Stephan Weiss, Samir Bendoukha, Ahmed Alzin, Fraser K Coutts, Ian K Proudler, and Jonathan A Chambers. Mvdr broadband beamforming using polynomial matrix techniques. In *2015 23rd European Signal Processing Conference (EUSIPCO)*, pages 839–843. IEEE, 2015.

[37] Ahmed Alzin, Fraser K. Coutts, Jamie Corr, Stephan Weiss, Ian K. Proudler, and Jonathon A. Chambers. Adaptive broadband beamforming with arbitrary array geometry. *2nd IET International Conference on Intelligent Signal Processing (ISP)*, pages 1–6, 2015.

[38] Ahmed Alzin, Fraser K Coutts, Jamie Corr, Stephan Weiss, Ian K Proudler, and Jonathon A Chambers. Polynomial matrix formulation-based capon beamformer. *11th International Conference on Mathematics in Signal Processing (IMA)*, 2016.

[39] Barry D Van Veen and Kevin M Buckley. Beamforming: A versatile approach to spatial filtering. *IEEE transactions on acoustics, speech, and signal processing magazine*, 5(2):4–24, 1988.

[40] Don H Johnson and Dan E Dudgeon. *Array signal processing: concepts and techniques*. PTR Prentice Hall Englewood Cliffs, 1993.

[41] Salvatore Bellofiore, Constantine A Balanis, Jeffry Foutz, and Andreas S Spanias. Smart-antenna systems for mobile communication networks. part 1. overview and antenna design. *IEEE Antennas and Propagation Magazine*, 44(3):145–154, 2002.

[42] Mark T Ma. *Theory and application of antenna arrays*. John Wiley & Sons, 1974.

[43] Robert J Mailloux. Antenna array architecture. *Proceedings of the IEEE*, 80(1):163–172, 1992.

[44] Darren B Ward, Rodney A Kennedy, and Robert C Williamson. Theory and design of broadband sensor arrays with frequency invariant far-field beam patterns. *The Journal of the Acoustical Society of America*, 97(2):1023–1034, 1995.

[45] Frank S Crawford. Waves, berkeley physics course. *berkeley physics course*, 1968.

[46] Alan V Oppenheim and Ronald W Schafer. *Discrete-time signal processing*. Pearson Education, 2014.

[47] Robert Roy, Arogyaswami Paulraj, and Thomas Kailath. Esprit–a subspace rotation approach to estimation of parameters of cisoids in noise. *IEEE transactions on acoustics, speech, and signal processing*, 34(5):1340–1342, 1986.

[48] Ralph O. Schmidt. Multiple emitter location and signal parameter estimation. *IEEE Transactions on Antennas and Propagation*, 34(3):276–280, 1986.

[49] Simon Haykin. *Adaptive filter theory*. Pearson Higher Ed, 2013.

[50] Jack Capon. High-resolution frequency-wavenumber spectrum analysis. *Proceedings of the IEEE*, 57(8):1408–1418, 1969.

[51] Lloyd Griffiths and Charles W. Jim. An alternative approach to linearly constrained adaptive beamforming. *IEEE Transactions on antennas and propagation*, 30(1):27–34, 1982.

[52] Barry D Van Veen. Optimization of quiescent response in partially adaptive beamformers. *IEEE transactions on acoustics, speech, and signal processing*, 38(3):471–477, 1990.

[53] Charles W Jim. A comparison of two LMS constrained optimal array structures. *Proceedings of the IEEE*, 65(12):1730–1731, 1977.

[54] Lal Chand Godara. *Smart antennas*. CRC press, 2004.

[55] Lloyd J Griffiths. A comparison of multidimensional wiener and maximum-likelihood filters for antenna arrays. *Proceedings of the IEEE*, 55(11):2045–2047, 1967.

[56] MR Sayyah Jahromi and Lal Chand Godara. Steering broadband beamforming without pre-steering. In *IEEE/ACES International Conference on Wireless Communications and Applied Computational Electromagnetics*, pages 987–990. IEEE, 2005.

[57] Soydan Redif, John McWhirter, and Stephan Weiss. Design of FIR paraunitary filter banks for subband coding using a polynomial eigenvalue decomposition. *IEEE Transactions on Signal Processing*, 59(11):5253–5264, November 2011.

[58] C. H. Ta and Stephan Weiss. Design of Precoding and Equalisation for MIMO Broadband Transmission. In S. Weiss, editor, *IEE/EURASIP Conference on DSP Enabled Radio*, volume 2005/11086, pages 30/1–30/5, Southampton, UK, September 2005.

[59] C. H. Ta and Stephan Weiss. A Jointly Optimal Precoder and Block Decision Feedback Equaliser Design With Low Redundancy. In *15th European Signal Processing Conference*, pages 489–492, Poznan, Poland, September 2007.

[60] Chi Hieu Ta and Stephan Weiss. A Design of Precoding and Equalisation for Broadband MIMO Systems. In *15th International Conference on Digital Signal Processing*, pages 571–574, Cardiff, UK, July 2007.

[61] Chi Hieu Ta and Stephan Weiss. A design of precoding and equalisation for broadband MIMO systems. In *Forty-First Asilomar Conference on Signals, Systems and Computers*, pages 1616–1620, Pacific Grove, CA, USA, November 2007.

[62] Stephan Weiss, Chi Hieu Ta, and Chunguang Liu. A wiener filter approach to the design of filter bank based single-carrier precoding and equalisation. In *IEEE International Symposium on Power Line Communications and Its Applications*, pages 493–498, Pisa, Italy, March 26-28 2007.

[63] Chi Hieu Ta, Chungguang Liu, and Stephan Weiss. An approach for block transmission based precoding and equalisation with improved performance. In *IEEE International Symposium on Power Line Communications and Its Applications*, pages 331–335, Jeju Island, Korea, April 2008.

[64] Waleed Al-Hanafy, Andrew P. Millar, Chi Hieu Ta, and Stephan Weiss. Broadband SVD and non-linear precoding applied to broadband MIMO channels. In *42nd Asilomar Conference on Signals, Systems and Computers*, pages 2053–2057, Pacific Grove, CA, USA, October 2008.

[65] Waleed Al-Hanafy and Stephan Weiss. Comparison of precoding methods for broadband mimo systems. In *Third International Workshop on Computational Advances in Multi-Sensor Adaptive Processing*, Aruba, Dutch Antilles, December 2009.

[66] Waleed Al-Hanafy and Stephan Weiss. Trade-off between complexity and ber performance of a polynomial svd-based broadband mimo transceiver. In *27th National Radio Science Conference*, Menoufia, Egypt, March 2010.

[67] Nicola Moret, Andrea Tonello, and Stephan Weiss. Mimo precoding for filter bank modulation systems based on psvd. In *IEEE 73rd Vehicular Technology Conference*, pages 1–5, May 2011. (best paper award).

[68] J. Foster, J. McWhirter, S. Lambotharan, I. Proudler, M. Davies, and J. Chambers. Polynomial matrix qr decomposition for the decoding of frequency selective multiple-input multiple-output communication channels. *IET Signal Processing*, 6(7):704–712, September 2012.

[69] Andre Sandmann, Andreas Ahrens, and Steffen Lochmann. Resource allocation in svd-assisted optical mimo systems using polynomial matrix factorization. In *Proceedings of 16. ITG Symposium Photonic Networks*, pages 1–7, May 2015.

[70] Andreas Ahrens, Andre Sandmann, E. Auer, and S. Lochmann. Optimal power allocation in zero-forcing assisted PMSVD-based optical MIMO systems. In *2017 Sensor Signal Processing for Defence Conference (SSPD)*, pages 1–5, December 2017.

[71] Stephan Weiss, Soydan Redif, Tom Cooper, C. Liu, P. Baxter, and John G. McWhirter. Paraunitary oversampled filter bank design for channel coding. *EURASIP Journal on Advances in Signal Processing*, 2006:1–10, 2006.

[72] Soydan Redif. Convolutive blind signal separation via polynomial matrix generalised eigenvalue decomposition. *Electronics Letters*, 53(2):87–89, 2017.

[73] Stephan Weiss, N. J. Goddard, S. Somasundaram, Ian K. Proudler, and P. A. Naylor. Identification of broadband source-array responses from sensor second order statistics. In *Sensor Signal Processing for Defence Conference*, pages 1–5, London, UK, December 2017.

[74] V. W. Neo, C. Evers, and P. A. Naylor. Speech enhancement using polynomial eigenvalue decomposition. In *2019 IEEE Workshop on Applications of Signal Processing to Audio and Acoustics (WASPAA)*, pages 125–129, New Paltz, NY, October 2019.

[75] Mohamed A. Alrmah, Mohamed Hussin, Stephan Weiss, and Sangarapillai Lambotharan. Comparison of broadband direction of arrival estimation algorithms. In *9th IMA Mathematics in Signal Processing Conference*, Birmingham, UK, December 2012.

[76] Mohamed Alrmah, Stephan Weiss, Soydan Redif, Sangarapillai Lambotharan, and John G. McWhirter. Angle of arrival estimation for broadband signals: A comparison. In *IET Intelligent Signal Processing*, London, UK, December 2013.

[77] Stephan Weiss, Mohamed Alrmah, Sangarapillai Lambotharan, John G. McWhirter, and M. Kaveh. Broadband angle of arrival estimation methods in a polynomial matrix decomposition framework. In *IEEE 5th International Workshop on Computational Advances in Multi-Sensor Adaptive Processing*, pages 109–112, December 2013.

[78] Mohamed A. Alrmah, Jamie Corr, Ahmed Alzin, Keith Thompson, and Stephan Weiss. Polynomial subspace decomposition for broadband angle of arrival estimation. In *Sensor Signal Processing for Defence*, pages 1–5, Edinburgh, Scotland, September 2014.

[79] A. Hogg, V. Neo, Stephan Weiss, C. Evers, and P.A. Naylor. A polynomial eigenvalue decomposition music approach for broadband sound source localization. In *Proc. IEEE Workshop on Applications of Signal Processing to Audio and Acoustics*, New Paltz, NY, October 2021.

[80] Parishwad P Vaidyanathan. *Multirate systems and filter banks*. Pearson Education India, 1993.

[81] John G McWhirter, Paul D Baxter, Tom Cooper, Soydan Redif, and Joanne Foster. An evd algorithm for para-hermitian polynomial matrices. *IEEE Transactions on Signal Processing*, 55(5):2158–2169, 2007.

[82] Stephan Weiss, Jennifer Pestana, Ian K Proudler, and Fraser K Coutts. Corrections to "on the existence and uniqueness of the eigenvalue decomposition of a

parahermitian matrix". *IEEE Transactions on Signal Processing*, 66(23):6325–6327, 2018.

[83] Stephan Weiss, Jennifer Pestana, and Ian K Proudler. On the existence and uniqueness of the eigenvalue decomposition of a parahermitian matrix. *IEEE Transactions on Signal Processing*, 66(10):2659–2672, 2018.

[84] Parishwad P Vaidyanathan. Theory of optimal orthonormal subband coders. *IEEE Transactions on Signal Processing*, 46(6):1528–1543, 1998.

[85] S. Icart and P. Comon. Some properties of Laurent polynomial matrices. In *9th IMA Conference on Mathematics in Signal Processing*, Birmingham, UK, December 2012.

[86] Soydan Redif, Stephan Weiss, and John G. McWhirter. An approximate polynomial matrix eigenvalue decomposition algorithm for para-hermitian matrices. In *11th IEEE International Symposium on Signal Processing and Information Technology*, pages 421–425, Bilbao, Spain, December 2011.

[87] Z. Wang, John G. McWhirter, Jamie Corr, and Stephan Weiss. Multiple shift second order sequential best rotation algorithm for polynomial matrix EVD. In *23rd European Signal Processing Conference*, pages 844–848, Nice, France, September 2015.

[88] Z. Wang, John G. McWhirter, Jamie Corr, and Stephan Weiss. Order-controlled multiple shift sbr2 algorithm for para-hermitian polynomial matrices. In *9th IEEE Sensor Array and Multichannel Signal Processing Workshop*, Rio de Janeiro, Brazil, July 2016.

[89] Soydan Redif, Stephan Weiss, and John G McWhirter. Sequential matrix diagonalization algorithms for polynomial evd of parahermitian matrices. *IEEE Transactions on Signal Processing*, 63(1):81–89, 2015.

[90] Jamie Corr, Keith Thompson, Stephan Weiss, John G. McWhirter, Soydan Redif, and Ian K. Proudler. Multiple shift maximum element sequential matrix diago-

nalisation for parahermitian matrices. In *IEEE Workshop on Statistical Signal Processing*, pages 312–315, Gold Coast, Australia, June 2014.

[91] Jamie Corr, Keith Thompson, Stephan Weiss, John G. McWhirter, and Ian K. Proudler. Causality-Constrained multiple shift sequential matrix diagonalisation for parahermitian matrices. In *22nd European Signal Processing Conference*, pages 1277–1281, Lisbon, Portugal, September 2014.

[92] Jamie Corr, Keith Thompson, Stephan Weiss, John G. McWhirter, and Ian .K. Proudler. Maximum energy sequential matrix diagonalisation for parahermitian matrices. In *48th Asilomar Conference on Signals, Systems and Computers*, pages 470–474, Pacific Grove, CA, USA, November 2014.

[93] Jamie Corr, Keith Thompson, Stephan Weiss, Ian K. Proudler, and John G. McWhirter. Reduced search space multiple shift maximum element sequential matrix diagonalisation algorithm. In *IET/EURASIP Intelligent Signal Processing*, London, UK, December 2015.

[94] Jamie Corr, Keith Thompson, Stephan Weiss, John .G. McWhirter, and Ian K. Proudler. Performance trade-offs in sequential matrix diagonalisation search strategies. In *IEEE 6th International Workshop on Computational Advances in Multi-Sensor Adaptive Processing*, pages 25–28, Cancun, Mexico, December 2015.

[95] V. W. Neo and P. A. Naylor. Second order sequential best rotation algorithm with householder reduction for polynomial matrix eigenvalue decomposition. In *IEEE International Conference on Acoustics, Speech and Signal Processing*, pages 8043–8047, Brighton, UK, May 2019.

[96] John G McWhirter, Paul D Baxter, Tom Cooper, and Soydan Redif. A novel technique for broadband subspace decomposition. In *IEEE 14th European Signal Processing Conference*, pages 1–5, 2006.

[97] John McWhirter and Zeliang Wang. A novel insight to the SBR2 algorithm for

diagonalising para-hermitian matrices. *11th International Conference on Mathematics in Signal Processing (IMA)*, 2016.

[98] Jamie Corr. *Advanced algorithms for polynomial matrix eigenvalue decomposition.* PhD thesis, University of Strathclyde, 2017.

[99] Jamie Corr, Keith Thompson, Stephan Weiss, John G. McWhirter, and Ian K. Proudler. Cyclic-by-row approximation of iterative polynomial EVD algorithms. In *Sensor Signal Processing for Defence*, pages 1–5, Edinburgh, Scotland, September 2014.

[100] Fraser K. Coutts, Jamie Corr, Keith Thompson, Stephan Weiss, Ian Proudler, and John G. McWhirter. Memory and complexity reduction in parahermitian matrix manipulations of PEVD algorithms. In *24th European Signal Processing Conference*, Budapest, Hungary, August 2016.

[101] Fraser K. Coutts, Jamie Corr, Keith Thompson, Stephan Weiss, Ian K. Proudler, and John G. McWhirter. Complexity and search space reduction in cyclic-by-row PEVD algorithms. In *50th Asilomar Conference on Signals, Systems and Computers*, Pacific Grove, CA, November 2016.

[102] Fraser K. Coutts, Keith Thompson, Stephan Weiss, and Ian K. Proudler. Analysing the performance of divide-and-conquer sequential matrix diagonalisation for large broadband sensor arrays. In *2017 IEEE International Workshop on Signal Processing Systems*, pages 1–6, Lorient, France, October 2017.

[103] Fraser Coutts, Jamie Corr, Keith Thompson, Ian Proudler, and Stephan Weiss. Divide-and-conquer sequential matrix diagonalisation for parahermitian matrices. In *Sensor Signal Processing for Defence Conference*, pages 1–5, London, UK, December 2017.

[104] Fraser K. Coutts, Keith Thompson, Ian K. Proudler, and Stephan Weiss. Restricted update sequential matrix diagonalisation for parahermitian matrices. In *IEEE 7th International Workshop on Computational Advances in Multi-Sensor Adaptive Processing*, Curacao, December 2017.

[105] Fraser K. Coutts, Ian K. Proudler, and Stephan Weiss. Efficient implementation of iterative polynomial matrix evd algorithms exploiting structural redundancy and parallelisation. *IEEE Transactions on Circuits and Systems I: Regular Papers*, 66(12):4753–4766, December 2019.

[106] Faizan Ahmad Khattak, Stephan Weiss, and Ian K. Proudler. Fast givens rotation approach to second order sequential best rotation algorithms. In *International Conference in Sensor Signal Processing for Defence*, Edinburgh, Scotland, September 2021.

[107] J. Foster, J. G. McWhirter, and J. Chambers. Limiting the order of polynomial matrices within the SBR2 algorithm. In *IMA International Conference on Mathematics in Signal Processing*, Cirencester, UK, December 2006.

[108] Chi Hieu Ta and Stephan Weiss. Shortening the order of paraunitary matrices in SBR2 algorithm. In *6th International Conference on Information, Communications & Signal Processing*, pages 1–5, Singapore, December 2007.

[109] Jamie Corr, Keith Thompson, Stephan Weiss, Ian K. Proudler, and John G. McWhirter. Shortening of paraunitary matrices obtained by polynomial eigenvalue decomposition algorithms. In *Sensor Signal Processing for Defence*, Edinburgh, Scotland, September 2015.

[110] Jamie Corr, Keith Thompson, Stephan Weiss, Ian K. Proudler, and John G. McWhirter. Impact of source model matrix conditioning on PEVD algorithms. In *IET/EURASIP Intelligent Signal Processing*, London, UK, December 2015.

[111] Fraser Coutts, Keith Thompson, Stephan Weiss, and Ian Proudler. Impact of fast-converging PEVD algorithms on broadband AoA estimation. In *Sensor Signal Processing for Defence Conference*, pages 1–5, London, UK, December 2017.

[112] Stephan Weiss, Connor Delaosa, J. Matthews, Ian Proudler, and B.A. Jackson. Detection of weak transient signals using a broadband subspace approach. In *International Conference on Sensor Signal Processing for Defence*, 2021.

[113] Jamie Corr, Keith Thompson, Stephan Weiss, Ian K Proudler, and John G McWhirter. Row-shift corrected truncation of paraunitary matrices for pevd algorithms. In *Signal Processing Conference (EUSIPCO), 2015 23rd European*, pages 849–853, 2015.

[114] Stephan Weiss, Ian K. Proudler, Fraser K. Coutts, and Jennifer Pestana. Iterative approximation of analytic eigenvalues of a parahermitian matrix EVD. In *IEEE International Conference on Acoustics, Speech and Signal Processing*, Brighton, UK, May 2019.

[115] Stephan Weiss, Ian K. Proudler, Fraser K. Coutts, and J. Deeks. Extraction of analytic eigenvectors from a parahermitian matrix. In *International Conference on Sensor Signal Processing or Defence*, E, 2020.

[116] Stephan Weiss, Ian K. Proudler, and Fraser K. Coutts. Eigenvalue decomposition of a parahermitian matrix: Extraction of analytic eigenvalues. *IEEE Transactions on Signal Processing*, 69:722–737, 2021.

[117] Henrik Hansen, Affes Sofiene, and Paul Mermelstein. A beamformer for cdma with enhanced near-far resistance. In *IEEE International Conference on Communications (Cat. No. 99CH36311)*, volume 3, pages 1583–1587, 1999.

[118] Jacob Benesty and Yiteng Huang. *Adaptive signal processing: applications to real-world problems*. Springer Science & Business Media, 2013.

[119] Soydan Redif, John G McWhirter, Paul D Baxter, and Thomas Cooper. Robust broadband adaptive beamforming via polynomial eigenvalues. In *IEEE OCEANS*, pages 1–6, 2006.

[120] Martin Davies, Sangarapillai Lambotharan, and John McWhirter. Broadband mimo beamforming using spatial-temporal filters and polynomial matrix decomposition. In *IEEE 15th International Conference on Digital Signal Processing*, pages 579–582, 2007.

[121] Chi Hieu Ta and Stephan Weiss. A design of precoding and equalisation for broadband mimo systems. In *Digital Signal Processing, 2007 15th International Conference on*, pages 571–574. IEEE, 2007.

[122] Mohamed Alrmah, Stephan Weiss, and Sangarapillai Lambotharan. An extension of the music algorithm to broadband scenarios using a polynomial eigenvalue decomposition. In *19th European Signal Processing Conference*, pages 629–633, 2011.

[123] Peter G Vouras and Trac D Tran. Robust transmit nulling in wideband arrays. *IEEE Transactions on Signal Processing*, 62(14):3706–3719, 2014.

[124] I Thng, Antonio Cantoni, and Yee Hong Leung. Derivative constrained optimum broad-band antenna arrays. *IEEE Transactions on Signal Processing*, 41(7):2376–2388, 1993.

[125] Shutao Zhang and Ian Li-Jin Thng. Robust presteering derivative constraints for broadband antenna arrays. *IEEE Transactions on Signal Processing*, 50(1):1–10, 2002.

[126] Michael Rubsamen and Alex B Gershman. Robust presteered broadband beamforming based on worst-case performance optimization. In *5th IEEE Sensor Array and Multichannel (SAM) Signal Processing Workshop*, pages 340–344, 2008.

[127] Jesus Selva. An efficient structure for the design of variable fractional delay filters based on the windowing method. *IEEE Transactions on Signal Processing*, 56(8):3770–3775, 2008.

[128] Vesa Valimaki and Timo Laakso. Fractional delay filters—design and applications. In *Nonuniform Sampling*, pages 835–895. Springer, 2001.

[129] Mohamed Alrmah, Stephan Weiss, and John McWhirter. Implementation of accurate broadband steering vectors for broadband angle of arrival estimation. In *IET Intelligent Signal Processing Conference (ISP)*, pages 1–6, 2013.

[130] Gene H Golub and Charles F Van Loan. *Matrix computations*, volume 3. JHU Press, 2012.

[131] Neil Bershad. Analysis of the normalized lms algorithm with gaussian inputs. *IEEE Transactions on Acoustics, Speech, and Signal Processing*, 34(4):793–806, 1986.

[132] Timo I Laakso, Vesa Valimaki, Matti Karjalainen, and Unto K Laine. Splitting the unit delay [fir/all pass filters design]. *IEEE Signal Processing Magazine*, 13(1):30–60, 1996.

[133] Lloyd J Griffiths. Adaptive monopulse beamforming. *Proceedings of the IEEE*, 64(8):1260–1261, 1976.

[134] Walter Kellermann. Analysis and design of multirate systems for cancellation of acoustical echoes. In *ICASSP-88., International Conference on Acoustics, Speech, and Signal Processing*, pages 2570–2573. IEEE, 1988.

[135] Stephan Weiss. *On adaptive filtering on oversampled subbands*. PhD thesis, Signal Processing Division, University of Strathclyde, Glasgow, 1998.

[136] Kevin M Buckley. Spatial/spectral filtering with linearly constrained minimum variance beamformers. *IEEE Transactions on Acoustics, Speech, and Signal Processing*, 35(3):249–266, 1987.

[137] Timo I Laakso, Vesa Valimaki, Matti Karjalainen, and Unto K Laine. Splitting the unit delay [fir/all pass filters design]. *IEEE Signal Processing Magazine*, 13(1):30–60, 1996.

[138] Jack Capon, Roy J. Greenfield, and R. J. Kolker. Multidimensional maximum-likelihood processing of a large aperture seismic array. *Proceedings of the IEEE*, 55(2):192–211, 1967.

[139] Connor Delaosa, Jennifer Pestana, Nicholas J Goddard, Samuel Somasundaram, and Stephan Weiss. Sample space-time covariance matrix estimation. In *IEEE*

*International Conference on Acoustics, Speech and Signal Processing (ICASSP)*, pages 8033–8037, 2019.

[140] Jian Li, Petre Stoica, and Zhisong Wang. On robust capon beamforming and diagonal loading. *IEEE transactions on signal processing*, 51(7):1702–1715, 2003.

[141] Blair D Carlson. Covariance matrix estimation errors and diagonal loading in adaptive arrays. *IEEE Transactions on Aerospace and Electronic systems*, 24(4):397–401, 1988.

[142] Stephan Weiss, Andrew P Millar, and Robert W Stewart. Inversion of paraher-mitian matrices. In *18th European Signal Processing Conference*, pages 447–451, 2010.

[143] Mohamed Alrmah and Stephan Weiss. Filter bank based fractional delay filter implementation for widely accurate broadband steering vectors. In *5th IEEE International Workshop on Computational Advances in Multi-Sensor Adaptive Processing (CAMSAP)*, pages 332–335, 2013.

[144] Jean-Marc Valin, François Michaud, Jean Rouat, and Dominic Létourneau. Robust sound source localization using a microphone array on a mobile robot. In *Intelligent Robots and Systems, 2003.(IROS 2003). Proceedings. 2003 IEEE/RSJ International Conference on*, volume 2, pages 1228–1233. IEEE, 2003.

[145] Efren Fernandez-Grande. Sound field reconstruction using a spherical microphone array. *The Journal of the Acoustical Society of America*, 139(3):1168–1178, 2016.

[146] S Lawrence Marple Jr and William M Carey. *Digital spectral analysis*. Dover puplications, INC., 2019.

[147] Connor Delaosa, Jennifer Pestana, Stephan Weiss, and Proudler Ian K. Subspace perturbation bounds with an application to angle ofarrival estimation using the music algorithm. In *International Conference on Sensor Signal Processing for Defence*, 2020.

[148] N Jablon. Adaptive beamforming with the generalized sidelobe canceller in the presence of array imperfections. *IEEE Transactions on Antennas and Propagation*, 34(8):996–1012, 1986.

[149] Mahdi Tohidian, Hamidreza Amindavar, and Ali M. Reza. A DFT-based approximate eigenvalue and singular value decomposition of polynomial matrices. *EURASIP Journal on Advances in Signal Processing*, 2013(1):1–16, 2013.

[150] Fraser K. Coutts, Keith Thompson, Stephan Weiss, and Ian K. Proudler. A comparison of iterative and DFT-based polynomial matrix eigenvalue decompositions. In *IEEE 7th International Workshop on Computational Advances in Multi-Sensor Adaptive Processing*, Curacao, December 2017.

[151] Fraser Kenneth Coutts, Keith Thompson, Jennifer Pestana, Ian Proudler, and Stephan Weiss. Enforcing eigenvector smoothness for a compact DFT-based polynomial eigenvalue decomposition. In *10th IEEE Workshop on Sensor Array and Multichannel Signal Processing*, pages 1–5, July 2018.

[152] Stephan Weiss and Malcolm D. Macleod. Maximally smooth dirichlet interpolation from complete and incomplete sample points on the unit circle. In *IEEE International Conference on Acoustics, Speech, and Signal Processing*, Brighton, UK, May 2019.

[153] Stephan Weiss, Ian K. Proudler, and Malcolm D. Macleod. Measuring smoothness of real-valued functions defined by sample points on the unit circle. In *Sensor Signal Processing in Defence Conference*, Brighton, UK, May 2019.

[154] Stephan Weiss, Jesus Selva, and Malcolm Macleod. Measuring smoothness of trigonometric interpolation through incomplete sample points. In *EUSIPCO*, 2020.

[155] Soydan Redif, Stephan Weiss, and John G McWhirter. Relevance of polynomial matrix decompositions to broadband blind signal separation. *Signal processing, Elsevier*, 134:76–86, 2017.

[156] Connor Delaosa, Fraser K Coutts, Jennifer Pestana, and Stephan Weiss. Impact of space-time covariance estimation errors on a parahermitian matrix evd. In *IEEE 10th Sensor Array and Multichannel Signal Processing Workshop (SAM)*, pages 164–168, 2018.

[157] I. Gohberg, P. Lancaster, and L. Rodman. *Matrix Polynomials*. Academic Press, New York, 1982.